Cationic Polymer Brush Coated Nanoparticles for Gene Delivery

Danyang Li

Supervisor: Dr. Julien Gautrot

School of Engineering and Materials Science

Queen Mary University of London

This dissertation is submitted for the degree of

Doctor of Philosophy

July 2018

Declaration

I certify that the present work is my own work during my studies at Queen Mary, University of London. It has not been submitted for a degree at this or any other University. Any words and/or figures from the work of other people and previously published material are fully acknowledged according to standard referencing.

This thesis fully complies with the regulations set by the University of London and the Queen Mary, University of London.

Danyang Li

Signature:

July 2018

Acknowledgement

Firstly, I would like to express my sincerest gratitude to my supervisor Dr Julien Gautrot for offering me the chance to do this PhD. I still remember the first day I met him. It was 8:30 am in the morning, Dr Julien Gautrot was working in the lab when a friend took me for a guide tour around the department. This thesis would not exist without all the suggestions, advices, constant encouragement and patience provided by Dr Julien Gautrot throughout the years. I really benefit a lot with the solid and extensive knowledge that Dr Julien Gautrot has. I was also deeply impressed by his conscientious and dedicated attitudes as an educator and researcher. Besides, he is always available to provide quality discussions and guidance for progress through group meetings, one-to-one meetings and emails.

I would also like to thank the funding provider, Chinese Scholarship Council, to support my living in London with such a fantastic experience.

My life would not have been as enjoyable as it was without all the friendly members of Dr Julien Gautrot's group. I would like to thank Dr Aji Alex Moothedathu Raynold, Alice Dowden, Dr Burcu Colak, Dr Chara Simitzi, Christian Jones, Denys Ewerton da Silva Santos, Dr Dexu Kong, Edward Cozens, Fauzia Quadir, Dr Fengfeng Zhang, Fengjin Qu, Dr Gloria Silva, Dr Khai Duong Quang Nguyen, Lihui Peng, Linke Wu, Dr Mahentha Krishnamoorthy, Dr Maria Crespo Ribadeneyra, Matt Dibble, Dr Pei Tang, Dr Shoghik Hakobyan, Dr Stefania Di Cio, William Megone, Dr Xi Zhang, Yaqi You, Dr Yiran An. They

Abstract

Polymer brushes generated *via* "grafting-from" approach emerged as an attractive surface modification tool offering chemical stability, synthetic flexibility and unprecedented control over the polymer grafting density, thickness, chemical composition and functionality. They display interesting features to many applications in regenerative medicine including cell culture, tissue engineering and as delivery systems due to exquisite control of physicochemical and biological properties. Cationic polymer brushes are particularly attractive in the field of designing effective vectors for gene delivery as polymer brush allows the design and coating of a variety of particles with well-defined core-shell architecture and chemistry to efficiently condense and deliver nucleic acids. This thesis concentrates on designing safe and efficient gene delivery vectors based on 'graft from' cationic polymer brush and understanding the interaction of nucleic acids with polymer brush.

Chapter one presented fundamental knowledge of polymer brush and its biomedical application. The first part of this chapter describes the definition of polymer brush, the preparation strategies, mechanism of atom transfer radical polymerisation and the responsiveness of polymer brush including solvent, pH and ionic strength. The second part discusses the state-of-art applications of polymer brush in regenerative medicine including protein resistant polymer brush for tissue engineering and as drug/gene delivery systems.

In chapter two, high density cationic polymer brushes was prepared to study the interactions with different nucleic acids. We further demonstrate the ease with which such coatings allow the design of highly structured nanomaterials for siRNA delivery using block copolymer-brush based nanoparticles that allow the protection of oligonucleotides by a protein resistant outer block. In particular these nanomaterials display a high serum stability and low cytotoxicity whilst retaining excellent knock down efficiencies.

Chapter three aims to fabricate polymer brush from macroinitiator adsorbed to a variety of templates with different core sizes, surface chemistries and shapes to further explore a more flexible way to generate polymer brushes on different particles as well as labelling them with stable fluorescence. Selected candidates were used to study the interaction of different brush chemistry coated particles with epidermal cells and for the delivery of siRNA.

In chapter four, three different polymer brushes coated silica nanoparticles (SiO$_2$-PDMAEMA, SiO$_2$-PDMAI and SiO$_2$-PDMABr) were prepared and the effect of different chemistries and pH responsiveness on siRNA transfection kinetics was evaluated. Moreover, fluorescently labelled vectors and siRNA were used to visualise siRNA complex uptake and siRNA release in HaCaT cells.

Chapter five summarises the main findings of this thesis and provides suggestions for future research.

List of Publications:

Accepted:

• **D. Li**, A. Sharili, J. Connelly, J. Gautrot*. Highly stable RNA encapsulation by dense cationic polymer brushes for siRNA delivery. ***Biomacromolecules***, 19 (2018), 606–615.

• **D. Li**, J. Gautrot*. Polymer and Biopolymer Brushes | chapter 20 | Design of polymer brushes for cell culture and cellular delivery: for materials science and biotechnology. ***Wiley***, December, (2) 2017, 557-603. (**Invited bookchapter**, editors: Prof. Omar Azzaroni and Prof. Igal Szleifer.)

• M. Krishnamoorthy†, **D. Li†**, A. Sharili, T. Gulin-Sarfraz, J. Rosenholm, J. Gautrot*. The solution conformation of polymer brushes determines their interactions with DNA and transfection efficiency, ***Biomacromolecules***, 18 (2017) 4121–4132. (**†Equal contribution first author**)

• S.J. Attwood, E. Cortes, A.W.M. Haining, B. Robinson, **D. Li**, J. Gautrot, A. del Río Hernández*. Adhesive ligand tether length affects the size and length of focal adhesions and influences cell spreading and attachment, ***Scientific Report***, 6 (2016) 34334.

• Y. An, **D. Li,** N. Roohpour, J.E. Gautrot*, A.H. Barber*. Failure mechanisms in denture adhesives, ***Dental Materials***, 32 (2016) 615-623.

In preparation:

• **D. Li**, J. Gautrot*. Preparation of fluorescent polymer brushes on different templates with macroinitiators for cell-particle interaction study.

• **D. Li**, J. Gautrot*. Quaternised cationic polymer brush coated silica nanoparticles for siRNA long-term and efficient delivery.

• D. Santos, **D. Li**, M. Ramstedt, J. Gautrot*, T. Soares*. Charged polymer brushes under different solvents and salt types: atomistic simulations of pDMAEMA and pMETAC.

Abbreviations and Symbol

kact	The rate constant of activation
KATRP	ATRP equilibrium constants
kdact	The rate constant of deactivation
α-BiB	Bromoisobutyryl bromide
Mw	Molecular weight
ATRP	Atom transfer radical polymerisation
AFM	Atomic force microscopy
BCA	Bicinchoninic acid
BCB	Block copolymer brush
Boc-AEMA	N-tertbutoxycarbonyl-aminoethyl methacrylate
Boc-AEAEMA	N,N-di(tertbutoxycarbonyl)-2-(2-aminoethylamino)ethyl methacrylate
$CaCO_3$	Calcium carbonate
CNCs	Cellulose nanocrystals
CP	Choline phosphate
CPB	Concentrated polymer brush
CysMA	Cysteine methacrylate
DAPI	4,6-diamidino-2-phenylindole
DCM	Dichloromethane
DEAEMA	2- (diethylamino)ethyl methacrylate
DMAP	4-dimethylaminopyridine
DMEM	Dulbecco's modified eagle medium
DMAEMA	2-(dimethylamino)ethylmethacrylate
DMAPMAA	N-(3-(dimethylamino)propyl) methacrylamide
DMF	Dimethylformamide
DLS	Dynamic light scattering
DOX	Doxorubicin
DPAEMA	2-(diisopropylamino)ethyl methacrylate
ECM	Extra cellular matrix (ECM)
EGFR	Epidermal growth factor receptors

Et$_3$N	Triethylamine
FBS	Fetal bovine serum
FCP	Fluorescent conjugated polyelectrolytes
FTIR-ATR	Fourier transform infrared spectroscopy-attenuated total reflectance
GAPDH	Glyceraldehyde 3-phosphate dehydrogenase
GFP	Green fluorescent protein
GO	Graphene oxide sheets
GPC	Gel permeation chromatography
HAEAPMA	(2- hydroxy-3-(2-aminoethyl)amino)propyl methacrylate
HIFU	High intensity focused ultrasound
HSNPs	Hollow silica nanoparticles
LBL	Layer-by-layer
LCST	Lower critical solution temperature
LDHs	Ayered double hydroxides
Lipo	Lipofectetamine 2000
MCP	2-(methacryloyloxy)ethyl choline phosphate
MeDMA	2-(methacryloyloxy)ethyl) trimethyl ammonium chloride
MI	Macroinitiator
mRNA	Messenger RNA
NC	Negative control
NITEC	Nitrile imine-mediated tetrazole-ene cycloadditions
P4VP	Poly(4-vinyl pyridine)
PAA	Poly(acrylic acid)
PAAEE	Poly(N-acryloylaminoethoxyethanol)
PAAm	Poly(acrylamide)
PAspAA	Poly(N-4-(2-methacrylamidoethyl)asparagine)
PBA	Phenylboronic acid
PBS	Phosphate-buffered saline
PCBMA	Poly(carboxybetaine methacrylate)
PCL	Poly(Ɛ-caprolactone)
PDEA	Poly((diethylamino)ethyl methacrylate)
PDA	Poly(dopamine)
PDEAEMA	Poly(2-(diethylamino)-ethyl methacrylate)
PDMAEMA	Poly((dimethylamino)ethyl methacrylate)
PDMS	Polydimethylsiloxane

PDMSA	1-(dimethoxymethylsiyl)propyl acrylate
PEG	Poly (ethylene glycol)
PEI	Polyethylenimine
PFA	Paraformaldehyde
PGA	Poly(glycolic acid)
PGluAA	Poly(N-5-(2- methacrylamidoethyl)glutamine)
PHEMA	Poly(2-hydroxyethyl methacrylate)
PHEA	Poly(2-hydroxyethyl acrylate)
PHPMA	Poly(hydroxypropyl methacrylamide)
PHPMAm	Poly(hydroxyl propyl methacrylamide)
PLA	Poly(lactic acid)
PLEDs	Polymer light-emitting diodes
PLL	Poly(L-lysine)
PMAA	Poly(methacrylic acid)
PMPC	Poly(2-methacryloyloxylethy phosphorylcholine)
PNIPAAm	Poly(N-isopropylacrylamide)
POEGMA	Poly(oligo(ethylene glycol) methacrylate)
POEGMEMA	Poly(oligo(ethylene glycol) methyl ether methacrylate)
POx	Poly(2-oxazoline)
PPEGMA	Poly(poly(ethylene glycol) methyl ether methacrylate)
P/S	PenicillinStreptomycin
PS	Polystyrene
PSBMA	Poly-(sulfobetaine methacrylate)
PSS	Poly(sodium 4-styrenesulfonate)
PVBIPS	Poly(3-(1-(4- vinylbenzyl)-1H-imidazol-3-ium-3-yl)propane-1-sulfonate)
QCM	Quartz crystal microbalance
REFs	Rat embryonic fibroblasts
RISC	RNA-induced silencing complex
RGD	Arg-Gly-Asp Peptide
RGE	Arg-Gly-Glu Peptide
RNAi	RNA interference
SAMs	Self-assembled monolayers
SDPB	Semi-dilute polymer brush
SDS-PAGE	Sodium dodecyl sulfate–polyacrylamide gel electrophoresis
SEM	Scanning electron microscopy

SiO$_2$	Silica nanoparticles
siRNA	Short interfering RNA
SPR	Surface plasmon resonance
SUS	Stainless steel
SWCNTs	Single-walled carbon nanotubes
TBS	Tris buffered saline
TEA	Triethylamine
TEM	Transmission electron microscope
TGA	Thermogravimetric analysis
THF	Tetrahydrofuran
UCNPs	Lanthanide-doped up conversion nanoparticles
UV	Ultraviolet

Contents

CHAPTER 1

Literature Review*

1.1 Polymer brush

1.1.1 Polymer brush definition

Polymer brushes are defined as dense layers of chains confined to a surface or interface where the distance between grafts (d) is much less than the unperturbed dimensions of the tethered (h). At high grafting densities, *i.e.* when the distance between neighbouring grafting points is small, steric repulsion leads to chain stretching and a brush-like (scheme 1a) conformation of the surface-tethered chains.[1, 2] At lower densities, surface-tethered polymer chains can adopt various other conformations, which are referred to as mushroom (scheme 1b) or pancake (scheme 1c).[1, 2]
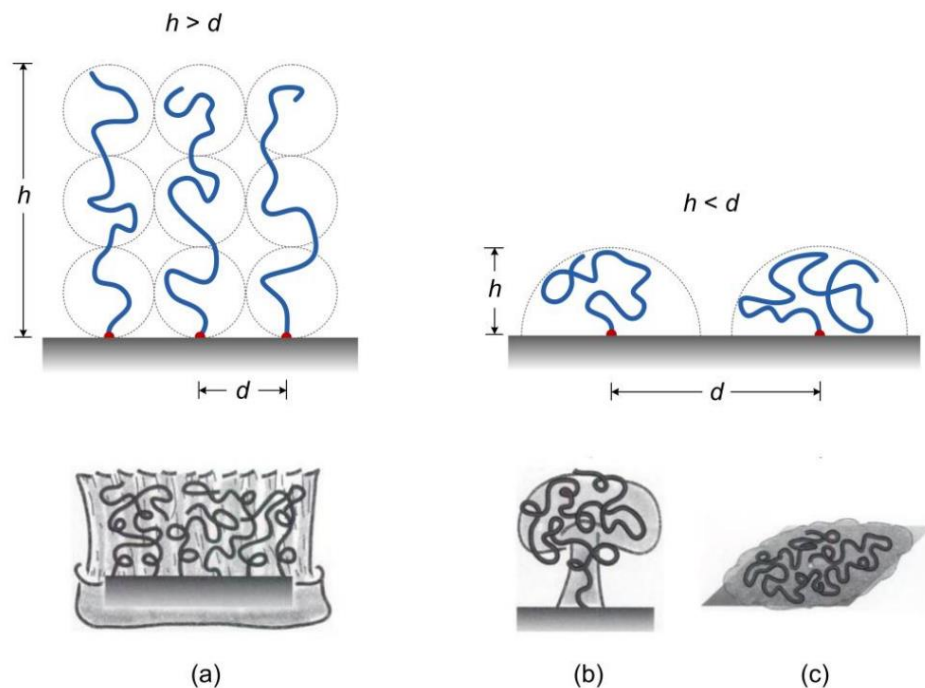
Figure 1.1. Illustration of possible conformations of polymers end-tethered to a surface: (a) brush-like, (b) mushroom-like and (c) pancake-like.

1.1.2 General preparation strategies of polymer brush

The two main strategies for the preparation of polymer brushes are the grafting to and the grafting from strategies[3]. The grafting to strategy involves attaching prefabricated polymers *via* either physisorption (scheme 2A) [4, 5] or covalent chemical bond (scheme 2B) [6]. However, there are several limitations for the grafting to strategy, which make it difficult to produce thick and dense polymer brushes due to the steric repulsions between polymer chains. Furthermore, the reaction between the complementary group at the surface and the polymer end-group typically becomes less efficient with increasing polymer molecular weight. In the grafting from approach (scheme 2C)[7, 8], the polymerisation is directly initiated from initiator-functionalised surfaces, which allows relatively accurate control over brush thickness, composition, and architecture. Living controlled surface-initiated polymerisation reactions, including atom transfer radical polymerisation (ATRP)[9-11], carbocationic polymerisation[12, 13], anionic polymerisation[14, 15], and ring-opening metathesis polymerisation[16, 17] are typically required to achieve such control. The different polymerisation reactions can be carried out on surfaces presenting very different topographies (planar[18], curved[19], and irregular surfaces[20]), and allow the generation of polymer brushes based on a wide spectrum of different monomers.
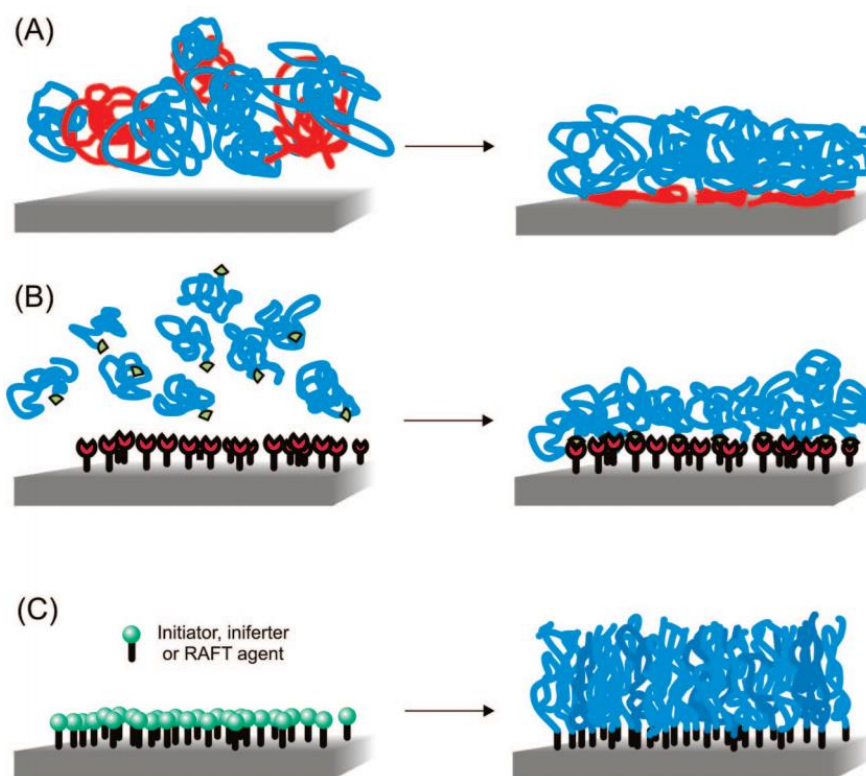
Figure 1.2. Synthetic strategies for the preparation of polymer brushes: (A) physisorption of diblock copolymers *via* preferential adsorption of the red blocks to the surface (grafting to approach); (B) chemisorption *via* reaction of appropriately end-functionalised polymers with complementary functional groups at the substrate surface (grafting to approach); (C) polymer brushes grown *via* surface-initiated polymerisation techniques (grafting from approach).[1]

1.1.3 Atom transfer radical polymerisation (ATRP)

Atom transfer radical polymerisation (ATRP), a living polymerisation technique, has proven particularly performant for the design of well-defined polymeric materials. ATRP is a highly robust and versatile synthetic strategy which enables the preparation of polymers with precisely controlled molecular weight, low dispersities (Mw/Mn<1.1) and diverse functionalities.[21] ATRP technique is particularly suited for the preparation of functional bioactive surfaces, including antibacterial[22, 23], antifouling[24, 25], stimuli

responsive[26-29], micropatterned[30] and biomolecule-coupled surfaces[31]. Also, it has been widely used for the preparation of well-structured functional biomaterials, such as hydrogels[32-36], cationic gene carriers[37-42] and polymer–protein conjugates[43, 44].

1.1.3.1 ATRP mechanism

As is shown in scheme 1.3[21], ATRP is controlled by an equilibrium between propagating radicals and dormant species, predominately in the form of initiating alkyl halides macromolecular species (P_n-X). The dormant species unfrequently react, based on the rate constant of activation (k_{act}), with transition metal complexes in their lower oxidation state, Mt^n/L (Mt^n represents the transition metal species in oxidation state m and L is a ligand). Mt^n/L act as activators to intermittently form growing radicals (P_n*), and deactivators-transition metal complexes in their higher oxidation state, coordinated with halide ligands $X-Mt^{n+1}$/L. The generated radical can then propagate with vinyl monomer (k_p), terminated by either recombination or disproportionation (which ATRP aims to reduce), or be reversibly deactivated (k_{deact}). ATRP is a catalytic process and can be mediated by many redox-active transition metal complexes (CuI/L and X–CuII/L have been the most often used transition metal catlysts, but other studied metals include Ru, Fe, Mo, Os, *etc)* [21, 45-47].

$$\text{Pn-X} + \text{Mt}^n/\text{L} \;\underset{K_{deact}}{\overset{K_{act}}{\rightleftharpoons}}\; \text{Pn*} + \text{X-Mt}^{n+1}/\text{L}$$

$$\left(K_p\right)$$

Monomers   Termination

Mt=transition metal
L=complexing ligand
Pn=polymer chain
X=Br or Cl
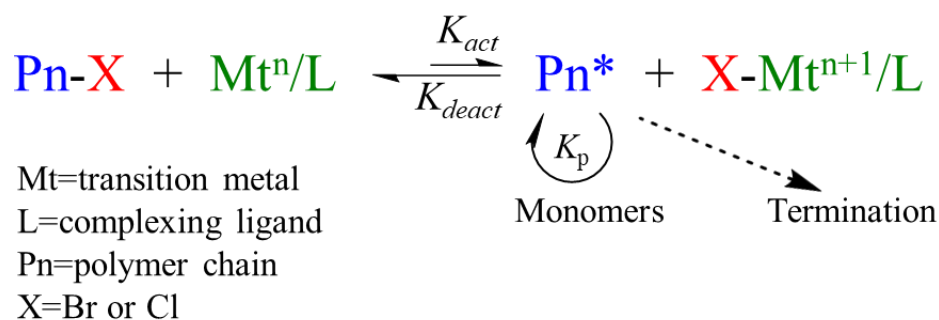
Figure 1.3. The mechanism of transition metal-catalysed ATRP.[21]

1.1.3.2 Factors influencing the rate in ATRP

ATRP depends largely on the equilibrium between the activation process (generation of radicals, k_{act}) and the deactivation process (formation of alkyl halides, k_{deact}) as described above. The equilibrium constants, $K_{ATRP}=k_{act}/k_{deact}$, determines the concentration of radicals and subsequently the rates of polymerisation and termination[48, 49]. Numerous studies have concentrated on measuring k_{act} for polymeric and monomeric and most of the values were obtained under various reaction conditions, such as different temperatures, solvents, *etc*. In addition, initiators and ligands can also strongly affect the ATRP rate constant. The work from Tang *et al.*[49] presented a large set of K_{ATRP} values determined for ATRP using various alkyl halide initiators and Cu catalysts with nitrogen-based ligands and discussed how the structures of the ligands and initiators affect the K_{ATRP} values. They found the activity of the Cu complex decreases as the ligand is changed from Cyclam-B > N4-branched > N4-linear > N3 > N2 (figure 1.4). The ethylene group provides a better linkage than the propylene group for the coordinating nitrogen in the ligand. They also demonstrate that the activity of the initiator decreases as the alkyl group is varied from 3°> 2°> 1°and its R-substituent varied from -CN < -Ph < -C(O)OR > -CH$_3$ (figure 1.5). The activities of alkyl bromide initiators are several times larger than

those of the corresponding chlorides. This work provides guidance for further design of efficient ATRP initiators and ligands.
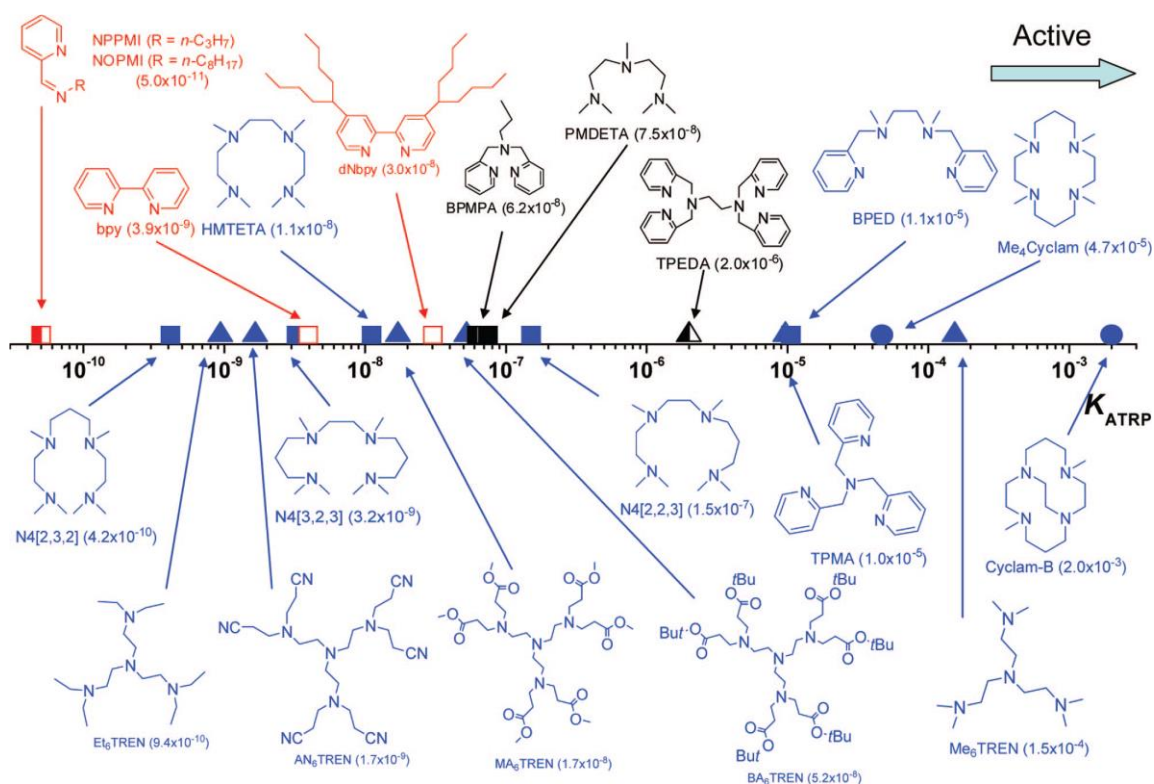
Figure 1.4. ATRP equilibrium constants K_{ATRP} for various N-based ligands with the initiator EtBriB in the presence of CuBr in MeCN at 22°C. Color key: (red) N2; (black) N3 and N6; (blue) N4. Symbol key: (solid) amine/imine; (open) pyridine; (left-half-solid) mixed; (□) linear; (△) branched; (○) cyclic.[49]
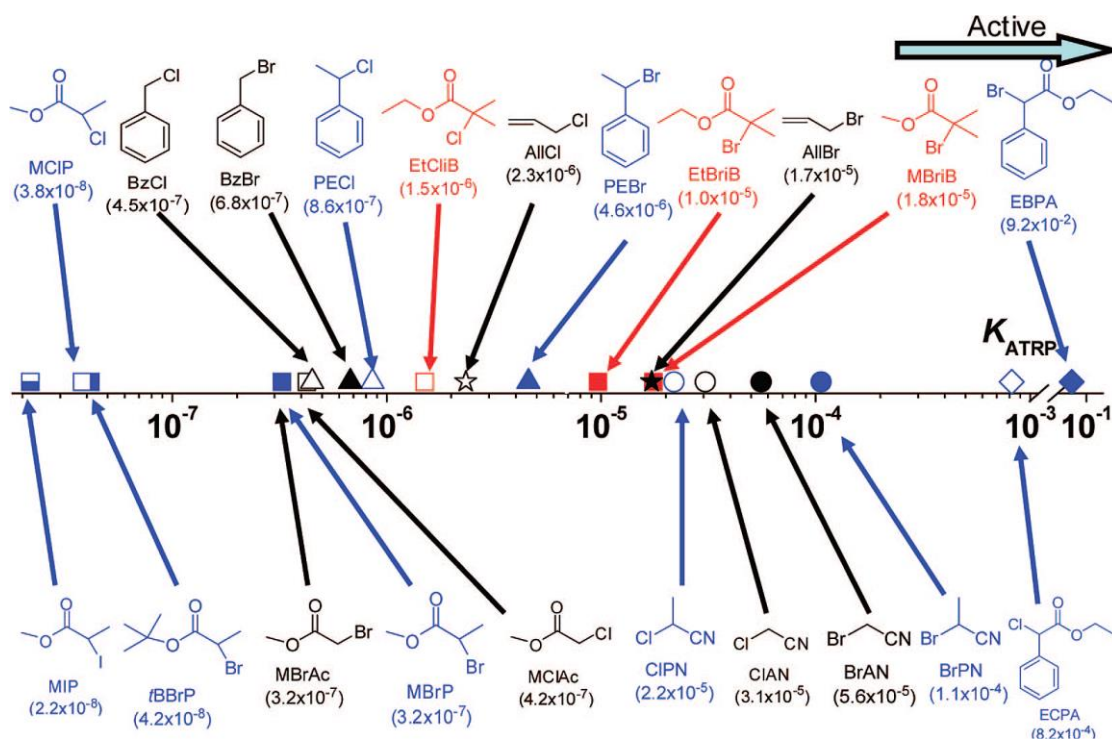
Figure 1.5. ATRP equilibrium constants for various initiators with CuX/TPMA (X=Br, Cl) in MeCN at 22 °C. Colour key: (red) 3°; (blue) 2°; (black) 1°. Symbol key: (solid) R-Br; (open) R-Cl; (bottom-half-solid) R-I; ($\triangle$) phenyl; ($\square$) ester; ($\circ$) nitrile; ($\diamond$) phenyl ester; ($\star$) allyl[49].

1.1.3.3 Macroinitiators (MIs)

Chlorosilane- or alkoxysilane-based small-molecule initiators are commonly synthesised by hydrosilylation using reagents that are highly toxic and flammable (*e.g.,* H_2PtCl_6 and $HSiCl_3$), which makes it hazardous to scale up.[50, 51] Moreover, silane initiators are prone to hydrolysis, making functionalisation of waterborne colloidal substrates somewhat problematic. Macroinitiators can overcome some of the disadvantages of conventional silane-based small-molecule initiators: they can be conveniently synthesised on a gram scale, have excellent chemical stability, and can be rapidly adsorbed onto various surfaces such as silica or metal oxide substrates from aqueous solution at ambient

temperature.[52-56] However, if their adsorption is not controlled, polyelectrolytic macroinitiatiors can produce polymer brushes with significantly lower grafting densities than those grown from silane-based initiators (as evidenced by the slower rate of polymerisation observed from corresponding substrates)[53].

Layer-by-layer (LBL) deposition is a thin film fabrication technique. The films are formed by depositing alternating layers of oppositely charged materials with wash steps in between. Applying LBL technique of both cationic and anionic macroinitiatiors can increase the chain grafting density (Figure 1.6)[53].
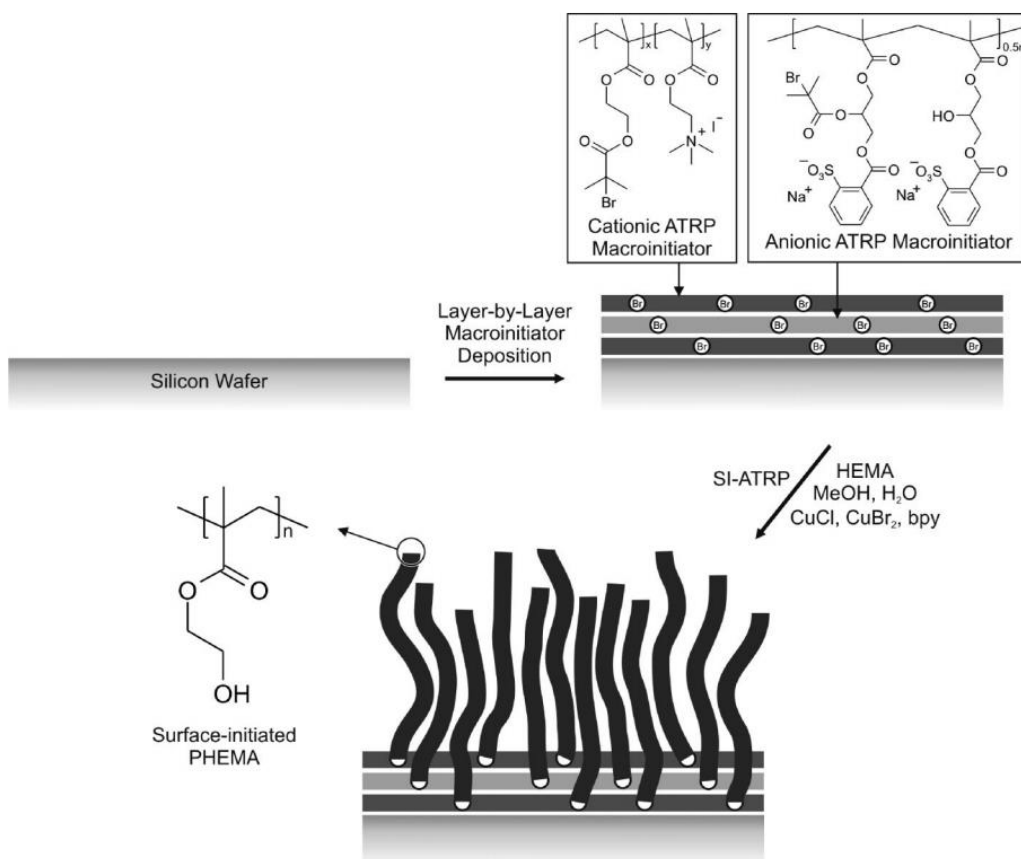
Figure 1.6. LBL electrostatic adsorption of oppositely charged polyelectrolyte macroinitiatiors on oxidised silicon wafers, followed by surface-initiated ATRP of HEMA.[53]

9

The thickness of coatings generated from cationic and anionic macroinitiators layers increased in an approximately linear fashion. And the bromoester initiator density ($\sim$4.9 $\pm$ 0.2 nm^{-2} for a 17-layer macroinitiator) was estimated to be comparable to that calculated for ATRP initiator monolayers obtained by either thiol or silane chemistry.[53] Increasing the number of macroinitiator layers led to a concomitant increase in brush thickness, which is attributed to an increase in the surface initiator density, and leads to more densely grafted brushes.[53] Since many biopolymers (proteins, nucleic acids and DNA) are polyelectrolytes, the LBL are interesting models for biomaterials and it should be worthwhile to study the internal structure of these layers in more detail using different techniques, including for example neutron reflectivity[57] and fluorescence microscopy[58].

1.1.4 Polymer brush responsiveness

The conformation and structure of a polymer brushes can be manipulated *via* a variety of external stimuli, *e.g.* solvent[59], temperature[60-63], pH[64-68], and ions regarding of the different architecture[69, 70] as well as the chemical composition of the polymer chains. These responsive properties potentially allow the development of "smart" surfaces.

1.1.4.1 Solvent

In a good solvent, the contacts between polymer chains and the solvent will be maximised, thus the brushes will tend to swell, while in a poor solvent the brush will collapse in order to reduce the interaction with solvent. This solvent effect highly contributes to the brush conformation. For instance, ABC triblock copolymer PDMS-b-

PS-b-PDMSA was synthesised with a combination of living anionic ring-opening and ATRP and covalently bond to a silicon wafer.[71] Surface properties of the copolymer ultrathin films could be reversibly controlled to present either PS or PDMS segments by treatment with toluene, or a mixture of toluene/hexane as shown in Figure 1.7A.[71] Tapping-mode AFM (Figure 1.7B)[72] observations revealed that the surfaces of brush films immersed in a good solvent for both segments (toluene) and subsequently dried under a stream of nitrogen exhibited fractal morphology characteristic for glassy polymers. In contrast, the surfaces of brush films exposed to toluene/hexane mixtures and dried under nitrogen, were completely featureless. This suggested that, following treatment with the solvent of lower affinity towards PS, "soft" PDMS segments were preferentially segregating to the surface to form a rubbery surface.
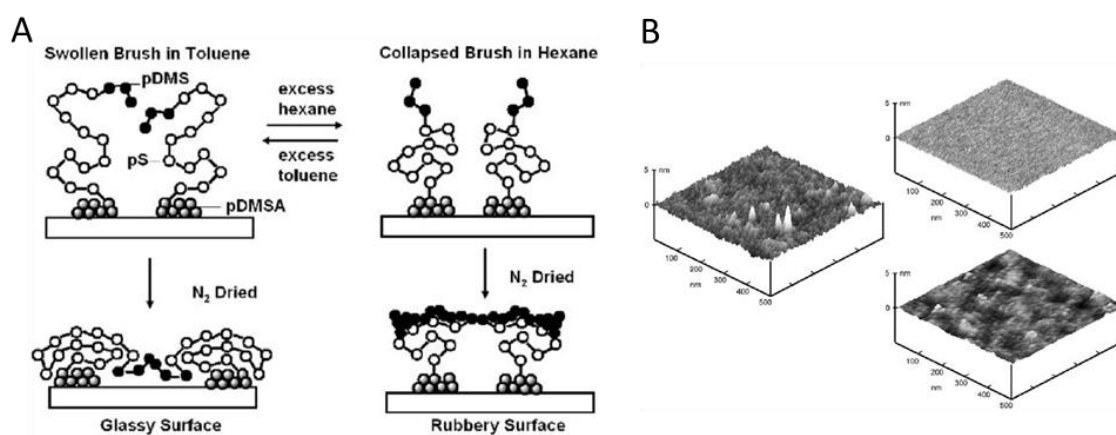
Figure 1.7. A: Scheme illustration of PDMS-b-PS-b-PDMSA triblock polymer brush treated with toluene and gradually adding hexane and drying with nitrogen to form either glassy or rubbery surface; [71] B: Tapping-mode AFM height images of PDMS-b-PS-b-PDMSA brushes after the following treatments. (left) After immersion in toluene and drying with nitrogen; (right) after immersion in toluene, gradual addition of hexane and drying with nitrogen imaged under both ultra-light (top) and normal (bottom) AFM tapping mode.[72]

1.1.4.2 Response to pH

In an acidic environment, hydronium ions (H_3O^+) are abundant, thus, for polyacid brushes, such as poly(acrylic acid) (PAA)[65] and poly(methacrylic acid) (PMAA)[68], the brush will be protonated, which usually renders it hydrophobic and collapsed, excluding water molecules. However, in base, the deprotonated polyacid brush is negatively charged and will swell due to the coulombic repulsion of the negative charges. The pH-response of polybase brushes (e.g. poly((dimethylamino)ethyl methacrylate) (PDMA), poly((diethylamino)ethyl methacrylate) (PDEA), and poly(4-vinylpyridine) (P4VP)) are opposite to that of polyacid brushes; their wet thickness decreases with increasing pH due to deprotonation of the charged side groups, which will also affect the aggregation of the particles when forming brush-particle composition.
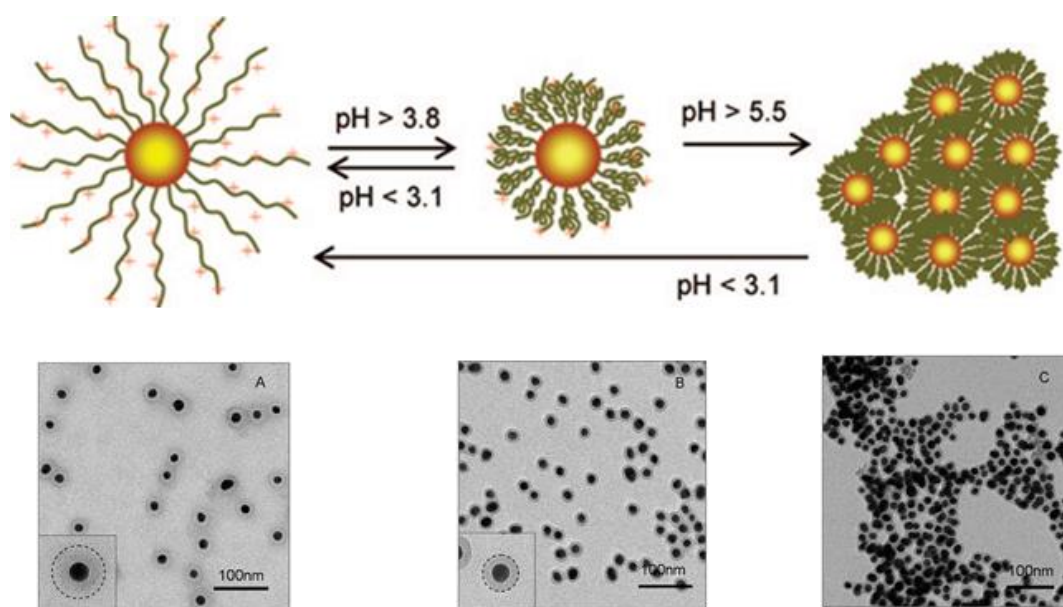
Figure 1.8. pH-responsive morphology changes of the gold/P4VP nanocomposites.[7]

For example, P4VP grafted gold nanoparticles exhibited a two-stage pH responsiveness (Figure 1.8)[73]: at low pH (<3.1), the polymer chains are positively charged due to the formation of pyridinium ions. Hence , hence, water is a good solvent and the polymer chains extend maximally under the electrostatic repulsion, and these highly charged particles are monodisperse in the suspension; at an intermediate pH range (3.8-4.4), the pyridinium groups are readily deprotonated, water becomes a poor solvent, thus the polymer chains are collapsed onto the gold cores, but the whole particles are also monodisperse, this response is reversible due to the protonation/deprotonation process of pyridine groups; while at higher pH (>5.5), the very low concentration of H^+ ions results in a drastic decrease and hence the nanocomposites aggregate.

1.1.4.3 Ionic strength

When a polymer brush is formed from strong or weak polyelectrolyte molecules, electrostatic interactions introduce a rich variety of behavioural regimes.[74] The internal charge fraction of a brush in the osmotic regime has complex dependencies upon the chemical environment. At low salt concentration, negatively charged salt ions may exchange with counterions, which may effectively change the pH of the brush and cause additional swelling. Therefore, the brush tended to swell at low salt concentration before collapsing again in the salted brush regime when increasing the concentration. An example of effect of ionic strength on brush conformation is shown in Figure 1.9[75], displaying a power law increase of thickness with salt concentration of 1/3 for low salt concentration (and −1/3 at high concentration). This is a key piece of experimental evidence for the expected behaviour of weak polyelectrolyte brushes, showing the

transition between the osmotic brush and salted brush regimes, and strongly supports the validity of the proposed scaling theory[75, 76].
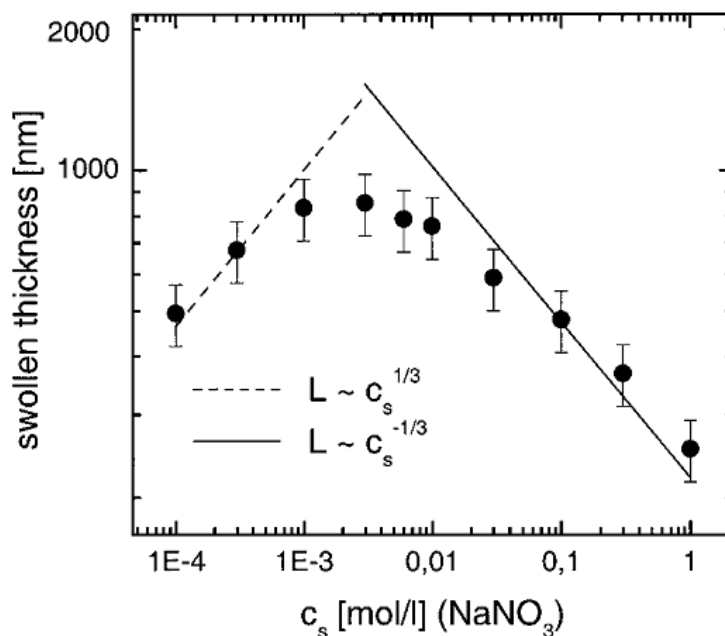
Figure 1.9. Swelling as a function of salt concentration for a weak polyelectrolyte.[75]

1.2 Polymer brush applications in regenerative medicine

Understanding the mechanisms regulating interactions between cells or tissues and the artificial material used as scaffold or substrate is of critical importance to develop new generation of implants and therapeutics for regenerative medicine. Over the last two decades, tuning physicochemical and biological properties of scaffolds and biomimicking substrates to understand and control such cell-interface interactions has received much attention and some of these concepts have been applied to a wide range of applications such as cell culture[77-80,] cell/tissue engineering[81, 82] and drug/gene delivery systems[83-85]. Polymer brushes generated *via* "grafting-from" approach display

interesting features for the design of such biointerfaces[79, 86]. Polymer brushes can be generated *via* several controlled polymerisation techniques as well as a wide variety of initiators for different types of substrates (e.g., silicon, gold, glass, graphene and hydroxyapatite) displaying a broad range of surface chemistry. Importantly, such chemical modification of scaffolds or implants does not alter bulk mechanical properties. The following section will concentrate exclusively on the state-of-the-art of polymer brushes applied in cell culture and as delivery systems.

1.2.1 Protein-resistant polymer brushes for tissue engineering and in vitro assays

Polymer brushes are capable of controlling surface protein absorption and of regulating specific cell behaviors by manipulating a number of important architectural and physicochemical features and the introduction of bioactive moieties or macromolecules. The altered interfaces between material and surrounding cells or a tissue should allow the control of a few behaviors such as cell adhesion, proliferation, spreading, motility, differentiation and recruitment of cells, which are of critical importance for tissue engineering and regenerative medicine.

1.2.1.1 Design of protein-resistant polymer brushes

Protein fouling from physiological fluids (e.g., blood, plasma, and serum) can lead to undesirable effects and failure of implants and devices. Poor control of fouling can result, for example, in the blockage of flow through separation columns and porous membranes[87], the non-specific response of affinity biosensors[88], the reduced circulation

time of nanocarriers in the blood stream due to colloidal instability or opsonization[89, 90], the attachment of bacteria on contact lenses[91] and synthetic implants[92], or the failure of cardiovascular devices *via* thrombus formation[92]. Protein adsorption is considered to be a key factor controlling the interaction between polymeric biomaterials and physiological fluids and affects important secondary interactions such as cell and tissue adhesion or immune response. Therefore, the design of low/anti-fouling surfaces is essential for the development of biosensors and regenerative medicine applications (e.g., protein biomarkers monitoring, biomedical implant coating to prevent biofilm formation and infections).[78]

Due to their ultra/low-fouling ability, resisting both protein and cell adhesion, and good cytocompatibility, poly (ethylene glycol) (PEG)-based materials have been widely studied and used in the biomedical field.[93, 94] However, the various factors controlling the stability of PEGylated surfaces (and the kinetics and thermodynamics of relevant events) are still debated and often not sufficient to protect surfaces from protein adsorption is harsh conditions (in particular undiluted physiological fluids)[95]. Thus, alternative antifouling surfaces are needed. Polymer brushes, with their characteristic high surface density, ease of formation, robustness in a relatively wide range of conditions and versatile architecture and chemistry, have been designed to restrict protein adsorption and some of these coatings display ultralow (<5 ng/cm^{-2}) fouling from defined single protein solution as well as more complex physiological fluids. Brushes based on oligo(ethylene glycol) and zwitterionic side chains are the most classic examples of antifouling polymer brushes, but other structures have been developed, with excellent performance, suggesting that design rules may be different to those

determined for monolayers[96]. Poly(oligo(ethylene glycol) methacrylate) (POEGMA) brushes, with their low fouling properties from fibronectin, lysozyme, BSA, and foetal bovine serum (amongst other proteins and samples tested) were the first protein resistant brush reported in the literature.[97-99] These brushes can be generated from a variety of substrates without compromising protein resistance properties[100], thus can be applied to a wide range of biotechnology platforms and biomedical devices capable of performing in physiological conditions prone to generate high protein fouling[101, 102]. The performance of POEGMA to restrict protein adsorption was correlated to brush properties such as thickness, grafting density and length of the oligo(ethylene glycol) (OEG) side chain.[97, 101, 103]

Poly(hydroxypropyl methacrylamide) (PHPMA) brushes and poly(2-hydroxyethyl methacrylate) (PHEMA) brushes are other neutral brushes displaying excellent protein resistant properties.[104] With the appropriate brush thickness of ~25-45 nm for PHPMA and ~20-45 nm for PHEMA, surfaces can achieve almost zero protein adsorption (<0.3 ng/cm^2, below detection thresholds for techniques such as quartz crystal microbalance (QCM) and surface plasmon resonance (SPR) from single-protein solution.[104] For undiluted human blood serum and plasma, PHEMA brushes with a film thickness of ~20-30 nm adsorb less than 3.5 ng/cm^2 proteins (Figure 1.10, A1), while PHPMA brushes at a film thickness of ~30 nm adsorb more proteins, between ~13.5 and ~50.0 ng/cm^2, respectively (Figure 1.10, A2).[104] However, important differences observed for the protein adsorption from different donors are observed and presumably reflect the important variations observed in blood composition from one patient to another (Figure 1.10, B)[105]. The protein resistance of PHEMA brushes, as for other anti-fouling brushes

was found to be strongly influenced by the grafting density[106]. These studies highlight the importance of size-exclusion effects to prevent the infiltration of proteins through polymer chains and adsorption to the underlying substrate.[106-108] Therefore, providing these brushes do not display strong affinity to proteins, their adsorption should be suppressed.
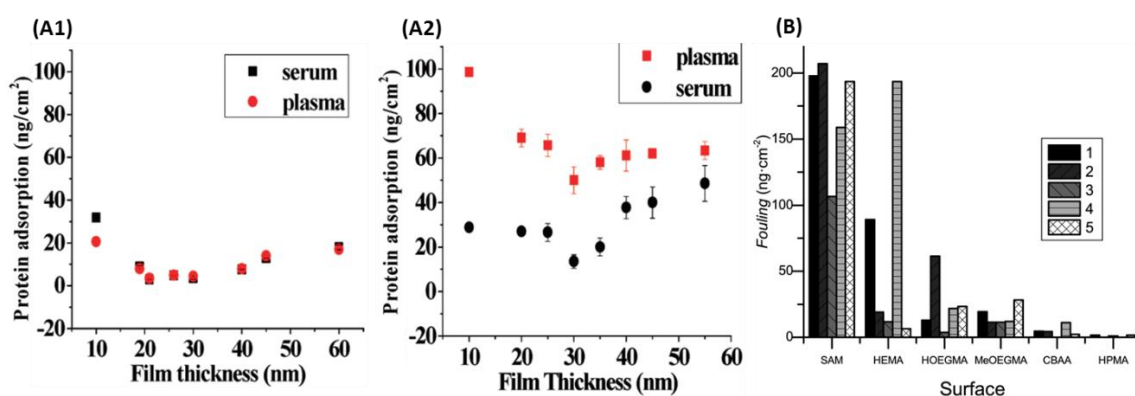
Figure 1.10. Adsorption of undiluted human blood serum and plasma on PHEMA (A1), PHPMA surfaces (A2)[104] and fouling from pooled blood plasmas from five single donors on six surfaces (B)[105], measured by SPR.

A wide range of substrates have been used for polymer brush growth[78]. This has allowed the functionalisation of silicon, gold and other surfaces with POEGMA and PHEMA brushes to control protein fouling at the surface of these materials.[14,22,109] Other materials relevant to the design of biomedical implants have also been coated with polymer brushes. For example, polyester block copolymer brushes (e.g., poly(lactic acid) (PLA), poly(glycolic acid) (PGA) and poly(ε-caprolactone) (PCL) prepared as the first layer and OEG as the outer layer) showed increased resistance to protein adsorption, regardless of decreasing rate of brush degradation.[110] Si-OEG-PGA brushes were found to be relatively more protein resistant compared with both Si-OEG-PLA and Si-OEG-PCL

brushes due to the higher density of grafting observed for the OEG component.[110] The topography of the substrates, for example *via* the introduction of wrinkled morphologies, can also be controlled, depending on the requirement of specific applications, independently of antifouling properties of the coatings (e.g., POEGMA brushes have been successfully grafted from a thermally triggered shape memory elastomers)[111].

Polyelectrolyte brushes, especially polycations, usually have poor biocompatibility due to their high surface charge resulting in significant adsorption of biomolecules and potential toxicity to cells (in particular for positively charged coatings). In contrast to traditional polyelectrolytes, zwitterionic polymer brushes, which have a positively and a negatively charged group associated within the same repeating unit, are reported to display high resistance to nonspecific protein adsorption. In this area, polymer brushes based on carboxybetaine, sulfobetaine and phosphorylcholine have proved particularly successful and performant to restrict protein adsorption, even from undiluted fluids such as serum, blood or plasms.[88, 112, 113] Amino acid-based methacrylate monomers, such as cysteine methacrylate (CysMA) were used to prepare novel zwitterionic PCysMA brushes *via* a facile high-yielding thia-Michael addition and exhibit excellent antibiofouling performance compared to poly(2-(methacryloyloxy)ethyl phosphorylcholine) (PMPC) and POEGMA brushes.[114] Similarly, with brush thicknesses as thin as 11–12 nm, the adsorption to poly(N-4-(2-methacrylamidoethyl)asparagine) (pAspAA) from serum and plasma was reduced to 0.75 and 5.18 ng/cm^2, respectively, and 1.88 and 10.15 ng/cm^2, respectively, for poly(N-5-(2-methacrylamidoethyl)glutamine) (pGluAA).[115] Such adsorption level is comparable to

and perhaps slightly lower than that measured for other amino acid based zwitterionic polymers such as poly(serine methacrylate) and poly(ornithine methacrylamide) under thinner thickness.[116] The peptoid system developed by Lau et al. allowed to conveniently prepare a set of zwitterionic peptoid brushes with defined spatial separations between charged groups and therefore overall charge densities.[117] This allowed to study structure-property relationships controlling the antifouling behavior of brushes. Normally, zwitterionic brushes possess greater swelling at higher ionic strength, which in turn will affect protein adsorption. Ion responsive zwitterionic poly(3-(1-(4-vinylbenzyl)-1H-imidazol-3-ium-3-yl)propane-1-sulfonate) (PVBIPS) brushes displayed high protein absorption in PBS (~145 ng/cm^2), while flowing with 1.0 M NaCl resulted in much lower adsorptions of ~18 and ~0.23 ng/cm^2 for blood plasma and serum, respectively.[118] The enhanced antifouling performance could be attributed to cooperative effects of enhanced surface hydration and electrostatic screening upon increasing the ionic strength of the solution.

Beyond brush thickness, chain flexibility, packing density and architecture, the formation of a stable hydration layer with the brush and associated penetration of water into the coating leads to reduced protein binding, primarily due to the enthalpic stability of the system. Some neutral but non-zwitterionic brushes display such behavior. Poly(hydroxyl propyl methacrylamide) (PHPMAm) brushes indeed displayed excellent antifouling properties despite the presence of two proton donor moieties in the structure of their repeat unit.[96] Similarly, poly(N-acryloylaminoethoxyethanol) (PAAEE) brushes, which integrate three proton donor hydrophilic groups displayed strong hydration and effectively resisted protein adsorption from single-protein solutions and

undiluted human blood plasma and serum (< 0.3 ng/cm^2).[119] Hence strong hydration of polymer brushes was proposed to control the fouling properties of these systems, although this remains to be fully characterised.

1.2.1.2 Cell-resistant polymer brushes

Cells interacting with artificial surfaces typically occurs between extra cellular matrix (ECM) molecules adsorbed on the biomaterial and transmembrane integrin receptors present on the cell surface. In most cases, non-biofouling surfaces may also resist cell adhesion-mediating proteins such as fibronectin, laminin and vitronectin, which will subsequently inhibit cell adhesion. Generally, cell-resistant polymer brushes can be classified into neutral brushes or zwitterionic brushes. POEGMA brushes displayed better cell-resistant properties up to 14 days than oligo(ethylene glycol) self-assembled monolayers (SAMs) which showed resistance to cell adhesion at early time point.[120] It was also found that those with shorter OEG side chain length (4 OEG units) of poly(oligo(ethylene glycol) methyl ether methacrylate) (POEGMEMA) brushes succumbed to 3T3 fibroblast cell fouling (7 weeks) more rapidly than those with longer OEG side chains (23 OEG units for 11 weeks cell resistance) in long-term cell culture study.[121] The underlying mechanism was possibly due to the gradual hydrolysis of the ester bonds linking OEG side chain to methacrylate backbone that would lead to a loss of antifouling moieties and eventually an increase in protein and cell adsorption,[121] which is quite similar to PEG degradation caused antifouling compromise over extended periods of time.[122] Cell adhesion occurred preferentially at low grafting density, namely the mushroom regime, which allowed the adsorption of ECM proteins such as

fibronectin, the while slight or no cell adhesion were observed for denser brushes, the so-called brush regime.[78] The concentrated PAAEE brushes discussed in 2.1.1 highly resist endothelial cells attachment up to 3 days when the film thickness is above 12 nm.[119] Similarly, concentrated polymer brush (CPB, poly(poly(ethylene glycol) methyl ether methacrylate) (PPEGMA), PHEMA, and poly(2-hydroxyethyl acrylate) (PHEA)) showed excellent HUVECs repellency up to 7 days, whilst significant cell adhesion occurred on all the semi-dilute polymer brush (SDPB) samples (Figure 1.11, A).[106]
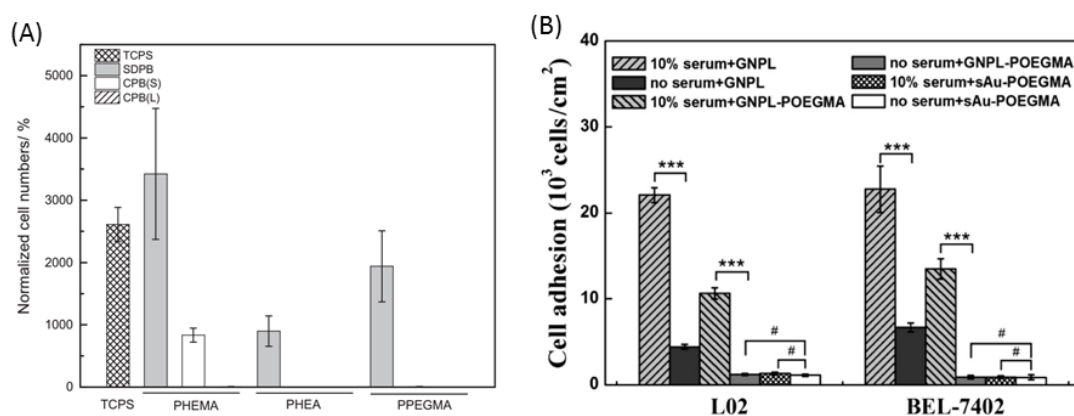
Figure 1.11. Normalised amount of adherent HUVECs on the brushes for 7 days on semi-dilute and concentrated PHEMA, PHEA and PPEGMA brushes (A)[106]; Adhesion of L02 and BEL-7402 cells on GNPL, sAuPOEGMA, and GNPL-POEGMA surfaces with and without FBS (B)[123].

In addition, CPB with higher hydrophilicity (PHEA and PPEGMA brushes) showed better cell-resistant properties than less hydrophilic PHEMA brushes with shorter chain (CPB(S)).[106] Zhang et al.[124] also showed low HUVECs adhesion on poly(2-oxazoline) (POx) polymer brushes with hydrophilic side chains such as poly(2-methyl-2-oxazoline) and poly(2-ethyl-2-oxazoline). Thus, the high grafting density and hydrophilicity of neutral polymer brushes are important to achieve cell repellency and it also allows us to control

the adhesion and spreading of fibroblasts by tuning the grafting density of PHEMA[125] or poly(acrylamide) (PAAm)[126] brushes.

It was also found that cells were more firmly attached to topographical surfaces than those on smooth surfaces. Shi et al.[123] prepared POEGMA brush coated topographical gold nanoparticle layer surfaces (GNPL-POEGMA) and smooth Au surfaces (sAu-POEGMA) by ATRP. It was found that topography promoted L02 and BEL-7402 cell adhesion only in the presence of vitronectin and fibronectin, which could be attributed to the 3D topographical structure of GNPL-POEGMA that adsorbed the minimal amounts of cell adhesive proteins to support initial cell adhesion (Figure 1.11, B).

Zwitterionic polymer brush films such as polysulfonate and polyacrylate-based polymer brushes have been extensively explored as protein resistant and cell-resistant surfaces due to the strong hydration layer formed on the surface. Jiang's group have been reported the effective fouling resistance of zwitterionic polymer brushes such as poly-(sulfobetaine methacrylate) (PSBMA), poly(carboxybetaine methacrylate) (PCBMA) and poly(2-methacryloyloxylethy phosphorylcholine) (PMPC) from pure serum and bacterial adhesion.[127-131]. These brushes have also been studied as ultra-low fouling surfaces restricting or suppressing cell attachment. For instance, PSBMA brush grafted biomedical grade stainless steel (SUS) showed excellent cell-resistant properties for both human MG63 osteoblast and HT1080 fibroblast cells compared with TCP, bare SUS and SUS with dopamine (SUS-D) and silane (SUS-Si) assembly layers up to 24 hours.[132] PMPC brush coated silicon wafers can significantly decrease protein and cell adhesion.[133, 134] Interestingly, Brooks et al.[126, 135, 136] developed novel monomer containing a choline phosphate (CP) head group and 2-(methacryloyloxy)ethyl choline phosphate (MCP), in

which CP has the inverse orientation of PC in the cell membranes and can bind to a variety of cell membranes driven by the unique CP–PC interaction, display protein resistance properties and while simultaneously promote cell adhesion.

1.2.1.3   Patterned anti-fouling brushes for the development of cell-based assays

The exceptional anti-fouling properties of polymer brushes, combined with the relative ease with which initiator molecules can be patterned at the nano- to micro-scale has allowed the development of nano- to micro-engineered platforms for cellular assays.[137-141] In particular the ease which polymer brushes can be micropatterned *via* micro-contact printing has enabled the design of substrates allowing the control of cell shape to study the impact of cell spreading on phenotype. [137, 138, 142,143] Circular adhesive islands with varied diameters (10-50 µm) were generated *via* the patterning of POEGMA brushes and allowed the regulation of keratinocyte spreading and shape.[143] Cells remained rounded on small islands (10-20 µm) and were induced to terminally differentiate, as evidenced by the expression of markers such as involucrin and transglutaminase. In contrast, larger islands (40-50 µm) allowed cells to spread, to remain proliferative and express stem cell markers. In addition, elliptical islands of intermediate sizes (corresponding to the area of 30 µm circular islands) allowed cell stretching along the main axis of the ellipsoid adhesive pattern and resulted in the reorganization of the actin cytoskeleton and decrease in keratinocyte differentiation. Importantly, a direct link was made between the reorganization of the cytoskeleton and the regulation of the activity of the Serum Response Factor *via* the cofactor MAL. Hence cells can sense the geometry of their adhesive environment very directly, *via* the

reorganization of their cytoskeleton and associated changes in the balance of free and polymerised actin. In addition, other physicochemical cues, such as exposure of the cell membrane to negative charges from poly(sulfopropyl methacrylate) (PSPMA) brushes, were found to modulate geometrical cues.[137] Keratinocyte differentiation on Arc-shaped patterns generated with POEGMA and PSBMA remained basal, comparable to that observed for cells spreading on large (50 μm) islands. However, cells spreading on patterns displaying the same shape but generated from negatively charged PSPMA brushes differentiated more frequently. This effect was not observed for large islands in which the cell membrane was not in direct contact with the brush, suggesting that charge repulsions between the negatively charge coating and the cell membrane resulted in the destabilization of the adhesions formed with the patterns. Beyond the study of biophysical processes allowing the regulation of cell phenotype, such micropatterned platforms are powerful tools for the systematic investigation of molecular pathway controlling stem cell fate decision. Hence, keratinocyte microarrays were used to identify the impact of histone acetylation on differentiation.[144] Further analysis of the shape of single cells spreading on micropatterns also highlighted important changes in nuclear morphology, depending on the shape and size of the micropattern.[145] This assay was further used to study the impact of the keratin network in regulating nuclear shape. It was found that the keratin network plays an important role in nuclear mechanotransduction and in defining nuclear size and shape, in addition to the actin cytoskeleton. Another approach to pattern polymer brushes is based on a photo-triggered conjugation strategy. POEGMA patterns were precisely controlled by combining the highly efficient nitrile imine-mediated tetrazole-ene cycloadditions (NITEC) conjugation with the versatility of bioinspired poly(dopamine) (PDA).[146]

Subsequently, rat embryonic fibroblasts (REFs) perfectly followed the pattern focal adhesions (evidenced by VASP and paxillin) selectively controlled at the non-irradiated regions, while cells were absent from patterned POEGMA brushes (Figure 1.12). Thus, patterned anti-fouling polymer brushes allow the study of the cross-talks and synergies between geometrical adhesive cues and physicochemical surface properties of polymer brushes on cell fate decision.
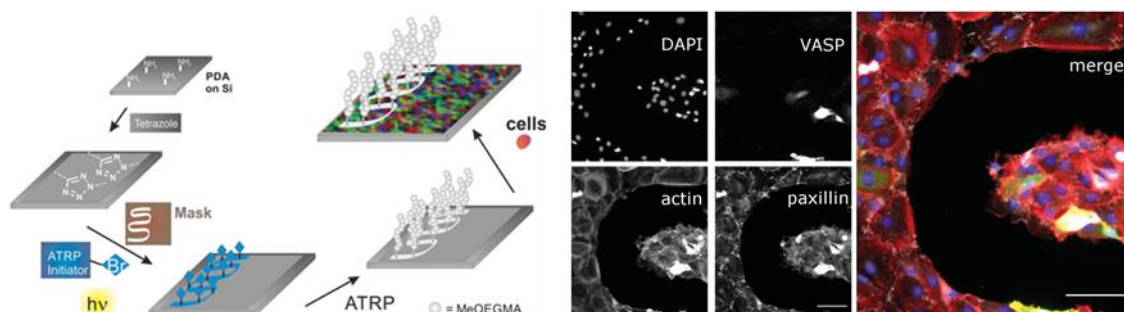
Figure 1.12. Surface patterning of POEGMA brushes on PDA films functionalised with a photoactive tetrazole (left); Images of fixed cells adhering between areas photopatterned with POEGMA brushes (right).[146]

In addition to the simple control of single cell shape and spreading, micropatterns can also allow the formation of cell clusters with defined sizes, shape and geometry of adhesion. POEGMA-functionalised brushes were used to pattern 100 µm adhesive islands to which 5-10 keratinocyte clusters adhered (Figure 1.13).[140] The cell assemblies generated were then found to segregate on different locations of the pattern, depending on their fate: differentiated cells were found in the centre of clusters whereas stem cells remained at the periphery. In addition, this process was affected by the geometry of the adhesive islands. Micro-rings in which a portion of the adhesive landscape was replaced by POEGMA brushes allowed stem cells to initially partition at

the periphery of the ring but allowed differentiated cells to migrate into the centre of the clusters, overlapping with non-adhesive areas. This was allowed by the competitive interactions and differential adhesion of differentiated cells and stem cells, which typically express different levels of proteins sustaining cell-matrix and cell-cell adhesions (i.e. integrins and cadherins). This platform was used to study the role of different adhesive proteins in establishing the compartmentalised structured of the micro-epidermis generated.

In addition, similar micro-arrays were used to control and study processes occurring during wound healing.[138] Cells were patterned into large clusters (400 μm) surrounded by a POEGMA coating. The brush was functionalised with alkene or alkyne moieties in order to allow the coupling of peptide sequences *via* thiol-ene chemistry.[142] This enabled the activation of the brush chemistry after cell seeding and formation of clusters, *via* a short photo-triggered reaction, in buffered conditions. When RGD was coupled to brushes surrounding cell clusters, they migrated out of the original pattern in a peptide-density dependent manner. Similarly, when RGE was used instead, cells were unable to escape the pattern. Such platform can therefore allow the systematic study of the impact of wound geometry and size as well as some of the biochemistry of the wound bed on processes mimicking wound healing. More generally, micro-arrays based on polymer brushes, and their exceptional stability over prolonged periods of cell culture, offer exciting opportunities for the study of processes, proteins and genes involved in controlling cell and tissue function, *in vitro* and in a human context.
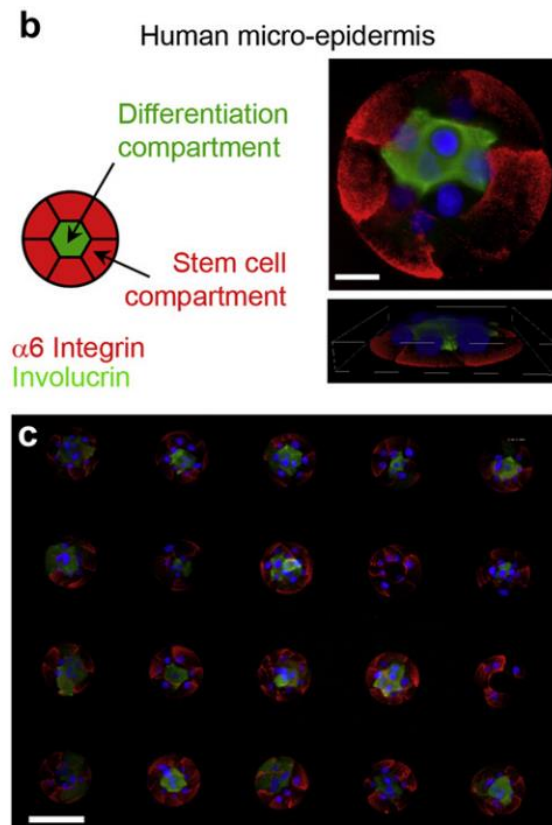
Figure 1.13. Probing the level of cell differentiation and the respective positioning of stem cells and differentiated cells using arrays of cell clusters.[140]

Polymer brushes have also been used to control the geometry of cell adhesions at the nanoscale[147]. Colloidal lithography was used to generate nanopatterns of gold discs (100 – 3000 nm) surrounded by a glass background.[148] The surface of the glass was subsequently functionalised with polymer brushes (generated *via* grafting to, as in poly(L-lysine) (PLL)-g-PEG, or *via* a grafting from approach with POEGMA, for improved protein resistance and control of adhesion size and geometry). The resulting patterns allowed the selective deposition of extra-cellular matrix proteins such as fibronectin to the gold nano-islands, which in turn restricted the size of single adhesions. This platform allowed to study the role of the geometrical maturation of adhesions on cell spreading. Focal adhesions, largely responsible for cell spreading on 2D and quasi-2D interfaces,

are indeed micron-sized complexes of proteins that link integrins and the extra-cellular matrix to the cytoskeleton. However, they arise from nascent adhesions, consisting of few (4-5) integrins clustered together that mature in size and shape. The nanopatterns generated allowed to block this process at different stages and allowed to highlight that protein recruitment was not impaired but that the stability and dynamics of proteins recruited at the adhesion was strengthened as their size matured. This in turns allowed the establishment of a more stable cytoskeleton, cell spreading and the control of fate decision.

1.2.2 Polymer brushes as delivery systems

Polymer brushes are attractive in the field of designing effective vectors for drug/gene delivery. These systems offer the ability to load drugs into carriers or covalently link the drugs to the polymer chains and trigger drug release in diseased tissue *via* external stimulation such as changes in local temperature or pH as well as the controlled degradation by cell-released enzymes. Polymer brushes facilitate the design and coating of a variety of particles such as gold, magnetic, silica nanoparticles and cellulose nanocrystals with well-defined core-shell architecture and chemistry. Cationic polymer brushes are also promising vectors and carriers for gene delivery applications.

1.2.2.1 Polymer brushes in drug delivery

Two important limitations for the delivery of conventional low molecular weight drugs are poor water solubility of hydrophobic compounds and systemic toxicity.[149-151] To tackle these issues, targeted drug delivery systems have been extensively explored as

effective means to deliver therapeutics to cells. Polymer-based drug delivery systems specifically targeting tissues or cells are particularly attractive for *in vivo* treatment of diseases. Indeed, they offer the possibility to load drugs into a carrier (typical examples include micelles and vesicles based on amphiphilic copolymers, dendrimers and cross-linked microgels/nanogels) or covalently link the drugs to the polymer (e.g. polymer–protein conjugates, polymer–drug conjugate) before functionalizing the resulting loaded carriers with specific ligands, recognised by receptors expressed at the surface of the targeted cells (e.g., cancer cells, brain endothelial cells etc.).[152-154] Another important aspect to take in consideration when designing polymeric carriers is the release mechanism, selectively when reaching the target site. Drug release can occur either due to vehicle disassembly or *via* passive diffusion of physically encapsulated drugs.[155, 156] For covalently linked drugs, conjugation chemistries such as pH sensitive linkage, enzyme-cleavable linkage and peptide-based linkage have been employed to trigger drug release in diseased tissue (e.g. in cancer).[157] Although brushes have a relatively low capacity to encapsulate and protect drugs for the delivery of therapeutics, owing to their relatively low thickness, some systems based on these coatings have been explored for drug delivery applications.

Thermo-responsive polymer brush-functionalised nanoparticles were explored as a potential drug delivery system. This approach is attractive in that it provides a reaction-free interior for loading of drugs. Copolymer brushes P(OEGMA-co-MEO$_2$MA) grafted single-walled carbon nanotubes (SWCNTs) exhibited LCST-dependent Rhodamine 6G loading and release properties.[158] During the Rh6G-loading process, below the LCST, brush chains were extended, thus the Rh6g could be easily adsorbed on

SWCNT@P(OEGMA-co-MEO$_2$MA), whereas above the LCST, the collapsed brush chains were able to retain some of the molecules. The thermally-controllable Rh6G release was confirmed *via* UV-vis spectroscopy and demonstrated that release rates of Rh6G below the LCSTs were faster than those above the LCST. Yavuz et al. anchored densely packed poly(N-isopropylacrylamide)-co-poly(acrylamide) (PNIPAAm-co-PAAm) copolymer brushes to Au nanocages to trigger the release of doxorubicin and lysozyme with a near-infrared laser by means of the photothermal effect (Figure 1.14).[83] The polymer chains collapsed above the LCST, opening the pores of the cage and thus releasing the loaded molecules. When the laser is turned off, the local temperature dropped and polymer chains relaxed back to their extended state, closing the cage and blocking any further release.[159] In combination with its high spatial and temporal resolution, this system is well suited for *in vivo* studies, owing to the high transparency of soft tissue in the near-infrared region. Similarly, drug release can also be triggered by heat generated by high-intensity focused ultrasound (HIFU), which can penetrate more deeply into soft tissue.[160] In addition, negatively charged poly(3-sulfopropyl methacrylate) (PSPMA) brushes were grafted on hollow silica nanoparticles (HSNPs) with dual functions of hydration lubrication and drug delivery. In aqueous conditions, aspirin can be released *via* the pores of HSNPs, due to the swelling of the hydrophilic, charged PSPMA brushes. This strategy is a promising approach for the design of injectable joint lubricant fluids for simultaneous lubrication and treatment.[161]
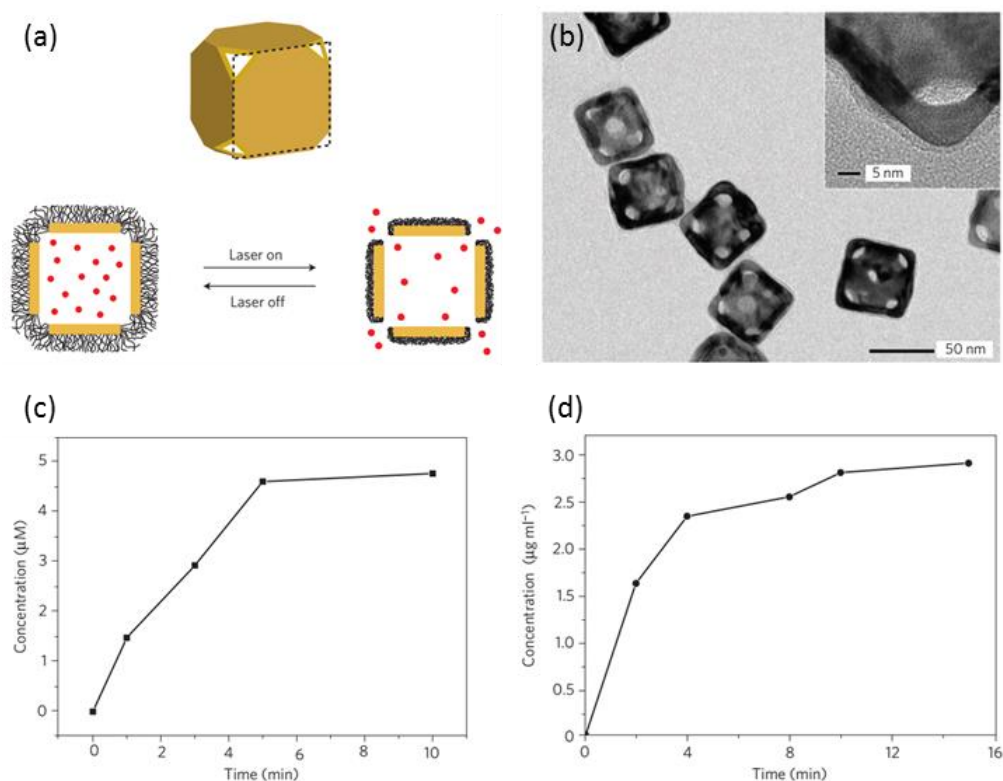
Figure 1.14. (a) Illustration of near-infrared laser triggered drug release of PNIPAAm-co-PAAm copolymer brushes coated Au nanocages; (b) TEM images of Au nanocages covered by copolymer brushes; a plot of the concentrations of Dox (c) and lysozyme (d) released from the Au nanocages.[83]

Other stimuli-triggered drug delivery systems include pH-sensitive polymer brush coatings.[85, 162-165] For instance, poly(4-vinyl pyridine) brush functionalised silica particles enabled the load of $[Ru(bipy)_3]Cl_2$ and calcein at high pH, at which PVP brushes were deprotonated and exhibited a hydrophobic collapsed morphology. At low pH, PVP brushes were permeable to molecule transport, leading to the pH-controlled release.[165] Introducing a biocompatible POEGMA layer after a poly(2-(diethylamino)-ethyl methacrylate) (PDEAEMA) polymer shell was found to reduce the toxicity of PDEAEMA-b-POEGMA copolymer brush-grafted silica nanotube, whist not affecting the pH controlled release of doxorubicin.[166] In addition, the incorporation of multiple stimuli

responsive moieties can greatly expand the application scope of functional polymer brush coatings in drug delivery systems. Zhang *et al*[85] developed a pH, reduction and light triple responsive drug delivery system based on PDEAEMA brush modified hollow mesoporous silica nanoparticles which were considered for potential scaffoldings in drug/gene delivery due to their good biocompatibility and large pore volume[167-169]. This design allowed higher DOX loading to be achieved and the resulting particles displayed excellent stability during blood circulation. In the presence of a reducing agent or in an acidic environment, as well as external UV irradiation.[85] As a result of the reversible opening and closure of the mesopores by PDEAEMA brushes, drugs were efficiently loaded, under mild conditions.[85]

Besides non-covalent drug loading and release approaches, bioconjugates of such polymer brush delivery systems with proteins and targeting molecules have also been designed.[170-173] Poly(methacrylic acid) (PMAA) was identified as a suitable candidate as its carboxylic groups can stabilise nanoparticles in water at physiological conditions and sequentially can be be further functionalised with targeting moieties. Phenylboronic acid (PBA) grafted PMAA *via* SI-ATRP on gold nanoshells (AuNSs) showed saccharide-sensitivity for controlled release of diol derivatives.[172]

Protein resistant polymer brushes may also be used to systematically investigate the pharmacokinetics of particles[170] in drug delivery or imaging applications, in particular if combined with targeting strategies. For example, lanthanide-doped upconversion nanoparticles (UCNPs) nanoparticles with a POEGMA shell functionalised with Concanavalin A were used for targeting and fluorescence imaging of cancer cells *in vitro* and tumors *in vivo*.[171]

1.2.2.2 Polymer brushes in gene delivery

Over the past decade, Gene therapy has shown much promise in therapies for various genetic diseases and cancers, such as immunodeficiency[174-177], cystic fibrosis[178, 179], and Parkinson's disease[180-183], also to be used as an alternative method to traditional chemotherapy used in treating cancers.

1.2.2.2.1 Mechanism and obstacles of gene delivery

Gene delivery is the process of delivering genetic-based materials (e.g., DNA or RNA) into host cells for applications such as genetic research or gene therapy. It is an important and necessary step in gene therapy for the introduction or silencing of a gene to promote therapeutic outcomes in patients. A critical part of gene delivery involves different delivery mechanism, most often, DNA is transported to the nucleus and RNA to the cytoplasm. The process of DNA transfection is complex and imposes challenges and demands on the delivery system, to overcome numerous extra- and intracellular obstacles to obtain decent transfection (Figure 1.15)[184-187].
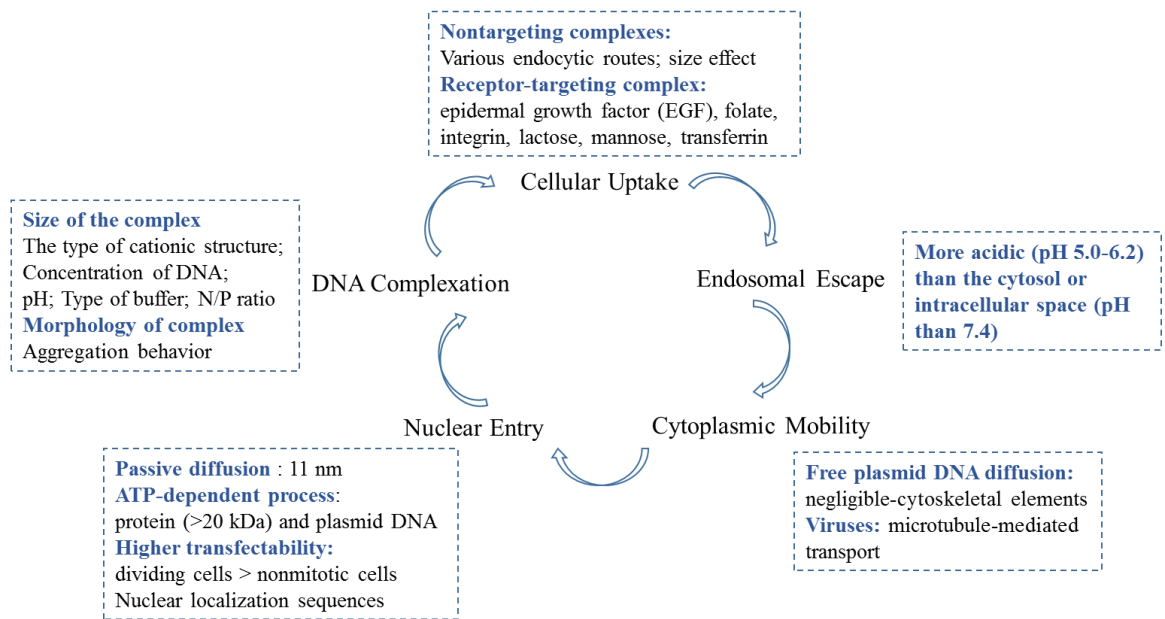
Figure 1.15. Extra- and intracellular obstacles in gene transfection.

The mechanism of RNA interference (RNAi) consists in two main stages: post-transcriptional gene silencing and transcriptional gene silencing. More specifically, endogenous double stranded RNA is identified by a ribonuclease protein called dicer, which cleaves it into 22-nucleotide (nt) pieces with 2-nt overhangs on the 3' ends (Figure 1.16).[188] These fragments are loaded into the RNA-induced silencing complex (RISC), subsequently, the guide strand is directed to the target mRNA, which is cleaved by the cleavage enzyme argonaute-2 into small pieces.[188] Thus, the process of mRNA translation can be interrupted by transporting short interfering RNA (siRNA) to the site of action in the cells of target tissues. A summary of the processes is shown in Figure 1.16.[188]
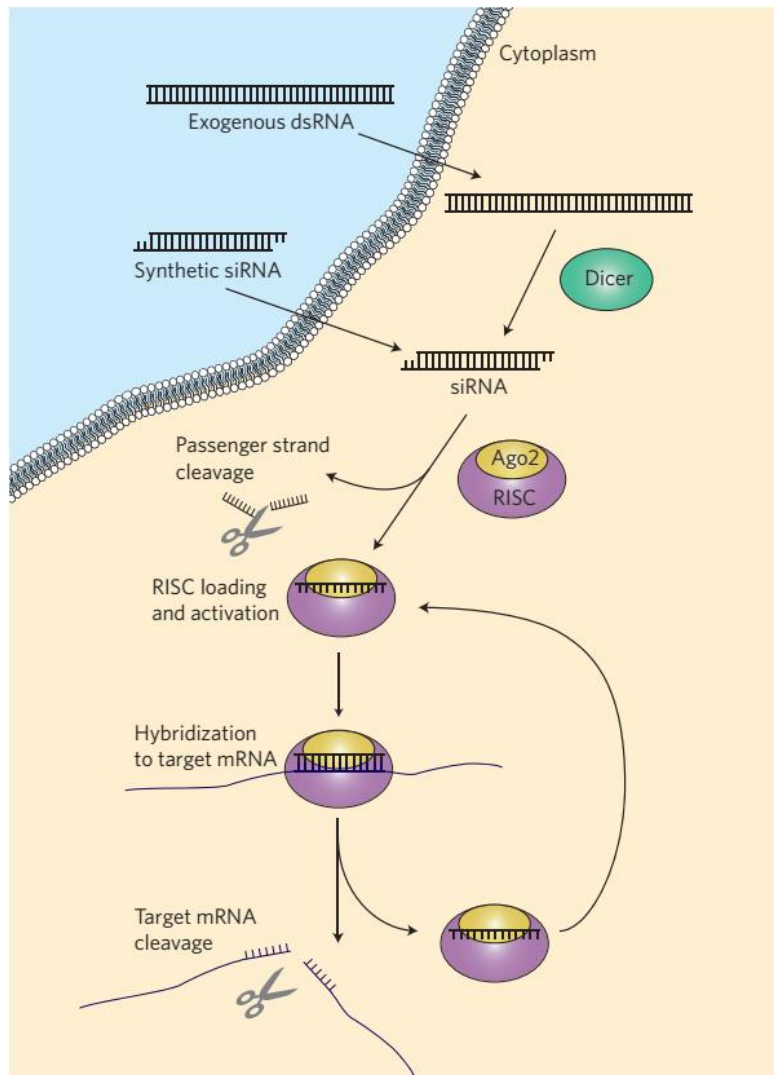
Figure 1.16. Mechanism of RNA interference.[188]

1.2.2.2.2 Non-viral gene delivery vectors

For efficient gene therapy, a gene carrier or vector is needed to escort negatively charged nucleic acids through cell membranes. The most challenging task in gene therapy is the design of gene delivery vectors with low cytotoxicity and high transfection efficiency[189-192]. Initial research efforts focused on the use of viral carriers, which showed high efficiency at delivering. However, numerous safety issues related with the use of viruses, such as immunogenicity and mutation of the host genome, encouraged

the investigation of non-viral vector delivery system. The commonly used nonviral

vector systems in gene delivery, including cationic lipsome[193], dendrimers[194-196], cationic

polymers[197-200], polypeptides[201-203] and nanoparticles[204-206] (Figure 1.17).

Cationic liposomes

DOTMA (Lipofectin™)
DOSPA (LipofectAMINE™)
DOGS (Transfectam ®)

Polypeptide

Tat-Based Peptides
Antennapedia Homeodomain Peptide
MPG Peptide
Transportan Peptide

Dendrimers

Polyamidoamine Dendrimers (PAMAM)
Poly(propylenimine) Dendrimers (PPI)
Poly(L-lysine) Dendrimers
Phosphorus-Containing Dendrimers
Carbosilane Dendrimers

Nanoparticles

Quantum Dots
Gold Nanoparticles
Silica Nanoparticles
Carbon Nanotubes
Lipid-Based Nanoparticles
Polymeric Hydrogels

Cationic polymers

Poly(L-lysine) (PLL)
Polyethylenimine (PEI)
Polymethacrylate
Carbohydrate-Based Polymers
Linear Poly(amido-amine) (PAA)
Biodegradable Polymers

Figure 1.17. Non-viral vectors for gene delivery.

The main requirements for a non-viral vector are: 1, good solubility in water/water

miscible solvents; 2, low toxicity; 3, high gene delivery efficiency; 4, ease of endosomal

escape; 5, appropriate degradation rate. Cationic polymers and lipids, the two main

types of non-viral gene delivery vectors, display low host immunogenicity and high

flexibility allowing the condensation of negatively charged nuclear acid into nano sized

particles through electrostatic interactions.

A great number of polycations, including polyethylenimine (PEI)[207], poly((2-dimethyl

amino)ethyl methacrylate) (PDMAEMA)[208, 209], poly(l-lysine) (PLL) and polyamidoamine

(PAAM), have been reported to be capable of delivering genes. Among these cationic

polymers, PEI homopolymers are widely used as gene carriers. Owing to its high

transfection efficiency branched PEI with a molecular weight of 25 kDa is considered to be the "gold standard" for polymeric non-viral vectors, however, at physiological pH, only 25 % of the amine groups are protonated with the cytotoxic (IC50 = ~ 30 µg/ml)[210].

1.2.2.2.3 'Grafted from' cationic polymer brush-based gene delivery vectors

Recently, polymer brushes have been widely employed for the design of new polymeric gene vectors as they allow the design and coating of a variety of particles such as nanodiamond, gold, iron oxide, silica nanoparticles and cellulose nanocrystals, with well-defined core−shell architecture and chemistry and hence are of high interest as vectors and carriers for gene delivery. The cationic monomers involved in ATRP synthesis of gene vectors include 2-(dimethylamino)ethylmethacrylate (DMAEMA), (2-hydroxy-3-(2-aminoethyl)amino)propyl methacrylate (HAEAPMA), 2-(diethylamino)ethyl methacrylate (DEAEMA), N-(3-(dimethylamino)propyl) methacrylamide (DMAPMAA), 2-(diisopropylamino)ethyl methacrylate (DPAEMA), (2-(methacryloyloxy)ethyl) trimethyl ammonium chloride (MeDMA), N-tert-butoxycarbonyl-aminoethyl methacrylate (Boc-AEMA) and N,N_-di-(tert-butoxycarbonyl)-2-(2-aminoethylamino)ethyl methacrylate (Boc-AEAEMA) (Figure 1.18)[211, 212].
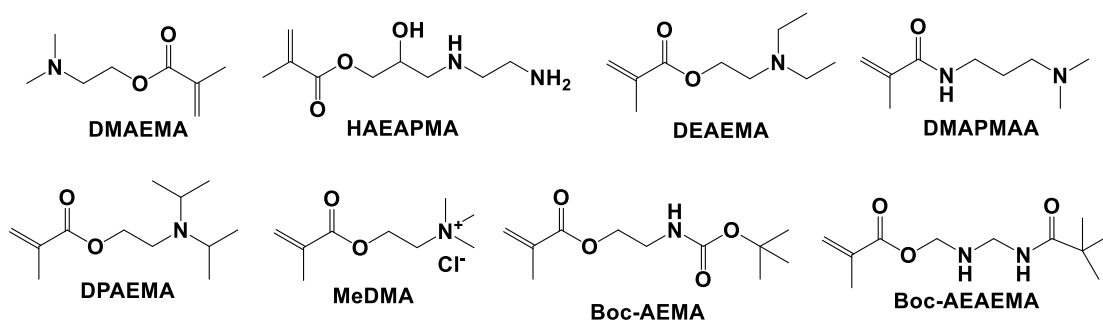
Figure 1.18. Cationic monomers involved in ATRP synthesis of gene vectors[211, 212].

Among all the monomers, DMAEMA is a monomer unit bearing a tertiary amine weak base with a pK of 7.5, falling within the range for optimal transfection. Also, PDMAEMA with controlled molecular weights, well-defined chain ends, and in different macromolecular architectures (such as block, star, and graft) could be easily made through ATRP[213-215].

PDMAEMA brushes grafted nanodiamaonds were able to condense plasmid DNA into stable nanoparticles and protect DNA from enzymatic degradation.[198] The use of magnetic particles as cores to grow cationic brushes allows the delivery of gene as well as magnetic cell separation and MRI imaging.[208, 216, 217] For example, ATRP initiators bearing a dopamine group were deposited on oleic acid stabilised superparamagnetic maghemite nanoparticles (γ-Fe$_2$O$_3$), *via* ligand exchange, to prepare PDMAEMA brush functionalised γ-Fe$_2$O$_3$ (γ-Fe$_2$O$_3$@PDMAEMA), which showed 2-fold increase in transfection efficiency of CHO-K1 cells without increasing cytotoxicity, as compared to polyethyleneimine (PEI). Transfected cells were selectively isolated using a magnet (Figure 1.19).[216] Similarly, also using magnetic sorting, PDMAEMA-bound iron oxide/pDNA magnetoplexes exhibited remarkably improved gene expression efficiency in the presence of 10% FBS compared to the commercial control, PolyMag/pDNA.[217] Due

to its biocompatibility and unique conjugated structure and ease of surface functionalization, graphene oxide has also been developed as efficient gene delivery system. Graphene sheets were functionalised with PDMAEMA brushes (SS–GPDs) *via* ATRP. The resulting nanosheets were found to display increase gene transfection efficiencies and lower cytotoxicity compared to the corresponding PDMAEMA homopolymers. In addition, the disulfide linkage between PDMAEMA chains and the graphene sheet allowed their cleavage under mild reductive conditions.[218] Transfection efficiencies with such SS–GPDs were affected by the chain length of PDMAEMA brushes and increased even at lower N/P ratios with longer PDMAEMA chains.[218] Other types of nanomaterials presenting surface hydroxyl groups such as layered double hydroxides (LDHs) were also shown to display efficient gene delivery properties after functionalization with cationic brushes.[219]
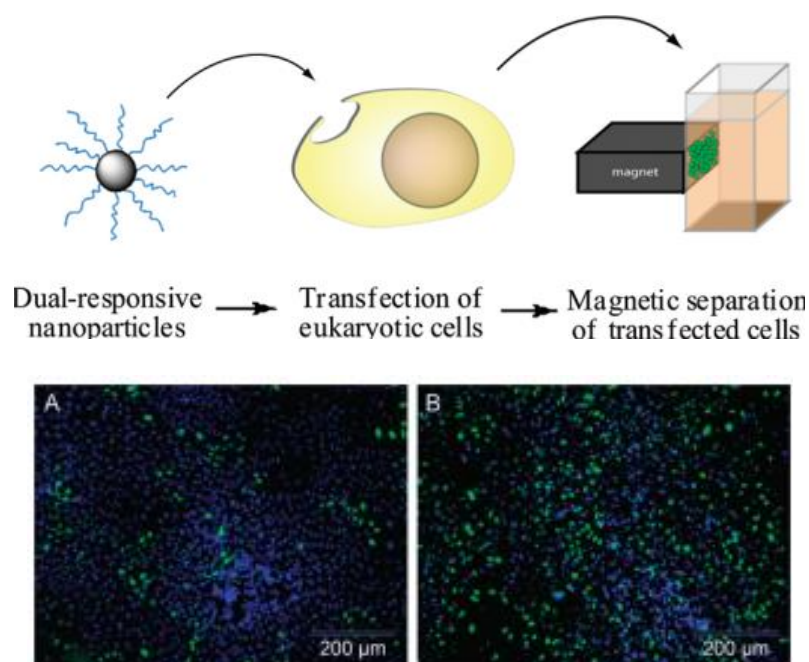
Figure 1.19. γ-Fe$_2$O$_3$@PDMAEMA (B) for transfection CHO-K1 cells compared to PEI (A).[216]

The morphology and geometry of polymer brush-functionalised vectors was also found to impact the transfection efficiency.[84, 220] Thus, a series of gene vectors based on PDMAEMA brush-functionalised Au nanoparticles (including Au nanospheres, Au nano-octahedra (Au NOs), arrow-headed Au nanorods (Au AHNRs), and Au nanorods with different aspect ratios (Au NRs and Au LNRs)) were designed to investigate the impact of morphology on gene transfection (Figure 1.20).[84] It was found that Au nanosphere-based carriers exhibited the poorest performance, whilst particles with sharper morphologies such as arrow-headed Au nanorods were the most efficient. In addition, Au nanorods with smaller aspect ratios perform better than longer ones.[84]
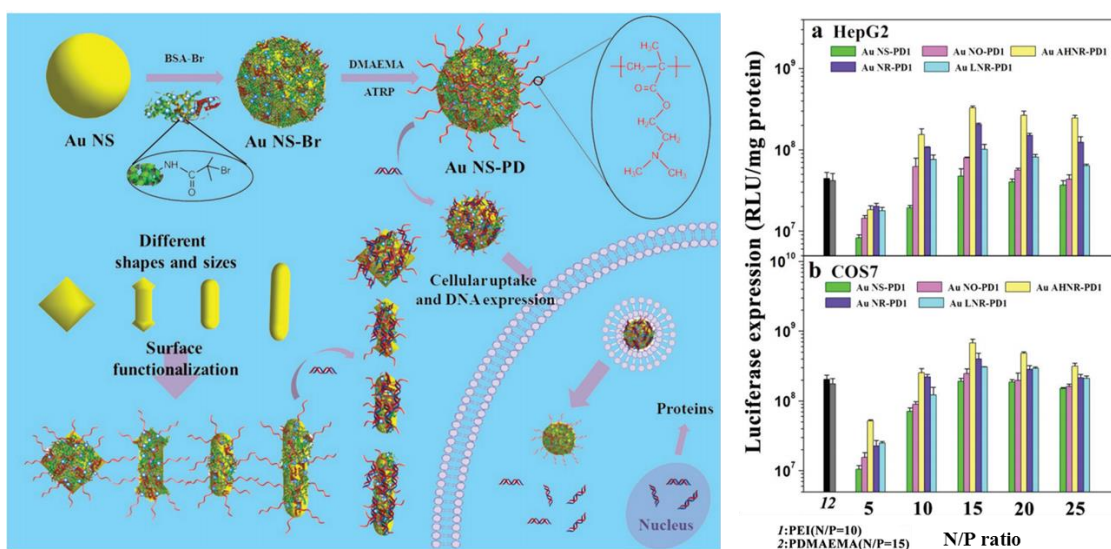
Figure 1.20. PDMAEMA-functionalised Au NPs generated *via* ATRP (Left). Transfection efficiencies (luciferase assay) measured for a range of Au NP-PD/pDNA complexes at various N/P ratios, in COS7 and HepG2 cell lines.[84]

Other types of elongated nanomaterials were also found to display efficient gene delivery properties. Spindly cellulose nanocrystals (CNCs) coated with PDMAEMA and Poly(poly(ethylene glycol)ethyl ether methacrylate) (PPEGEEMA) brushes were

prepared as novel non-spherical gene carriers. The cationic PDMAEMA chains condensed genes effectively with uncharged PPEGEEMA brushes spread outwards and reduce the cytotoxicity significantly.[221] Similar types of morphologies were also found to affect gene transfection in the silica-based nanomaterials. Hollow nanosphere-based vectors exhibited improved gene transfections compared to their solid counterparts.[220]

1.3 Summary and project overview

Polymer brushes have emerged as an attractive surface modification tool offering chemical stability, synthetic flexibility and unprecedented control over the polymer grafting density, thickness, chemical composition and functionality. Surface modification strategies of polymer brushes have proved particularly versatile and have been applied to a wide range of biomedical fields, including cell culture, tissue engineering and as delivery systems. The controlled physicochemical and biological properties enabled by the combination of polymer brush architecture and chemistry enable an exquisite control of interfacial properties and demonstrate their ability to mimic some of the properties and functions of natural ECM. These interfaces also allow the study of complex biological behaviors by simultaneously controlling protein resistance properties, cell adhesion/detachment *et al*. This offers interesting opportunities for the study of mechanisms controlling cell adhesion and phenotype at such interfaces and may result in novel concepts in biomaterials design. In addition, the combination of polymer brushes with nanotechnology has already shown its potential for applications in drug/gene delivery, *via* the precise design of brush chemistry, charge and architecture for controlled drug/gene encapsulation and release. Nanotechnologies

based on these coatings would provide increased basic understandings and the development of novel systems for the regenerative medicine and drug/gene delivery where finely tuned interfaces and associated physicochemical properties are required.

This project focuses on designing safe and efficient gene delivery vectors based on 'graft from' cationic polymer brush and understanding the interaction of nucleic acids with polymer brush. Briefly, cationic polymer brushes will be prepared both on flat surfaces (*e.g.* silicon wafer and gold surface) and particles. The interaction of polymer brushes and nucleic acid materials will be systematically investigated. Finally, cationic polymer brush-based gene delivery vectors will be prepared and applied to delivering nucleic acid materials of interest (Figure 1.21).
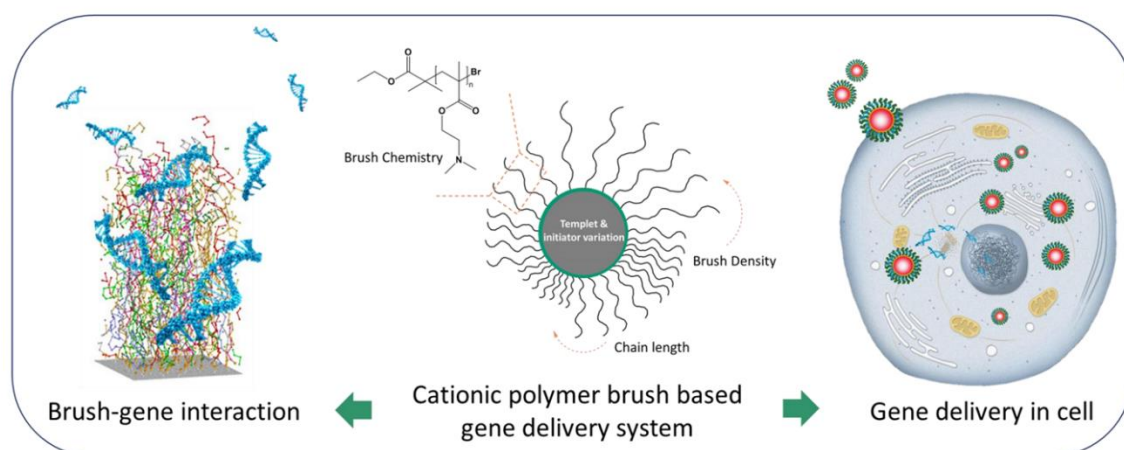

Figure 1.21. Overview of the project.

References

(1) Barbey, R.; Lavanant, L.; Paripovic, D.; Schuwer, N.; Sugnaux, C.; Tugulu, S.; Klok, H. A., *Chemical Reviews* **2009,** *109* (11), 5437-5527.

(2) Ruhe, J.; Ballauff, M.; Biesalski, M.; Dziezok, P.; Grohn, F.; Johannsmann, D.; Houbenov, N.; Hugenberg, N.; Konradi, R.; Minko, S.; Motornov, M.; Netz, R. R.; Schmidt, M.; Seidel, C.; Stamm, M.; Stephan, T.; Usov, D.; Zhang, H. N., *Adv Polym Sci* **2004,** *165*, 79-150.

(3) Zhao, B.; Brittain, W. J., *Prog Polym Sci* **2000,** *25* (5), 677-710.

(4) Brandani, P.; Stroeve, P., *Macromolecules* **2004,** *37* (17), 6640-6643.

(5) Lee, S.; Voros, J., *Langmuir* **2005,** *21* (25), 11957-11962.

(6) Tran, Y.; Auroy, P., *J Am Chem Soc* **2001,** *123* (16), 3644-3654.

(7) Matyjaszewski, K., *Prog Polym Sci* **2005,** *30* (8-9), 858-875.

(8) Radhakrishnan, B.; Ranjan, R.; Brittain, W. J., *Soft Matter* **2006,** *2* (5), 386-396.

(9) Hovlid, M. L.; Lau, J. L.; Breitenkamp, K.; Higginson, C. J.; Laufer, B.; Manchester, M.; Finn, M. G., *ACS Nano* **2014,** *8* (8), 8003-14.

(10) Matyjaszewski, K.; Tsarevsky, N. V., *J Am Chem Soc* **2014,** *136* (18), 6513-33.

(11) O'Connor, J.; Lang, Y.; Chao, J.; Cao, H.; Collins, L.; Rodriguez, B. J.; Dockery, P.; Finn, D. P.; Wang, W.; Pandit, A., *Small* **2014,** *10* (3), 469-73.

(12) Chernykh, A.; Alam, S.; Jayasooriya, A.; Bahr, J.; Chisholm, B. J., *Green Chem* **2013,** *15* (7), 1834-1838.

(13) Ouardad, S.; Deffieux, A.; Peruch, F., *Polym Chem-Uk* **2013,** *4* (6), 1874-1882.

(14) Cosemans, I.; Wouters, J.; Cleij, T.; Lutsen, L.; Maes, W.; Junkers, T.; Vanderzande, D., *Macromol Rapid Commun* **2012,** *33* (3), 242-7.

(15) Dane, E. L.; Grinstaff, M. W., *J Am Chem Soc* **2012,** *134* (39), 16255-64.

(16) Paley, D. W.; Sedbrook, D. F.; Decatur, J.; Fischer, F. R.; Steigerwald, M. L.; Nuckolls, C., *Angew Chem Int Ed Engl* **2013,** *52* (17), 4591-4.

(17) Park, H.; Lee, H. K.; Choi, T. L., *J Am Chem Soc* **2013,** *135* (29), 10769-75.

(18) Whitehorne, T. J.; Schaper, F., *Inorg Chem* **2013,** *52* (23), 13612-22.

(19) Buey, R. M.; Diaz, J. F.; Andreu, J. M., *Biochemistry* **2006,** *45* (19), 5933-8.

(20) Barink, M.; Van der Mark, P. C.; Fennis, W. M.; Kuijs, R. H.; Kreulen, C. M.; Verdonschot, N., *Biomaterials* **2003,** *24* (8), 1427-35.

(21) Matyjaszewski, K., *Macromolecules* **2012,** *45* (10), 4015-4039.

(22) Singh, P.; Srivastava, A.; Kumar, R., *J Polym Sci Pol Chem* **2012,** *50* (8), 1503-1514.

(23) Tang, F.; Zhang, L. F.; Zhang, Z. B.; Cheng, Z. P.; Zhu, X. L., *J Macromol Sci A* **2009,** *46* (10), 989-996.

(24) Patrucco, E.; Ouasti, S.; Vo, C. D.; De Leonardis, P.; Pollicino, A.; Armes, S. P.; Scandola, M.; Tirelli, N., *Biomacromolecules* **2009,** *10* (11), 3130-3140.

(25) Yue, W. W.; Li, H. J.; Xiang, T.; Qin, H.; Sun, S. D.; Zhao, C. S., *J Membrane Sci* **2013,** *446*, 79-91.

(26) Yamagami, T.; Kitayama, Y.; Okubo, M., *Langmuir* **2014,** *30* (26), 7823-7832.

(27) Babin, J.; Lepage, M.; Zhao, Y., *Macromolecules* **2008,** *41* (4), 1246-1253.

(28) Pan, K.; Ren, R. M.; Li, H. Z.; Cao, B., *Polym Advan Technol* **2013,** *24* (1), 22-27.

(29) Rowe, M. A.; Hammer, B. A. G.; Boyes, S. G., *Macromolecules* **2008,** *41* (12), 4147-4157.

(30) Maeng, I. S.; Park, J. W., *Langmuir* **2003,** *19* (23), 9973-9976.

(31) Xu, F. J.; Neoh, K. G.; Kang, E. T., *Prog Polym Sci* **2009,** *34* (8), 719-761.

(32) Galbis, E.; de Paz, M. V.; McGuinness, K. L.; Angulo, M.; Valencia, C.; Galbis, J. A., *Polym Chem-Uk* **2014,** *5* (18), 5391-5402.

(33) He, W. W.; Zhang, L. F.; Zhu, G. H.; Zhang, Z. B.; Zhou, N. C.; Cheng, Z. P.; Zhu, X. L., *J Control Release* **2011,** *152*, E210-E211.

(34) Reinicke, S.; Schmalz, H., *Colloid Polym Sci* **2011,** *289* (5-6), 497-512.

(35) Yoon, J. A.; Gayathri, C.; Gil, R. R.; Kowalewski, T.; Matyjaszewski, K., *Macromolecules* **2010,** *43* (10), 4791-4797.

(36) Yoon, J. A.; Kowalewski, T.; Matyjaszewski, K., *Macromolecules* **2011,** *44* (7), 2261-2268.

(37) Forbes, D. C.; Peppas, N. A., *Acs Nano* **2014,** *8* (3), 2908-2917.

(38) Johnson, R. P.; Uthaman, S.; John, J. V.; Heo, M. S.; Park, I. K.; Suh, H.; Kim, I., *Macromol Biosci* **2014,** *14* (9), 1239-1248.

(39) Li, S. Z.; Xiao, M. M.; Zheng, A. N.; Xiao, H. N., *Mat Sci Eng C-Mater* **2014,** *43*, 350-358.

(40) Liu, X. H.; Yin, H.; Zhang, Z. X.; Diao, B. S.; Li, J., *Colloid Surface B* **2015,** *125*, 230-237.

(41) Pan, Y. F.; Xue, Y.; Snow, J.; Xiao, H. N., *Macromol Chem Phys* **2015,** *216* (5), 511-518.

(42) Yang, X. C.; Niu, Y. L.; Zhao, N. N.; Mao, C.; Xu, F. J., *Biomaterials* **2014,** *35* (12), 3873-3884.

(43) Ha, E. J.; Kim, M.; Kim, J.; An, S. S. A.; Paik, H. J., *Polym-Korea* **2014,** *38* (4), 550-556.

(44) Steinbach, T.; Wurm, F.; Klok, H. A., *Polym Chem-Uk* **2014,** *5* (13), 4039-4047.

(45) Matyjaszewski, K., *Abstr Pap Am Chem S* **1999,** *218*, U510-U510.

(46) Nicolay, R.; Kwak, Y.; Matyjaszewski, K., *Macromolecules* **2008,** *41* (13), 4585-4596.

(47) Wang, J. S.; Matyjaszewski, K., *Abstr Pap Am Chem S* **1995,** *210*, 226-Pmse.

(48) Matyjaszewski, K., *Abstr Pap Am Chem S* **2001,** *221*, U297-U297.

(49) Tang, W.; Kwak, Y.; Braunecker, W.; Tsarevsky, N. V.; Coote, M. L.; Matyjaszewski, K., *J Am Chem Soc* **2008,** *130* (32), 10702-10713.

(50) Nunez, R.; Gonzalez-Campo, A.; Vinas, C.; Teixidor, F.; Sillanpaa, R.; Kivekas, R., *Organometallics* **2005,** *24* (26), 6351-6357.

(51) Zhang, G. B.; Fan, X. D.; Kong, J.; Liu, Q.; Liu, Y. Y.; Wang, S. J., *Acta Polym Sin* **2007,** (8), 780-784.

(52) Dupayage, L.; Nouvel, C.; Six, J. L., *J Polym Sci Pol Chem* **2011,** *49* (1), 35-46.

(53) Edmondson, S.; Vo, C. D.; Armes, S. P.; Unali, G. F.; Weir, M. P., *Langmuir* **2008,** *24* (14), 7208-7215.

(54) Fulghum, T. M.; Millan, M. D.; Oncescu, C.; Byers, R.; Advincula, R. C., *Abstr Pap Am Chem S* **2005,** *229*, U961-U961.

(55) Li, W. W.; Matyjaszewski, K., *J Am Chem Soc* **2009,** *131* (30), 10378-+.

(56) Ranganathan, K.; von Srinivasan, K. S., *Abstr Pap Am Chem S* **2002,** *224*, U406-U406.

(57) Kharlampieva, E.; Kozlovskaya, V.; Chan, J.; Ankner, J. F.; Tsukruk, V. V., *Langmuir* **2009,** *25* (24), 14017-14024.

(58) Zhou, C.; Qi, K.; Wooley, K. L.; Walker, A. V., *Colloid Surface B* **2008,** *65* (1), 85-91.

(59) Dong, J. Q.; Zhou, J., *Macromol Theor Simul* **2013,** *22* (3), 174-186.

(60) Ito, Y.; Park, Y. S.; Imanishi, Y., *Langmuir* **2000,** *16* (12), 5376-5381.

(61) Kitano, H.; Kago, H.; Matsuura, K., *J Colloid Interf Sci* **2009,** *331* (2), 343-350.

(62) Men, Y. J.; Drechsler, M.; Yuan, J. Y., *Macromol Rapid Comm* **2013,** *34* (21), 1721-1727.

(63) Nomura, K.; Makino, H.; Nakaji-Hirabayashi, T.; Kitano, H.; Ohno, K., *Colloid Polym Sci* **2015,** *293* (3), 851-859.

(64) Cheng, L.; Liu, A. P.; Peng, S.; Duan, H. W., *Acs Nano* **2010,** *4* (10), 6098-6104.

(65) Lee, H. S.; Dastgheyb, S. S.; Hickok, N. J.; Eckmann, D. M.; Composto, R. J., *Biomacromolecules* **2015,** *16* (2), 650-659.

(66) Liu, H. L.; Li, Y. Y.; Sun, K.; Fan, J. B.; Zhang, P. C.; Meng, J. X.; Wang, S. T.; Jiang, L., *J Am Chem Soc* **2013,** *135* (20), 7603-7609.

(67) Liu, T. W.; Liu, B.; Fu, X. M.; Sun, S. X.; Liu, W.; Bian, G. M.; Qi, Y. L.; Yang, X. L., *Colloid Polym Sci* **2015,** *293* (3), 809-816.

(68) Schuwer, N.; Klok, H. A., *Langmuir* **2011,** *27* (8), 4789-4796.

(69) Banquy, X.; Burdynska, J.; Lee, D. W.; Matyjaszewski, K.; Israelachvili, J., *J Am Chem Soc* **2014,** *136* (17), 6199-6202.

(70) Gowneni, S.; Ramanjaneyulu, K.; Basak, P., *Acs Nano* **2014,** *8* (11), 11409-11424.

(71) Pyun, J.; Jia, S. J.; Kowalewski, T.; Savin, D. A.; Patterson, G. D.; Liu, T. Q.; Matyjaszewski, K., *Abstr Pap Am Chem S* **2002,** *224*, U360-U360.

(72) Pyun, J.; Jia, S. J.; Kowalewski, T.; Matyjaszewski, K., *Macromol Chem Phys* **2004,** *205* (4), 411-417.

(73) Li, D. X.; He, Q.; Yang, Y.; Mohwald, H.; Li, J. B., *Macromolecules* **2008,** *41* (19), 7254-7256.

(74) Boyes, S. G.; Granville, A. M.; Baum, M.; Akgun, B.; Mirous, B. K.; Brittain, W. J., *Surf Sci* **2004,** *570* (1-2), 1-12.

(75) Pincus, P., *Macromolecules* **1991,** *24* (10), 2912-2919.

(76) Borisov, O. V.; Birshtein, T. M.; Zhulina, E. B., *J Phys Ii* **1991,** *1* (5), 521-526.

(77) Moroni, L.; Klein Gunnewiek, M.; Benetti, E. M., *Acta biomaterialia* **2014,** *10* (6), 2367-78.

(78) Krishnamoorthy, M.; Hakobyan, S.; Ramstedt, M.; Gautrot, J. E., *Chemical Reviews* **2014,** *114* (21), 10976-11026.

(79) Barbey, R.; Lavanant, L.; Paripovic, D.; Schuwer, N.; Sugnaux, C.; Tugulu, S.; Klok, H. A., *Chem Rev* **2009,** *109* (11), 5437-527.

(80) Mizutani, A.; Kikuchi, A.; Yamato, M.; Kanazawa, H.; Okano, T., *Biomaterials* **2008,** *29* (13), 2073-2081.

(81) Matsuura, K.; Utoh, R.; Nagase, K.; Okano, T., *Journal of controlled release : official journal of the Controlled Release Society* **2014,** *190*, 228-39.

(82) Petrie, T. A.; Raynor, J. E.; Dumbauld, D. W.; Lee, T. T.; Jagtap, S.; Templeman, K. L.; Collard, D. M.; Garcia, A. J., *Sci Transl Med* **2010,** *2* (45).

(83) Yavuz, M. S.; Cheng, Y. Y.; Chen, J. Y.; Cobley, C. M.; Zhang, Q.; Rycenga, M.; Xie, J. W.; Kim, C.; Song, K. H.; Schwartz, A. G.; Wang, L. H. V.; Xia, Y. N., *Nat Mater* **2009,** *8* (12), 935-939.

(84) Yan, P.; Wang, R. R.; Zhao, N. N.; Zhao, H.; Chen, D. F.; Xu, F. J., *Nanoscale* **2015,** *7* (12), 5281-5291.

(85) Zhang, Y. Y.; Ang, C. Y.; Li, M. H.; Tan, S. Y.; Qu, Q. Y.; Luo, Z.; Zhao, Y. L., *Acs Appl Mater Inter* **2015,** *7* (32), 18179-18187.

(86) Edmondson, S.; Osborne, V. L.; Huck, W. T. S., *Chem Soc Rev* **2004,** *33* (1), 14-22.

(87) Rana, D.; Matsuura, T., *Chem Rev* **2010,** *110* (4), 2448-2471.

(88) Jiang, S. Y.; Cao, Z. Q., *Adv Mater* **2010,** *22* (9), 920-932.

(89) Rodriguez-Emmenegger, C.; Jager, A.; Jager, E.; Stepanek, P.; Alles, A. B.; Guterres, S. S.; Pohlmann, A. R.; Brynda, E., *Colloid Surface B* **2011,** *83* (2), 376-381.

(90) Verma, A.; Stellacci, F., *Small* **2010,** *6* (1), 12-21.

(91) Thissen, H.; Gengenbach, T.; du Toit, R.; Sweeney, D. F.; Kingshott, P.; Griesser, H. J.; Meagher, L., *Biomaterials* **2010,** *31* (21), 5510-5519.

(92) Ratner, B. D., *Biomaterials* **2007,** *28* (34), 5144-5147.

(93) Banerjee, I.; Pangule, R. C.; Kane, R. S., *Adv Mater* **2011,** *23* (6), 690-718.

(94) Marruecos, D. F.; Kastantin, M.; Schwartz, D. K.; Kaar, J. L., *Biomacromolecules* **2016,** *17* (3), 1017-1025.

(95) Hucknall, A.; Rangarajan, S.; Chilkoti, A., *Adv Mater* **2009,** *21* (23), 2441-2446.

(96) Rodriguez-Emmenegger, C.; Brynda, E.; Riedel, T.; Houska, M.; Subr, V.; Alles, A. B.; Hasan, E.; Gautrot, J. E.; Huck, W. T. S., *Macromol Rapid Comm* **2011,** *32* (13), 952-957.

(97) Ma, H. W.; Li, D. J.; Sheng, X.; Zhao, B.; Chilkoti, A., *Langmuir* **2006,** *22* (8), 3751-3756.

(98) Ma, H. W.; Hyun, J. H.; Stiller, P.; Chilkoti, A., *Adv Mater* **2004,** *16* (4), 338-+.

(99) Ferris, R.; Hucknall, A.; Kwon, B. S.; Chen, T.; Chilkoti, A.; Zauscher, S., *Small* **2011,** *7* (21), 3032-3037.

(100) Rodriguez-Emmenegger, C.; Kylian, O.; Houska, M.; Brynda, E.; Artemenko, A.; Kousal, J.; Alles, A. B.; Biederman, H., *Biomacromolecules* **2011,** *12* (4), 1058-1066.

(101) Trmcic-Cvitas, J.; Hasan, E.; Ramstedt, M.; Li, X.; Cooper, M. A.; Abell, C.; Huck, W. T. S.; Gautrot, J. E., *Biomacromolecules* **2009,** *10* (10), 2885-2894.

(102) Harrison, R. H.; Steele, J. A. M.; Chapman, R.; Gormley, A. J.; Chow, L. W.; Mahat, M. M.; Podhorska, L.; Palgrave, R. G.; Payne, D. J.; Hettiaratchy, S. P.; Dunlop, I. E.; Stevens, M. M., *Adv Funct Mater* **2015,** *25* (36), 5748-5757.

(103) Kizhakkedathu, J. N.; Janzen, J.; Le, Y.; Kainthan, R. K.; Brooks, D. E., *Langmuir* **2009,** *25* (6), 3794-3801.

(104) Zhao, C.; Li, L. Y.; Wang, Q. M.; Yu, Q. M.; Zheng, J., *Langmuir* **2011,** *27* (8), 4906-4913.

(105) Pereira, A. D.; Rodriguez-Emmenegger, C.; Surman, F.; Riedel, T.; Alles, A. B.; Brynda, E., *Rsc Adv* **2014,** *4* (5), 2318-2321.

(106) Yoshikawa, C.; Qiu, J.; Huang, C. F.; Shimizu, Y.; Suzuki, J.; van den Bosch, E., *Colloid Surface B* **2015,** *127*, 213-220.

(107) Yoshikawa, C.; Goto, A.; Tsujii, Y.; Fukuda, T.; Kimura, T.; Yamamoto, K.; Kishida, A., *Macromolecules* **2006,** *39* (6), 2284-2290.

(108) Yoshikawa, C.; Goto, A.; Tsujii, Y.; Ishizuka, N.; Nakanishi, K.; Fukuda, T., *J Polym Sci Pol Chem* **2007,** *45* (21), 4795-4803.

(109) Sugnaux, C.; Lavanant, L.; Klok, H. A., *Langmuir* **2013,** *29* (24), 7325-33.

(110) Hu, X.; Gorman, C. B., *Acta biomaterialia* **2014,** *10* (8), 3497-504.

(111) Jackson, A. M. S.; Sheiko, S. S.; Ashby, V. S., *Langmuir* **2015,** *31* (19), 5489-5494.

(112) Shao, Q.; Jiang, S. Y., *Adv Mater* **2015,** *27* (1), 15-26.

(113) Wu, C. J.; Huang, C. J.; Jiang, S. Y.; Sheng, Y. J.; Tsao, H. K., *Rsc Adv* **2016,** *6* (30), 24827-24834.

(114) Alswieleh, A. M.; Cheng, N.; Canton, I.; Ustbas, B.; Xue, X.; Ladmiral, V.; Xia, S. J.; Ducker, R. E.; El Zubir, O.; Cartron, M. L.; Hunter, C. N.; Leggett, G. J.; Armes, S. P., *J Am Chem Soc* **2014,** *136* (26), 9404-9413.

(115) Li, W. C.; Liu, Q. S.; Liu, L. Y., *Langmuir* **2014,** *30* (42), 12619-12626.

(116) Liu, Q. S.; Li, W. C.; Singh, A.; Cheng, G.; Liu, L. Y., *Acta biomaterialia* **2014,** *10* (7), 2956-2964.

(117) Lau, K. H. A.; Sileika, T. S.; Park, S. H.; Sousa, A. M. L.; Burch, P.; Szleifer, I.; Messersmith, P. B., *Adv Mater Interfaces* **2015,** *2* (1).

(118) Yang, J. T.; Chen, H.; Xiao, S. W.; Shen, M. X.; Chen, F.; Fan, P.; Zhong, M. Q.; Zheng, J., *Langmuir* **2015,** *31* (33), 9125-9133.

(119) Chen, H.; Zhang, M. Z.; Yang, J. T.; Zhao, C.; Hu, R. D.; Chen, Q.; Chang, Y.; Zheng, J., *Langmuir* **2014,** *30* (34), 10398-10409.

(120) Raynor, J. E.; Petrie, T. A.; Garcia, A. J.; Collard, D. M., *Adv Mater* **2007,** *19* (13), 1724-+.

(121) Fan, X. W.; Lin, L. J.; Messersmith, P. B., *Biomacromolecules* **2006,** *7* (8), 2443-2448.

(122) Sharma, S.; Johnson, R. W.; Desai, T. A., *Langmuir* **2004,** *20* (2), 348-356.

(123) Shi, X. J.; Wang, Y. Y.; Li, D.; Yuan, L.; Zhou, F.; Wang, Y. W.; Song, B.; Wu, Z. Q.; Chen, H.; Brash, J. L., *Langmuir* **2012,** *28* (49), 17011-17018.

(124) Zhang, N.; Pompe, T.; Amin, I.; Luxenhofer, R.; Werner, C.; Jordan, R., *Macromol Biosci* **2012,** *12* (7), 926-936.

(125) Desseaux, S.; Klok, H. A., *Biomaterials* **2015,** *44*, 24-35.

(126) Lilge, I.; Schonherr, H., *Langmuir* **2016,** *32* (3), 838-847.

(127) Ladd, J.; Zhang, Z.; Chen, S.; Hower, J. C.; Jiang, S., *Biomacromolecules* **2008,** *9* (5), 1357-1361.

(128) Cheng, G.; Zhang, Z.; Chen, S. F.; Bryers, J. D.; Jiang, S. Y., *Biomaterials* **2007,** *28* (29), 4192-4199.

(129) Chang, Y.; Shih, Y. J.; Lai, C. J.; Kung, H. H.; Jiang, S. Y., *Adv Funct Mater* **2013,** *23* (9), 1100-1110.

(130) Gao, C. L.; Li, G. Z.; Xue, H.; Yang, W.; Zhang, F. B.; Jiang, S. Y., *Biomaterials* **2010,** *31* (7), 1486-1492.

(131) Schlenoff, J. B., *Langmuir* **2014,** *30* (32), 9625-9636.

(132) Sin, M. C.; Sun, Y. M.; Chang, Y., *ACS Appl Mater Interfaces* **2014,** *6* (2), 861-73.

(133) Feng, W.; Zhu, S. P.; Ishihara, K.; Brash, J. L., *Langmuir* **2005,** *21* (13), 5980-5987.

(134) Iwata, R.; Suk-In, P.; Hoven, V. P.; Takahara, A.; Akiyoshi, K.; Iwasaki, Y., *Biomacromolecules* **2004,** *5* (6), 2308-2314.

(135) Yu, X. F.; Liu, Z. H.; Janzen, J.; Chafeeva, I.; Horte, S.; Chen, W.; Kainthan, R. K.; Kizhakkedathu, J. N.; Brooks, D. E., *Nat Mater* **2012,** *11* (5), 468-476.

(136) Yu, X. F.; Yang, X. Q.; Horte, S.; Kizhakkedathu, J. N.; Brooks, D. E., *Chem Commun* **2013,** *49* (61), 6831-6833.

(137) Tan, K. Y.; Lin, H.; Ramstedt, M.; Watt, F. M.; Huck, W. T. S.; Gautrot, J. E., *Integr Biol-Uk* **2013,** *5* (6), 899-910.

(138) Costa, P.; Gautrot, J. E.; Connelly, J. T., *Acta biomaterialia* **2014,** *10* (6), 2415-2422.

(139) Takahashi, H.; Nakayama, M.; Itoga, K.; Yamato, M.; Okano, T., *Biomacromolecules* **2011,** *12* (5), 1414-1418.

(140) Gautrot, J. E.; Wang, C. M.; Liu, X.; Goldie, S. J.; Trappmann, B.; Huck, W. T. S.; Watt, F. M., *Biomaterials* **2012,** *33* (21), 5221-5229.

(141) Yu, Q.; Johnson, L. M.; Lopez, G. P., *Adv Funct Mater* **2014,** *24* (24), 3751-3759.

(142) Tan, K. Y.; Ramstedt, M.; Colak, B.; Huck, W. T. S.; Gautrot, J. E., *Polym Chem-Uk* **2016,** *7* (4), 979-990.

(143) Connelly, J. T.; Gautrot, J. E.; Trappmann, B.; Tan, D. W. M.; Donati, G.; Huck, W. T. S.; Watt, F. M., *Nat Cell Biol* **2010,** *12* (7), 711-U177.

(144) Connelly, J. T.; Mishra, A.; Gautrot, J. E.; Watt, F. M., *Plos One* **2011,** *6* (11).

(145) Almeida, F. V.; Walko, G.; McMillan, J. R.; McGrath, J. A.; Wiche, G.; Barber, A. H.; Connelly, J. T., *J Cell Sci* **2015,** *128* (24), 4475-4486.

(146) Rodriguez-Emmenegger, C.; Preuss, C. M.; Yameen, B.; Pop-Georgievski, O.; Bachmann, M.; Mueller, J. O.; Bruns, M.; Goldmann, A. S.; Bastmeyer, M.; Barner-Kowollik, C., *Adv Mater* **2013,** *25* (42), 6123-7.

(147) Gautrot, J. E.; Malmstrom, J.; Sundh, M.; Margadant, C.; Sonnenberg, A.; Sutherland, D. S., *Nano Lett* **2014,** *14* (7), 3945-3952.

(148) Malmstrom, J.; Christensen, B.; Jakobsen, H. P.; Lovmand, J.; Foldbjerg, R.; Sorensen, E. S.; Sutherland, D. S., *Nano Lett* **2010,** *10* (2), 686-694.

(149) Fleisher, D.; Bong, R.; Stewart, B. H., *Advanced Drug Delivery Reviews* **1996,** *19* (2), 115-130.

(150) Keerti, J.; Neelesh Kumar, M.; Narendra, K. J., *Current Pharmaceutical Design* **2015,** *21* (29), 4252-4261.

(151) Lin, H.; Yue, Y.; Maidana, D. E.; Bouzika, P.; Atik, A.; Matsumoto, H.; Miller, J. W.; Vavvas, D. G., *Seminars in Ophthalmology* **2016,** *31* (1-2), 1-9.

(152) das Neves, J.; Nunes, R.; Machado, A.; Sarmento, B., *Advanced Drug Delivery Reviews* **2015,** *92*, 53-70.

(153) Oupicky, D., *Advanced Drug Delivery Reviews* **2008,** *60* (9), 957.

(154) Sokolsky-Papkov, M.; Agashi, K.; Olaye, A.; Shakesheff, K.; Domb, A. J., *Advanced Drug Delivery Reviews* **2007,** *59* (4), 187-206.

(155) zur Muhlen, A.; Schwarz, C.; Mehnert, W., *Eur J Pharm Biopharm* **1998,** *45* (2), 149-55.

(156) Manzoor, A. A.; Lindner, L. H.; Landon, C. D.; Park, J.-Y.; Simnick, A. J.; Dreher, M. R.; Das, S.; Hanna, G.; Park, W.; Chilkoti, A.; Koning, G. A.; ten Hagen, T. L. M.; Needham, D.; Dewhirst, M. W., **2012,** *72* (21), 5566-5575.

(157) Ulbrich, K.; Holá, K.; Šubr, V.; Bakandritsos, A.; Tuček, J.; Zbořil, R., *Chemical Reviews* **2016,** *116* (9), 5338-5431.

(158) Jia, X.; Zhang, G. X.; Li, W.; Sheng, W. B.; Li, C. H., *J Polym Sci Pol Chem* **2014,** *52* (13), 1807-1814.

(159) Chen, J. Y.; Yang, M. X.; Zhang, Q. A.; Cho, E. C.; Cobley, C. M.; Kim, C.; Glaus, C.; Wang, L. H. V.; Welch, M. J.; Xia, Y. N., *Adv Funct Mater* **2010,** *20* (21), 3684-3694.

(160) Li, W. Y.; Cai, X.; Kim, C. H.; Sun, G. R.; Zhang, Y.; Deng, R.; Yang, M. X.; Chen, J. Y.; Achilefu, S.; Wang, L. V.; Xia, Y. N., *Nanoscale* **2011,** *3* (4), 1724-1730.

(161) Liu, G.; Cai, M.; Zhou, F.; Liu, W., *The Journal of Physical Chemistry B* **2014,** *118* (18), 4920-4931.

(162) Jia, X. K.; Yin, J. J.; He, D. G.; He, X. X.; Wang, K. M.; Chen, M.; Li, Y. H., *J Biomed Nanotechnol* **2013,** *9* (12), 2063-2072.

(163) Gao, Q.; Xu, Y.; Wu, D.; Sun, Y. H.; Li, X. A., *J Phys Chem C* **2009,** *113* (29), 12753-12758.

(164) Tang, H. Y.; Guo, J.; Sun, Y.; Chang, B. S.; Ren, Q. G.; Yang, W. L., *Int J Pharmaceut* **2011,** *421* (2), 388-396.

(165) Liu, R.; Liao, P. H.; Liu, J. K.; Feng, P. Y., *Langmuir* **2011,** *27* (6), 3095-3099.

(166) Zhou, J.; Zhang, W.; Hong, C.; Pan, C., *ACS Appl Mater Interfaces* **2015,** *7* (6), 3618-25.

(167) Zhang, Y.; Ang, C. Y.; Li, M.; Tan, S. Y.; Qu, Q.; Zhao, Y., *ACS Appl Mater Interfaces* **2016,** *8* (11), 6869-79.

(168) Sun, J. T.; Hong, C. Y.; Pan, C. Y., *J Phys Chem C* **2010,** *114* (29), 12481-12486.

(169) Chen, T. C.; Wu, W.; Xiao, H.; Chen, Y. X.; Chen, M.; Li, J. S., *Acs Macro Lett* **2016,** *5* (1), 60-63.

(170) Ohno, K.; Akashi, T.; Tsujii, Y.; Yamamoto, M.; Tabata, Y., *Biomacromolecules* **2012,** *13* (3), 927-36.

(171) Zhang, W. J.; Peng, B.; Tian, F.; Qin, W. J.; Qian, X. H., *Anal Chem* **2014,** *86* (1), 482-489.

(172) Liu, H. B.; Yan, Q.; Wang, C. E.; Liu, X.; Wang, C.; Zhou, X. H.; Xiao, S. J., *Colloid Surface A* **2011,** *386* (1-3), 131-134.

(173) Zhou, H.; Wang, X.; Tang, J.; Yang, Y. W., *Polym Chem-Uk* **2016,** *7* (12), 2171-2179.

(174) Williams, D. A.; Thrasher, A. J., *Stem Cell Transl Med* **2014,** *3* (5), 636-642.

(175) van Til, N. P.; de Boer, H.; Poliani, P. L.; Antoniou, M. N.; Villa, A.; Cavazzana-Calvo, M.; Zhang, F.; Thrasher, A. J.; Wagemaker, G., *J Clin Immunol* **2012,** *32*, 10-11.

(176) Booth, C.; Gaspar, H. B.; Thrasher, A. J., *Curr Opin Pediatr* **2011,** *23* (6), 659-666.

(177) Burtner, C. R.; Humbert, O.; O'Donnell, P.; Hubbard, N.; Humphrys, D.; Adair, J. E.; Trobridge, G. D.; Torgerson, T. R.; Scharenberg, A. M.; Rawlings, D.; Felsburg, P. J.; Kiem, H. P., *Blood* **2014,** *124* (21).

(178) Yan, Z. Y.; Stewart, Z. A.; Sinn, P. L.; Olsen, J. C.; Hu, J.; McCray, P. B.; Engelhardt, J. F., *Hum Gene Ther Cl Dev* **2015,** *26* (1), 38-49.

(179) Davies, L. A.; Nunez-Alonso, G. A.; McLachlan, G.; Hyde, S. C.; Gill, D. R., *Hum Gene Ther Cl Dev* **2014,** *25* (2), 97-107.

(180) Stoessl, A. J., *Lancet* **2014,** *383* (9923), 1107-1109.

(181) Rowland, N. C.; Starr, P. A.; Larson, P. S.; Ostrem, J. L.; Marks, W. J.; Lim, D. A., *Movement Disord* **2015,** *30* (2), 190-195.

(182) Palfi, S.; Gurruchaga, J. M.; Ralph, G. S.; Lepetit, H.; Lavisse, S.; Buttery, P. C.; Watts, C.; Miskin, J.; Kelleher, M.; Deeley, S.; Iwamuro, H.; Lefaucheur, J. P.; Thiriez, C.; Fenelon, G.; Lucas, C.; Brugieres, P.; Gabriel, I.; Abhay, K.; Drouot, X.; Tani, N.; Kas, A.; Ghaleh, B.; Le Corvoisier, P.; Dolphin, P.; Breen, D. P.; Mason, S.; Guzman, N. V.; Mazarakis, N. D.; Radcliffe, P. A.; Harrop, R.; Kingsman, S. M.; Rascol, O.; Naylor, S.; Barker, R. A.; Hantraye, P.; Remy, P.; Cesaro, P.; Mitrophanous, K. A., *Lancet* **2014,** *383* (9923), 1138-1146.

(183) Kordower, J. H., *Neuropsychopharmacol* **2015,** *40* (1), 255-256.

(184) Xing, H. B.; Pan, H. M.; Fang, Y.; Zhou, X. Y.; Pan, Q.; Li, D., *Oncol Lett* **2014,** *7* (2), 487-492.

(185) Rekha, M. R.; Sharma, C. P., *Curr Nanosci* **2011,** *7* (6), 879-885.

(186) Perez-Martinez, F. C.; Guerra, J.; Posadas, I.; Cena, V., *Pharm Res-Dordr* **2011,** *28* (8), 1843-1858.

(187) Mathew, A.; Cao, H. L.; Collin, E.; Wang, W. X.; Pandit, A., *Int J Pharmaceut* **2012,** *434* (1-2), 99-105.

(188) Kanasty, R.; Dorkin, J. R.; Vegas, A.; Anderson, D., *Nature Materials* **2013,** *12* (11), 967-977.

(189) Zhou, J. B.; Liu, J.; Cheng, C. J.; Patel, T. R.; Weller, C. E.; Piepmeier, J. M.; Jiang, Z. Z.; Saltzman, W. M., *Nat Mater* **2012,** *11* (1), 82-90.

(190) Lindberg, M. F.; Carmoy, N.; Le Gall, T.; Fraix, A.; Berchel, M.; Lorilleux, C.; Couthon-Gourves, H.; Bellaud, P.; Fautrel, A.; Jaffres, P. A.; Lehn, P.; Montier, T., *Biomaterials* **2012,** *33* (26), 6240-6253.

(191) Li, P.; Zhang, N., *Curr Gene Ther* **2011,** *11* (1), 58-73.

(192) Godinho, B. M. D. C.; McCarthy, D. J.; Torres-Fuentes, C.; Beltran, C. J.; McCarthy, J.; Quinlan, A.; Ogier, J. R.; Darcy, R.; O'Driscoll, C. M.; Cryan, J. F., *Biomaterials* **2014,** *35* (1), 489-499.

(193) Hu, S. H.; Hsieh, T. Y.; Chiang, C. S.; Chen, P. J.; Chen, Y. Y.; Chiu, T. L.; Chen, S. Y., *Adv Healthc Mater* **2014,** *3* (2), 273-282.

(194) Wang, F.; Wang, Y. T.; Wang, H.; Shao, N. M.; Chen, Y. Y.; Cheng, Y. Y., *Biomaterials* **2014,** *35* (33), 9187-9198.

(195) Shan, Y. B.; Luo, T.; Peng, C.; Sheng, R. L.; Cao, A. M.; Cao, X. Y.; Shen, M. W.; Guo, R.; Tomas, H.; Shi, X. Y., *Biomaterials* **2012,** *33* (10), 3025-3035.

(196) Du, X.; Xiong, L.; Dai, S.; Kleitz, F.; Qiao, S. Z., *Adv Funct Mater* **2014,** *24* (48), 7627-7637.

(197) Zhao, F.; Yin, H.; Zhang, Z. X.; Li, J., *Biomacromolecules* **2013,** *14* (2), 476-484.

(198) Zhang, P.; Yang, J. H.; Li, W. C.; Wang, W.; Liu, C. J.; Griffith, M.; Liu, W. G., *J Mater Chem* **2011,** *21* (21), 7755-7764.

(199) Han, S. C.; Wan, H. Y.; Lin, D. S.; Guo, S. T.; Dong, H. X.; Zhang, J. H.; Deng, L. D.; Liu, R. M.; Tang, H.; Dong, A. J., *Acta Biomater* **2014,** *10* (2), 670-679.

(200) Bechler, S. L.; Lynn, D. M., *Biomacromolecules* **2012,** *13* (2), 542-552.

(201) Yin, L. C.; Zheng, N.; Lu, H.; Gabrielson, N.; Kim, K. H.; Song, Z. Y.; Tang, H. Y.; Zhang, R. J.; Deng, X. J.; Wang, R. B.; Cheng, J. J., *Abstr Pap Am Chem S* **2014,** *248*.

(202) Byrne, M.; Victory, D.; Cryan, S. A.; Heise, A., *Abstr Pap Am Chem S* **2014,** *247*.

(203) Zhang, R. J.; Song, Z. Y.; Yin, L. C.; Zheng, N.; Tang, H. Y.; Lu, H.; Gabrielson, N. P.; Lin, Y.; Kim, K.; Cheng, J. J., *Wires Nanomed Nanobi* **2015,** *7* (1), 98-110.

(204) Peng, L. H.; Niu, J.; Zhang, C. Z.; Yu, W.; Wu, J. H.; Shan, Y. H.; Wang, X. R.; Shen, Y. Q.; Mao, Z. W.; Liang, W. Q.; Gao, J. Q., *Biomaterials* **2014,** *35* (21), 5605-5618.

(205) Park, W.; Yang, H. N.; Ling, D.; Yim, H.; Kim, K. S.; Hyeon, T.; Na, K.; Park, K. H., *Biomaterials* **2014,** *35* (25), 7239-7247.

(206) Eltoukhy, A. A.; Sahay, G.; Cunningham, J. M.; Anderson, D. G., *Acs Nano* **2014,** *8* (8), 7905-7913.

(207) Cheng, W.; Yang, C.; Hedrick, J. L.; Williams, D. F.; Yang, Y. Y.; Ashton-Rickardt, P. G., *Biomaterials* **2013,** *34* (14), 3697-3705.

(208) Majewski, A. P.; Stahlschmidt, U.; Jerome, V.; Freitag, R.; Muller, A. H. E.; Schmalz, H., *Biomacromolecules* **2013,** *14* (9), 3081-3090.

(209) Agarwal, S.; Zhang, Y.; Maji, S.; Greiner, A., *Mater Today* **2012,** *15* (9), 388-393.

(210) Taranejoo, S.; Liu, J.; Verma, P.; Hourigan, K., *J Appl Polym Sci* **2015,** *132* (25).

(211) Siegwart, D. J.; Oh, J. K.; Matyjaszewski, K., *Prog Polym Sci* **2012,** *37* (1), 18-37.

(212) Schubert, U. S.; von der Ehe, C.; Weber, C.; Yildirim, T., *Abstr Pap Am Chem S* **2014,** *248*.

(213) Song, Y. H.; Zhang, T. B.; Song, X. Y.; Zhang, L.; Zhang, C. Q.; Xing, J. F.; Liang, X. J., *J Mater Chem B* **2015,** *3* (5), 911-918.

(214) Zhu, C. H.; Zheng, M.; Meng, F. H.; Mickler, F. M.; Ruthardt, N.; Zhu, X. L.; Zhong, Z. Y., *Biomacromolecules* **2012,** *13* (3), 769-778.

(215) Dai, F. Y.; Liu, W. G., *Biomaterials* **2011,** *32* (2), 628-638.

(216) Majewski, A. P.; Schallon, A.; Jerome, V.; Freitag, R.; Muller, A. H. E.; Schmalz, H., *Abstracts of Papers of the American Chemical Society* **2012,** *243*.

(217) Huang, S. J.; Ke, J. H.; Chen, G. J.; Wang, L. F., *J Mater Chem B* **2013,** *1* (43), 5916-5924.

(218) Yang, X. C.; Zhao, N. N.; Xu, F. J., *Nanoscale* **2014,** *6* (11), 6141-6150.

(219) Hu, H.; Xiu, K. M.; Xu, S. L.; Yang, W. T.; Xu, F. J., *Bioconjugate Chem* **2013,** *24* (6), 968-978.

(220) Lin, X.; Zhao, N.; Yan, P.; Hu, H.; Xu, F. J., *Acta biomaterialia* **2015,** *11*, 381-392.

(221) Hu, H.; Hou, X.-J.; Wang, X.-C.; Nie, J.-J.; Cai, Q.; Xu, F.-J., *Polym Chem-Uk* **2016,** *7* (18), 3107-3116.

CHAPTER 2

Highly Stable RNA Capture by Dense Cationic Polymer Brush for Design of SiRNA Delivery Vectors*

Abstract

The high density of polymer brushes confers on their unique physico-chemical properties, in particular for the regulation of biomolecular interactions and the design of highly selective coatings for biosensors and protein patterning. Here we show that high density poly(N,N-dimethylaminoethyl methacrylate) (PDMAEMA) cationic polymer brushes enable the stable uptake of high levels of oligonucleotides. This is proposed to result from the high degree of crowding and associated increase in entropic driving force for the binding of polyelectrolytes such as nucleic acid molecules. We further demonstrate the ease with which such coatings allow the design of highly structured nanomaterials for siRNA delivery using block copolymer-brush based nanoparticles that allow the protection of oligonucleotides by a protein resistant outer block. In particular these nanomaterials display a high serum stability and low cytotoxicity whilst retaining excellent knock down efficiencies. Polymer brush-based nanomaterials therefore appear particularly attractive for the rational design of a new generation of high performance theranostics and RNA delivery probes.

2.1 Introduction

Polymer brushes have attracted considerable attention, due to their ease of synthesis *via* controlled radical polymerisations, offering unprecedented control over the coating structure and architecture[1, 2]. Brushes have been applied in the biomedical field for the design of highly specific biosensors and the restriction of protein adsorption and cell adhesion[3]. The very dense crowding of polymer brushes has proved extremely important to reduce protein adsorption to surfaces, beyond detection levels. This has enabled their use for the design of bacterial resistant coatings[4-6] and the patterning of protein and cell adhesions at the nano- to micro-scale[7-10]. In contrast, despite the exceptional level of control of structure and architecture that can be achieved using polymer brushes, including their potential for the design of theranostic probes and the systematic study of nanoparticle-cell interactions, polymer brush-functionalised nanomaterials have found limited applications in drug and gene delivery, perhaps as a result of their limited loading capacity. However, plasmid DNA and RNA (siRNA and miRNA) delivery typically only require very low loading levels (a few copies per cell). Hence a few articles have recently reported the delivery of plasmid DNA using polymer brush-functionalised nanoparticles. For example, PDMAEMA brushes containing only tertiary amines which is positively charged at physiological pH were grown from ATRP initiator functionalised silsesquioxane[11], silica nanoparticles[12], nanodiamond[13], gold nanomaterials[14] and magnetic nanoparticle[15] cores for the capture and delivery of plasmid DNA. Although moderate gene transfection efficiencies were obtained (up to 55% in some cases), one of the key advantages of polymer brushes is to enable the introduction of cores with different chemistry, shapes and sizes (e.g. for imaging

properties *via* fluorescence[12, 13] or MRI[14, 16, 17]), whilst retaining the same coating chemistry. Therefore, polymer brush decorated nanomaterials offer exciting opportunities for the systematic study of parameters impacting gene delivery and transfection (core type, brush chemistry, thickness and grafting density). However, relatively poor infiltration of large plasmid DNA molecules (4.0 kbp) through PDMAEMA brushes[12], implying sub-optimal loading and limiting the design freedom of brush-based delivery vectors.

Here we report the high loading level of small RNA molecules within densely packed PDMAEMA brushes and their stabilisation *via* multiple interactions within such highly crowded polycationic environment. Indeed, in contrast to low density polymer coatings typically achieved *via* a "grafting to" approach, the grafting density of polymer brushes grown *via* surface-initiated polymerisation techniques is not limited by thermodynamically controlled surface adsorption but is determined by the initiator density deposited and the kinetic control of polymerisation and termination reactions. As a result of such structural control, we report the use of PDMAEMA brush-functionalised nanoparticles with high knock down efficiency. In addition, we demonstrate the high flexibility of structural design of such nanomaterials, using block copolymer brushes, for their stabilisation in complex protein mixtures such as sera and the reduction of cytotoxicity.

2.2 Controlling polymer brush growth on flat surface

The growth kinetics of PDMAEMA brush generated *via* ATRP was investigated both on silicon wafers and gold substrates for later control of the brush growth on silica

nanoparticles and SPR chips (gold coated on glass). Progress of the polymerisation was monitored by characterising the dry brush thickness *via* ellipsometry (Figure 2.1).
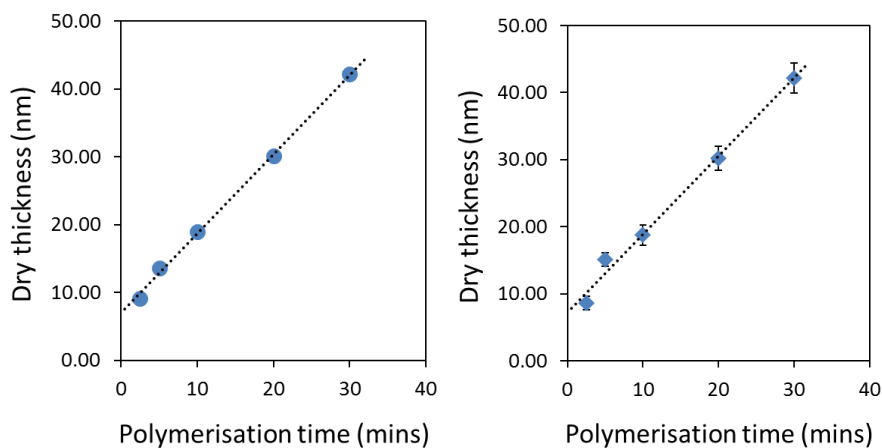
Figure 2.1. PDMAEMA brush growth kinetics on silicon wafer (left) and gold substrate (right) (brush thickness measurement as a function of polymerisation time).

The brush growth rate can be controlled by varying the monomer concentration, the ratio of Cu(I) to Cu(II), the nature of the ligands, and the solvent composition. In this study, addition of ethanol resulted in particularly well-controlled growth of PDMAEMA brush especially for thin brushes below 45 nm, as the PDMAEMA brush thickness profile is linear with no initial jump. Moreover, by diluting the initiator with its non-reactive analogues, the desired grafting density of PDMAEMA can be easily achieved according to Equation 2.1.

$$\sigma = \frac{\rho_m N_A h_{dry}}{M_n} \qquad (2.1)$$

Equation 2.1 (PDMAEMA brush density on flat surfaces): ρ_m is the mass density of DMAEMA (1.318 g/cm3), N_A is Avogadro's number, h_{dry} is the dry thickness of the brushes, and M_n is the average molecular weight of the tethered polymer chains [18, 19].

2.3   Monitoring the interaction of PDMAEMA brush with nucleic acids

The interactions of double stranded DNA and RNA probes with PDMAEMA brushes was investigated *via* surface plasmon resonance (SPR), in order to establish how brush density and nucleic acid probe size control their interactions and infiltration. 30 nm PDMAEMA brushes with dense and sparse grafting density (Figure 2.2) were involved in this study.
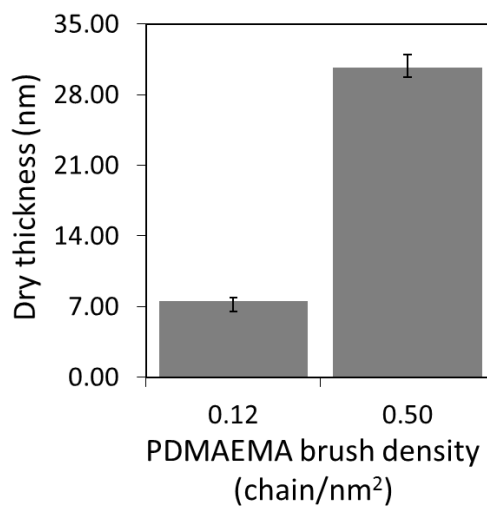
Figure 2.2. PDMAEMA brush thickness measurements with 0.50 chain/nm^2 density and 0.12 chain/nm^2 density brushes polymerised for the same period of time.

The binding amount of nucleic acid in pmol/cm^2 was determined according to equation

2.2. The adsorption of DNA probes, with sizes ranging from 10 to 4.5 kbp and a 22 bp RNA probe, to PDMAEMA brushes was monitored *via* SPR (Figure 2.3 A and 2.3B).

$$B = \frac{RU*100}{M_w} \tag{2.2}$$

Equation 2.2 (binding amount of nucleic acids on PDMAEMA brush in pmol/cm^2): RU is response unit measured from SPR, and Mw is the molecular weight of the nucleic acid.
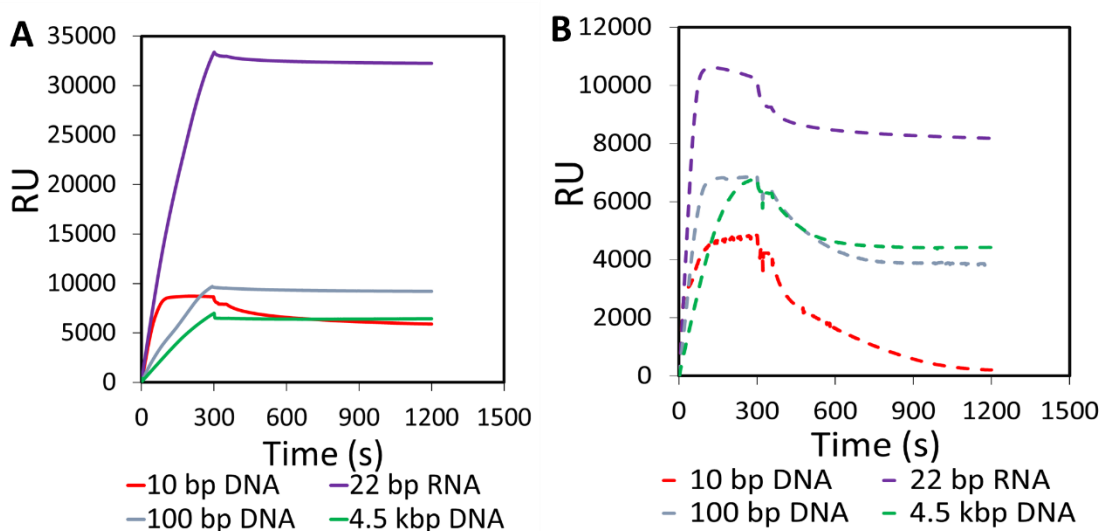
Figure 2.3. SPR traces for different nucleic acids adsorbing to dense (A) and sparse PDMAEMA brushes (B).

On dense brushes (0.50 chains/nm^2 [18-20]), fast adsorption was observed for all probes, but in particular for the shorter 10 bp DNA and 22 bp RNA molecules. Upon washing with phosphate-buffered saline (PBS), stable retention was observed, except for the smallest DNA probe, implying a weaker entropic drive for the adsorption of such small molecules. In contrast, the adsorption profile of nucleic acid molecules to lower density

brushes (0.12 chains/nm^2) displayed no significant differences in the initial rate of adsorption (with the exception of the large plasmid DNA), followed by a relatively fast desorption upon washing with PBS, in particular for the 10 bp DNA probe. Hence our results imply that nucleic acid adsorption to polymer brushes is kinetically limited by molecular crowding but results in considerable stabilisation of adsorbed nucleic acid molecules with intermediate sizes. In all cases, the calculated negative charge density (phosphates) of molecules adsorbed remained significantly lower (< 7,800 pmol/cm^2 for 22 bp RNA, calculations can be found in table 2.1.) than the positive charge density measured for high density PDMAEMA brushes (26,500 pmol/cm^2, calculations can be found in table 2.2.).
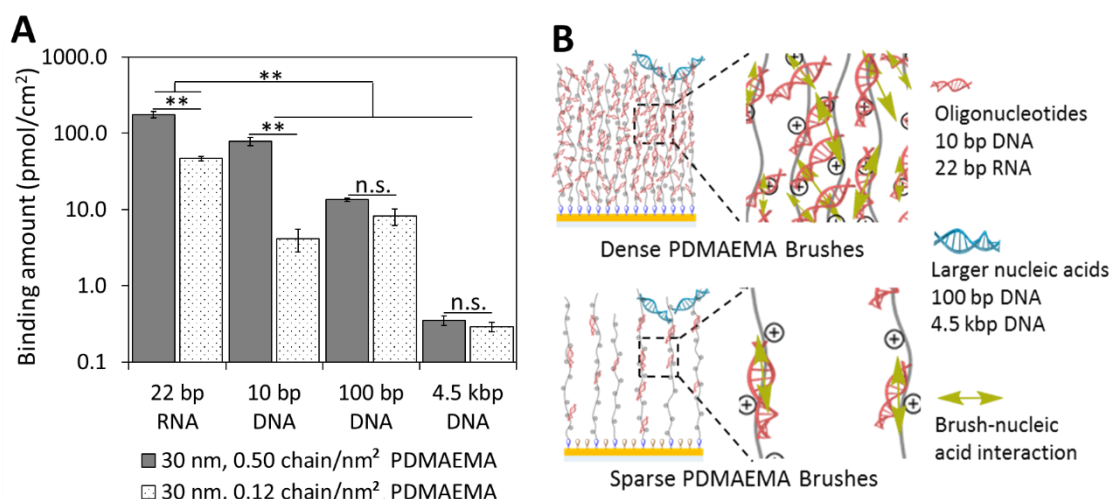
Figure 2.4. SiRNA binding quantification (A); Schematic illustration of nucleic acid molecules interacting with PDMAEMA brushes (B).

Therefore, molecular crowding and local desorption/re-adsorption phenomena[21] combined with entropic stabilisation, resulting in stable retention of the corresponding molecules in polymer brushes (Figure 2.4B). Entropic stabilisation of oligonucleotides may also be enhanced in polymer brushes, due to the frustrated conformation of

polymer chains. Surprisingly, this effect was particularly pronounced in the case of 22 bp RNA molecules (Figure 2.4A), perhaps as a result of additional hydroxyl groups and the presence of uridyl bases present on RNA probes[22]. The short length and stiffer structure of RNA molecules, compared with larger DNA molecules and plasmids, is typically thought to reduce interactions and condensation, with cationic polymeric non-viral delivery agents.[23-25] Consequently, a higher N/P ratio is typically required to form polyplexes with siRNA molecules, to optimise knock down efficiencies.[23] Therefore the dense crowding of cationic polymer brushes constitutes a unique environment for highly stable RNA uptake.

Table 2.1. Negative charge density calculation for different base pairs of nucleic acids.

Negative charge density of different bp of nucleic acids				
Nucleic acid (bp)	10	22	100	4000
Dense brush chain density (pmol/cm^2)	78.2	176.5	13.5	0.4
Dense brush charge density (pmol/cm^2) = bp*2*chain density	1564	7766	2700	3200
Sparse brush chain density (pmol/cm^2)	4.1	46.7	8.2	0.3
Sparse brush charge density (pmol/cm^2) = bp*2*chain density	82	2055	1640	2400

Table 2.2. Positive charge density calculation for dense and sparse PDMAEMA brush.

Positive charge density of PDMAEMA brush		
Brush type	Dense brush	Sparse brush
Chain density (chain/nm^2)	0.5	0.12
PDMAEMA molecular weight (Mn)	50000	50000
DMAEMA molar mass	157	157
DP=PDMAEMA Mn/DMAEMA molar mass	318	318
Charge density (charge/nm^2) =DP/chain density	159	38
Charge density (mol/nm^2)	2.64511E-22	6.34827E-23
Charge density (pmol/cm^2)	26451	6348

2.4 Synthesis and characterisation of PDMAEMA brush coated silica nanoparticles

The high binding capacity of RNA probes within dense PDMAEMA brushes suggested their use for siRNA delivery and the regulation of gene expression. Firstly, PDMAEMA brush coated 300 nm silica nanoparticles (SiO$_2$-PDMAEMA, measured with DLS in PBS) were prepared *via* ATRP with well dispersed particle size of 443 ± 6 nm in PBS (Figure 2.5) and zeta potential of 15.8 ± 4.4 mV.
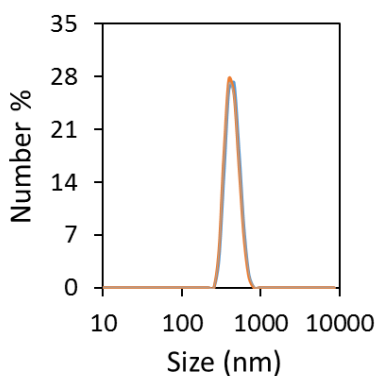
Figure 2.5. Size measurements of SiO$_2$-PDMAEMA in PBS by DLS.

Our previous study has shown PDMAEMA brush thickness on SiO$_2$ can also be controlled by stopping the polymerisation at different time points[12]. The morphology of SiO$_2$-PDMAEMA was confirmed by transmission electron microscope (TEM) in Figure 2.6, which showed an obvious organic layer of PDMAEMA on SiO$_2$ was around 8 nm. The appearance of absorbance band at 1730 cm^{-1} in fourier transform infrared spectroscopy (FTIR, Figure 2.7) was characteristic of C=O vibrations for PDMAEMA. The amount of PDMAEMA on the surface of SiO$_2$ was determined by thermogravimetric analysis (TGA) analysis with 24 % (Table1 and Figure 2.8) weight loss difference compared with initiator coated SiO$_2$. According to Equation 2.3, PDMAEMA dry brush thickness on SiO$_2$ was

calculated as 28 nm. By cleavage of PDMAEMA chains from silica nanoparticles by hydrofluoric acid, the resulting PDMAEMA was characterised by gel permeation chromatography (GPC in Figure 2.9) and by using Equation 2.4, the PDMAEMA density on SiO_2 can be characterised with 0.45 nm^{-2} which was close to the dense brush on silicon wafer. Thus, dense PDMAEMA brush coated silica nanoparticles were prepared for further siRNA knock down study.
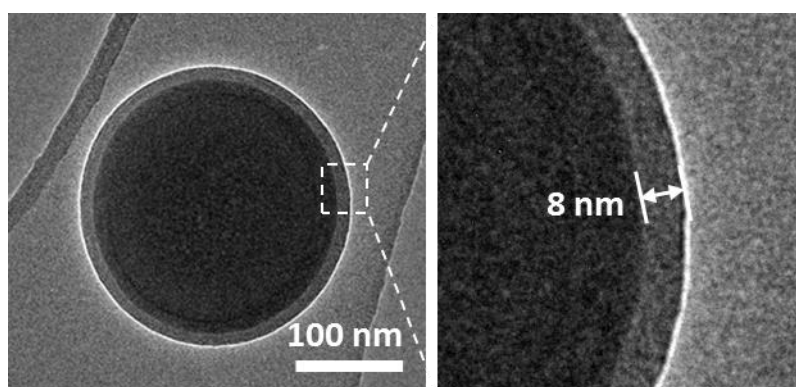
Figure 2.6. TEM image of SiO_2-PDMAEMA nanoparticles.
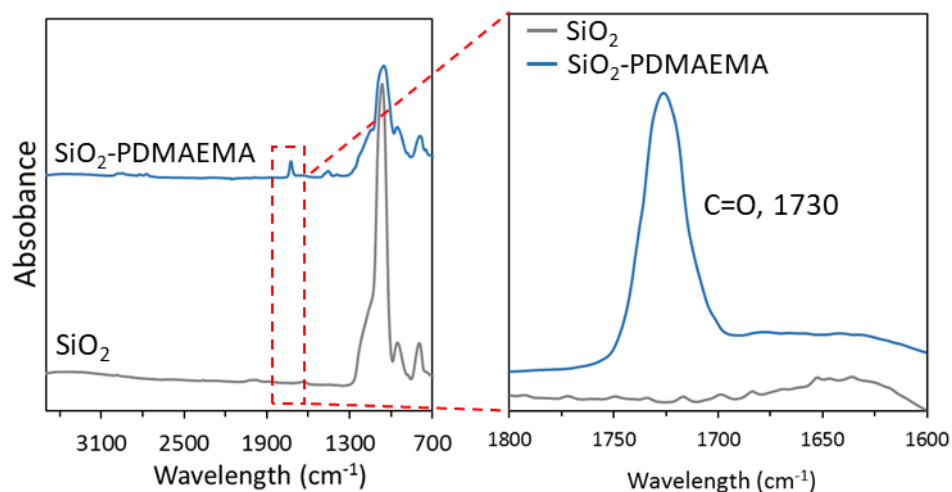
Figure 2.7. FTIR characterisation of SiO_2-PDMAEMA.

$$h = R\left(\frac{W_{brush}\rho_{SiO_2}}{W_{SiO_2}\rho_{brush}} + 1\right)^{\wedge}(1/3) - R \qquad (2.3)$$

Equation 2.3 (brush thickness on silica nanoparticles): W_{brush} is the weight loss percentage corresponding to the decomposition of polymer brush component, W_{SiO2} is the residual weight percentage, ρ_{brush} is the mass density of polymer brush ($\rho_{PDMAEMA}$, 1.318 g/cm^3, ρ_{POEGMA}, 1.105 g/cm^3), ρ_{SiO_2} is the density of bulk SiO$_2$ (2.4 g/cm^3), R is the radius of SiO$_2$ (150 nm).
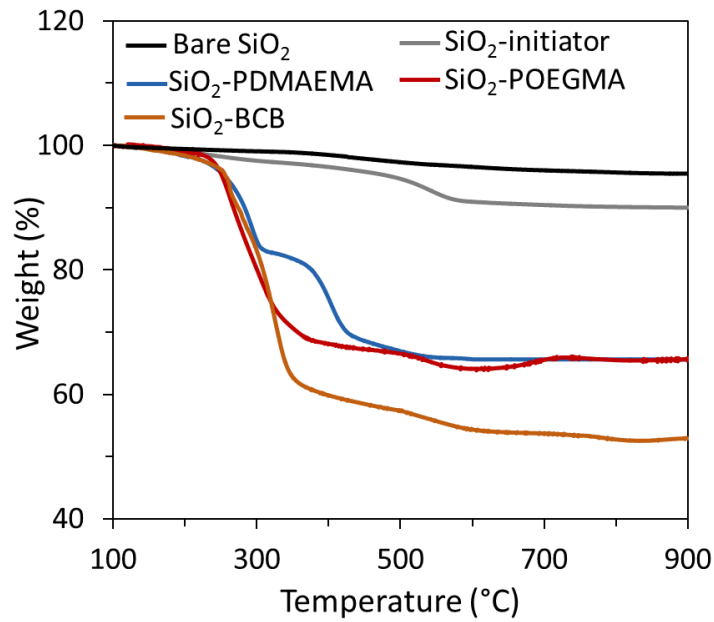
Figure 2.8. TGA characterisation of SiO$_2$-PDMAEMA, SiO$_2$-POEGMA and SiO$_2$-BCB nanoparticles.

$$\delta = \frac{\frac{W_{PDMAEMA}}{W_{SiO2}}\rho_{SiO_2}V_{SiO_2}N_A}{M_{PDMAEMA}S_{SiO_2}} \qquad (2.4)$$

Equation 2.4 (PDMAEMA brush density on silica nanoparticles): $W_{PDMAEMA}$ is the weight loss percentage corresponding to the decomposition of PDMAEMA, W_{SiO2} is the residual weight percentage, ρ_{SiO2} is the density of bulk SiO$_2$ (2.4 g/cm^3), V_{SiO2} is the volume of SiO$_2$ nanoparticle calculated from the average diameter of SiO$_2$ (300 nm), N_A is Avogadro's number, $M_{PDMAEMA}$ is the molecular weight of PDMAEMA cleaved from SiO$_2$, and S_{SiO2} is

the surface area of SiO$_2$ nanoparticle calculated from the average diameter of SiO$_2$ (300 nm)[12].
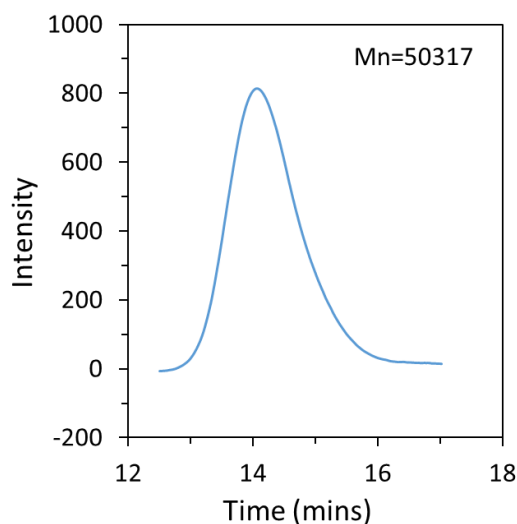
Figure 2.9. GPC measurement of PDMAEMA chains cleaved from silica nanoparticle.

2.5   SiO$_2$-PDMAEMA knock down efficiency and cell viability

A keratinocytes cell line expressing actin-GFP was selected for simple quantification of siRNA efficiency using GFP siRNA, allowing imaging of endogenous actin after phalloidin staining. The fluorescent intensity ratio of GFP (green)/ phalloidin (red) was measured after transfection and compared with the ratio of blank cells, which was then determined as the knock down efficiency. Transfection assay were tested with different N/P ratio (nitrogen to phosphate ratio, where N refers to the nitrogen of PDMAEMA brush, P refers to the phosphate of nucleic acids) of 5, 10 and 15, and commercialised transfection agent lipofectamine 2000 was used as a positive control. Highest knock down efficiencies (66 $\pm$ 6 %) were measured at N/P=10, comparable with those measured with lipofectamine (Figure 2.10A and 2.10B), whilst there was no significant

increase for transfection at N/P=15. In comparison, green fluorescence in the blank and negative control (NC) siRNA groups remained unaltered (Figure 2.10A). However, the toxicity of SiO$_2$-PDMAEMA/siRNA complexes was found to be lower than that of lipofectamine (Figures 2.10C), in which cell viability at N/P=5 or 10 were maintained above 65 %. Indeed, the inherent toxicity of cationic vectors remains an important issue to address in the field of gene delivery[26, 27] *via* non-viral cationic vectors. In addition, cationic vectors typically display poor stability in complex protein solutions, such as serum and blood, limiting the bloodstream circulation time and translation of these technologies[28].
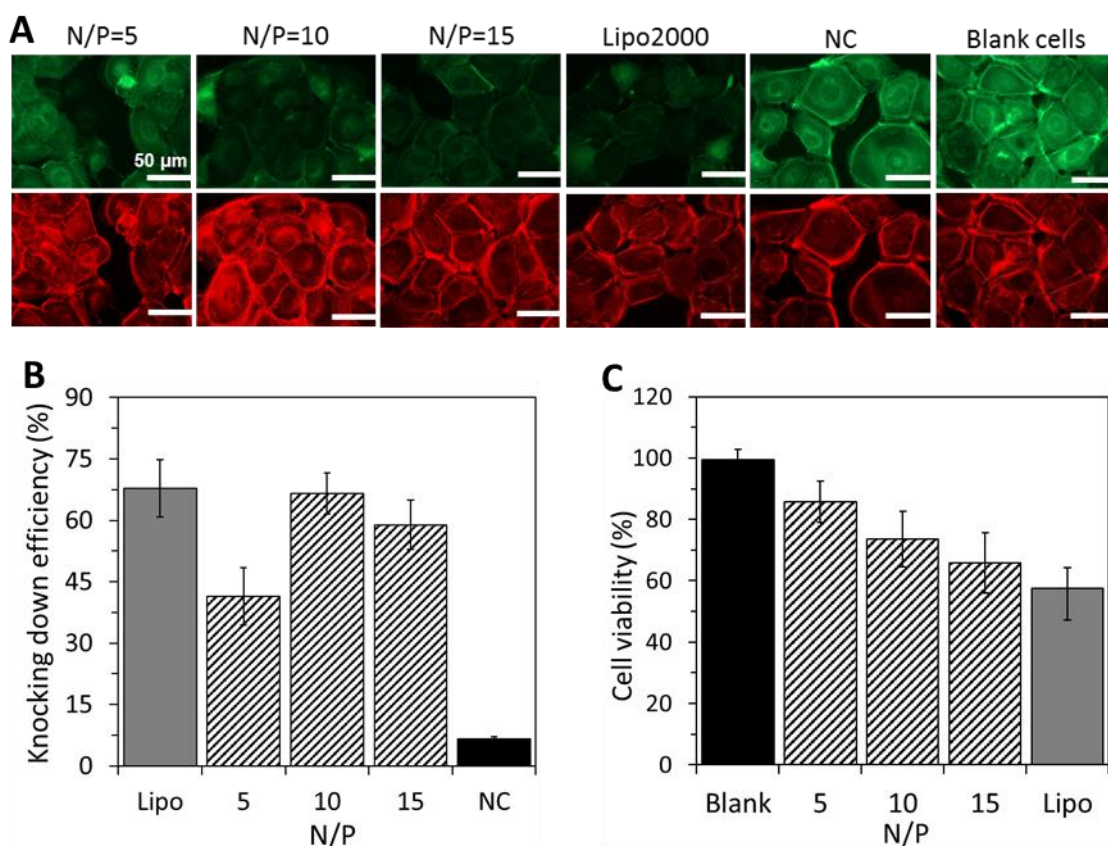
Figure 2.10. Knock down efficiency of SiO$_2$-PDMAEMA/GFP siRNA with HaCaT-GFP cells at N/P=5, 10 and 15 compared with Lipofectamine 2000/GFP siRNA (or NC siRNA, A and

B, scale bar: 50 μm); HaCaT cell viability test with live/dead assay on siRNA complexes with different N/P (C).

2.6 Synthesis and characterisation of block copolymer brush coated flat surfaces and silica nanoparticles

In order to address simultaneously cytotoxicity and stability issues, we developed a double shell approach enabling the coating of the PDMAEMA shell with a protein resistant and cytocompatible POEGMA shell[9, 29-31], to reduce protein adsorption and shield cell membranes from toxic cationic moieties. However, despite the wide range of block copolymer brushes generated and studied on flat substrates[1, 32], few reports have presented the synthesis of block copolymer brushes from nanoparticles[33]. In addition, "grafting to" approaches do not allow high grafting densities suitable for stable RNA loading (Figure 2.4). Hence, we re-initiated POEGMA blocks from the PDMAEMA first shell on both flat surfaces and silica nanoparticles (chemical structures on silica nanoparticle was illustrated in Figure 2.11) via the growth of a mixed PDMAEMA/POEGMA block (1/10 ratio, particles designated as SiO$_2$-BCB).
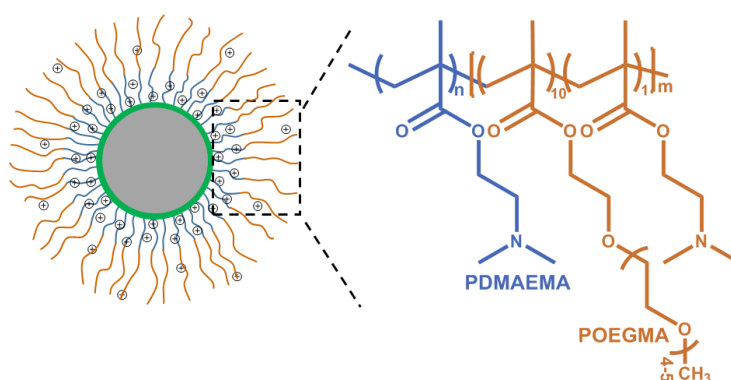
Figure 2.11. Schematic illustration and chemical structures of SiO$_2$-BCB.

Ellipsometry tracking of dry brush thickness in Figure 2.12 and 2.13 showed the good control on block copolymer brush growth regenerated from both 10 and 30 nm PDMAEMA brush.
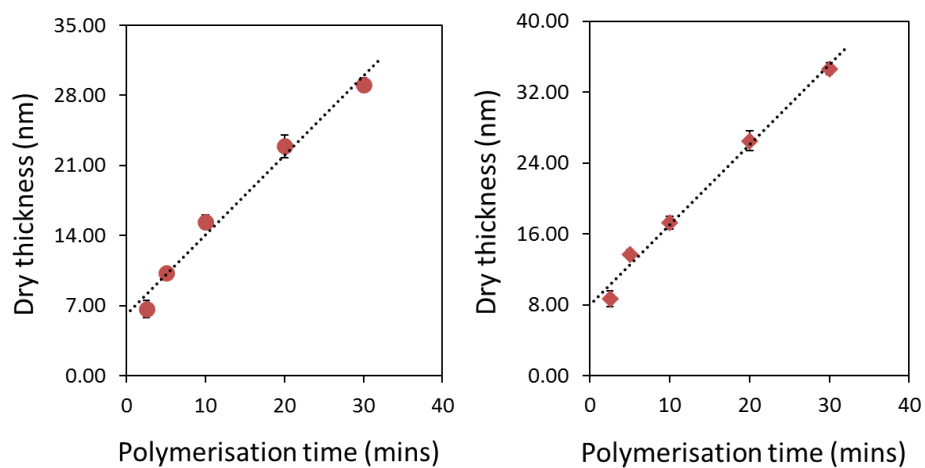
Figure 2.12. POEGMA brush growth kinetics on silicon wafer (left) and gold substrate (right).
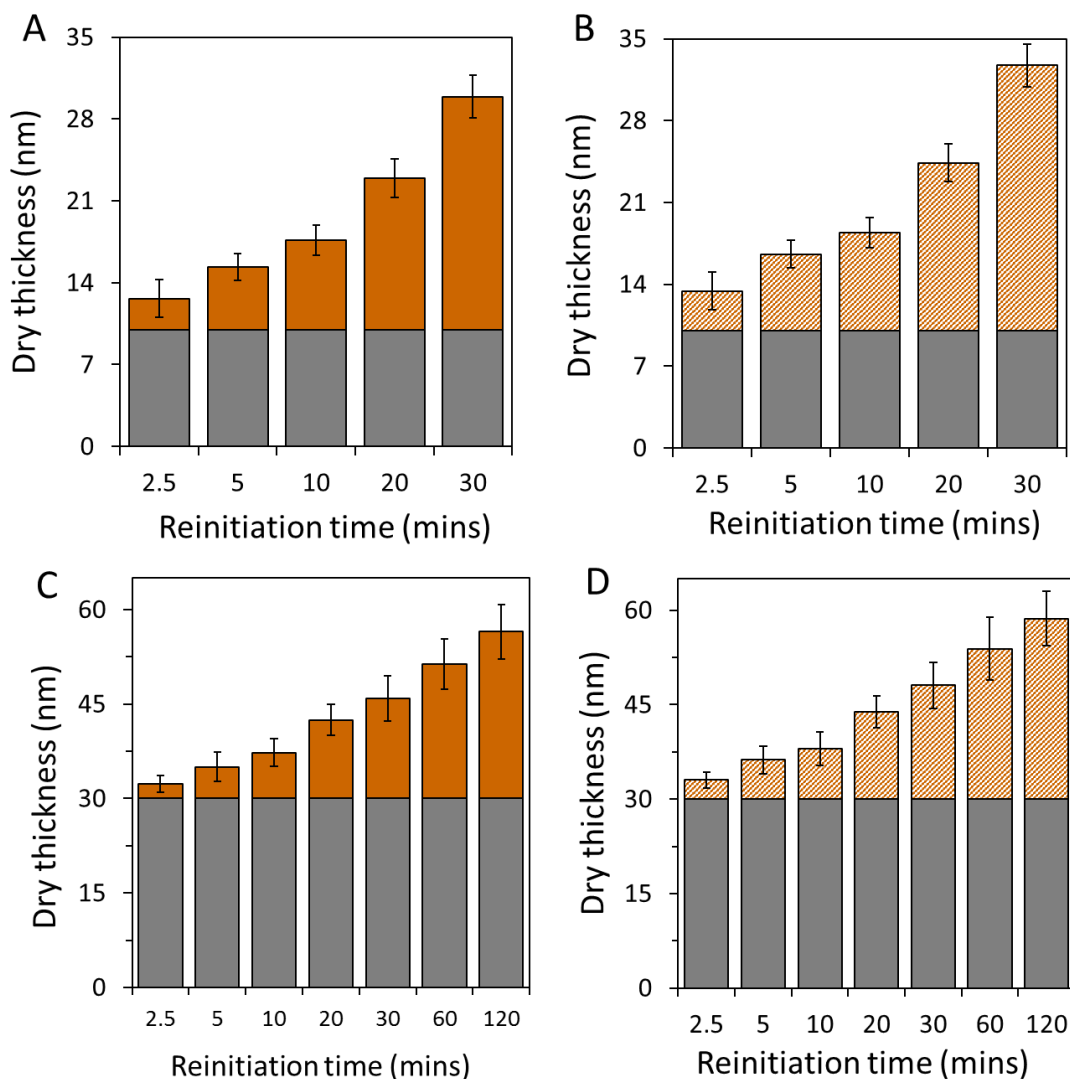
Figure 2.13. Re-initiation kinetics of POEGMA block from PDMAEMA brushes (10 nm (A and B) or 30 nm (C and D)) on silicon wafer (left, A and C) and gold substrate (right, B and D).

The obtained SiO_2-BCB was well characterised by various techniques. A number-average hydrodynamic radius of 550 ± 14 nm was determined by DLS as shown in Figure 2.14A and a reduced zeta potential of 4.4 ± 2.4 mV was characterised compared with SiO_2-PDMAEMA. Additionally, from FTIR measurements of SiO_2-PDMAEMA, SiO_2-POEGMA and SiO_2-BCB in Figure 2.14C, it is notable that both characteristic peaks of PDMAEMA at 2767 cm^{-1} and 2820 cm^{-1} and vibrations at 2870 cm^{-1} (characteristic of

POEGMA) can be found in SiO$_2$-BCB, which indicated the successful synthesis of SiO$_2$-BCB. The increased organic polymer layer of 16 nm was found under TEM (Figure 2.14B). It was in agreement with TGA analysis (Figure 2.8) that more weight loss and increased dry brush thickness (Table 2.3) was found with SiO$_2$-BCB.
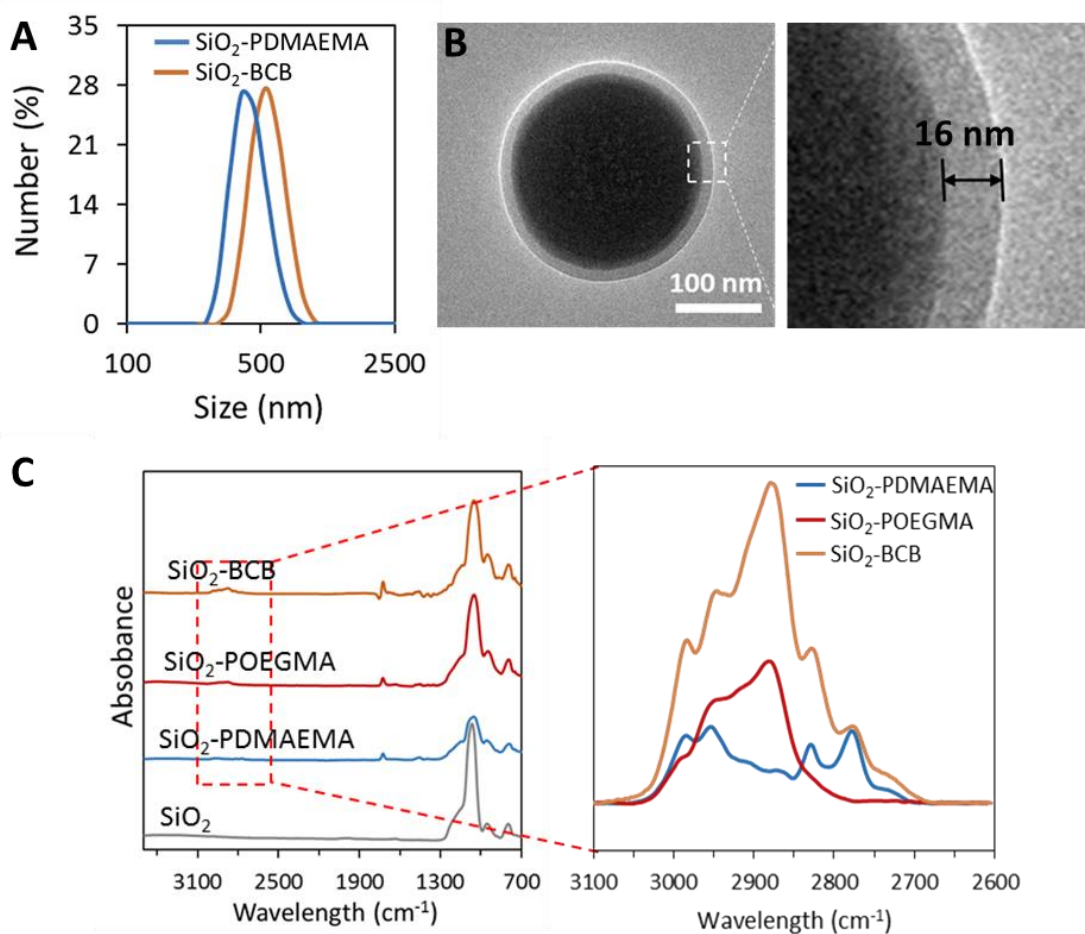
Figure 2.14. Characterisation of particles *via* DLS, in PBS (A); TEM image of SiO$_2$-BCB (B); FTIR characterisation (C).

Table 2.3. TGA characterisation and dry brush thickness on SiO_2.

Sample	Initiator (w %)	PDMAEMA (w %)	POEGMA (w %)	SiO_2 (w %)	PDMAEMA (nm)	POEGMA (nm)
Bare SiO_2	0	0	0	95	0	0
SiO_2-initiator	5	0	0	90	0	0
SiO_2-PDMAEMA	5	24	0	66	28	0
SiO_2-POEGMA	5	0	25	65	0	33
SiO_2-BCB	5	24	14	52	28	25

2.7   Block copolymer brushes interactions with nucleic acids and serum proteins

We then characterised RNA loading within the block copolymer brushes generated (Figure 2.15). SPR experiments demonstrated that 22 bp RNA molecules rapidly diffused through the outer block of the brush and bound to the PDMAEMA block at levels comparable to those measured for mono-block PDMAEMA brushes. We confirmed that POEGMA brushes did not bind any detectable level of RNA. SPR was also used to investigate the binding of proteins (10 % fetal bovine serum, FBS) on polymer brushes. Similarly, the protein adsorption of the block copolymer brushes synthesised reduced by about 50 %, compared to pure PDMAEMA brushes, in good agreement with differential adsorption to PDMAEMA and POEGMA brushes from serum[7, 8, 29]. Therefore, our results indicate that a block copolymer brush structure reduces significantly protein adsorption whilst retaining high levels of RNA uptake.
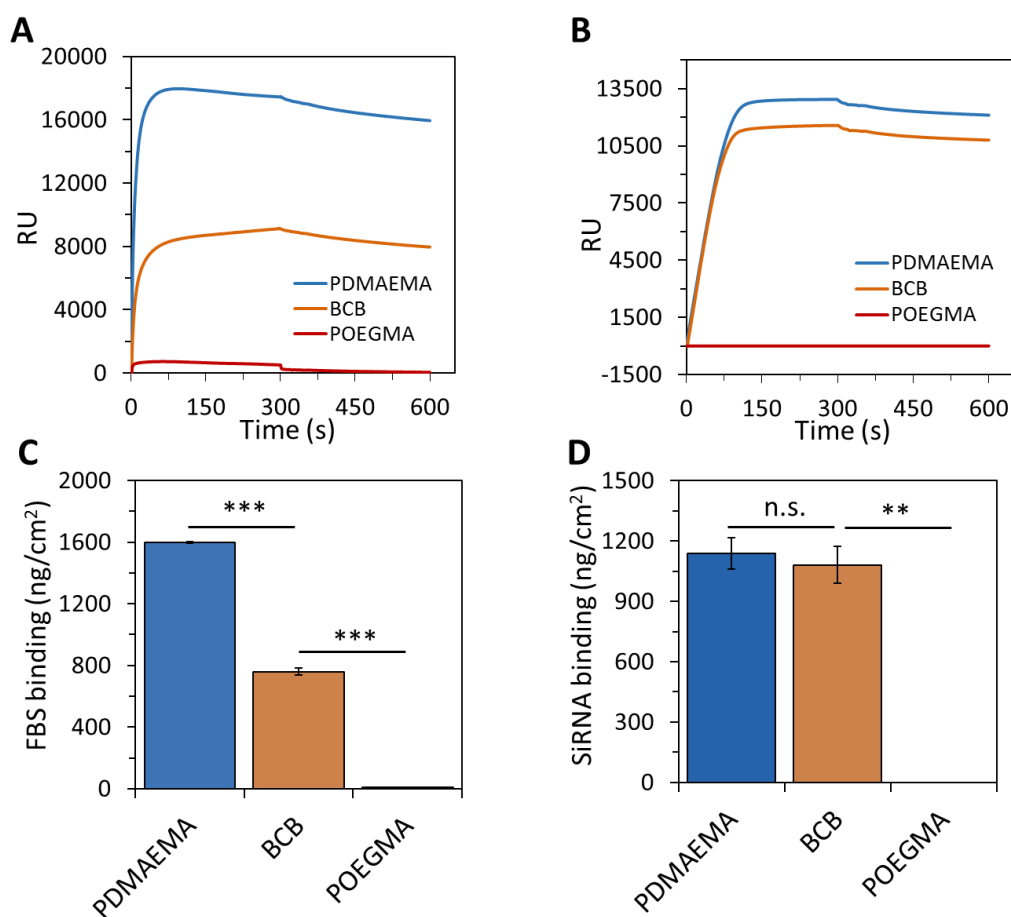
Figure 2.15. FBS (A and C) and siRNA (B and D) binding levels on PDMAEMA brushes, BCB (10 nm PDMAEMA + 10 nm second block) and POEGMA brushes.

2.8 SiO$_2$-BCB serum protein stability and cell viability

The potential of SiO$_2$-BCB particles to improve the safe delivery of siRNA to cells and to resist to aggregation and destabilisation in complex protein solutions was evaluated. We first characterised the stability of these colloids in 10% FBS solutions from 0 min to 48 h. Particles were then collected by centrifugation and washed three times in PBS before characterisation *via* DLS shown in Figure 2.16. SiO$_2$-POEGMA was also prepared as a negative control. In agreement with the high level of protein adsorption measured by SPR from 10% FBS solutions (Figure 2.15), SiO$_2$-PDMAEMA particles aggregated and sedimented rapidly (with charge reversal +16 mV to -5 mV) within 30 mins. In

comparison, SiO_2-POEGMA and SiO_2-BCB particles did not display notable signs of aggregation, even after 48 h (Figure 2.16). Similarly, the cytotoxicity of SiO_2-BCB remained low (96 $\pm$ 4 % viability at an N/P of 10), in contrast to that observed for SiO_2-PDMAEMA and lipofectamine in Figure 2.17A and 2.17B. Together, these results demonstrate that the addition of a POEGMA outer block to the PDMAEMA brush significantly improves cell viability, in addition to particle stability in the presence of serum.
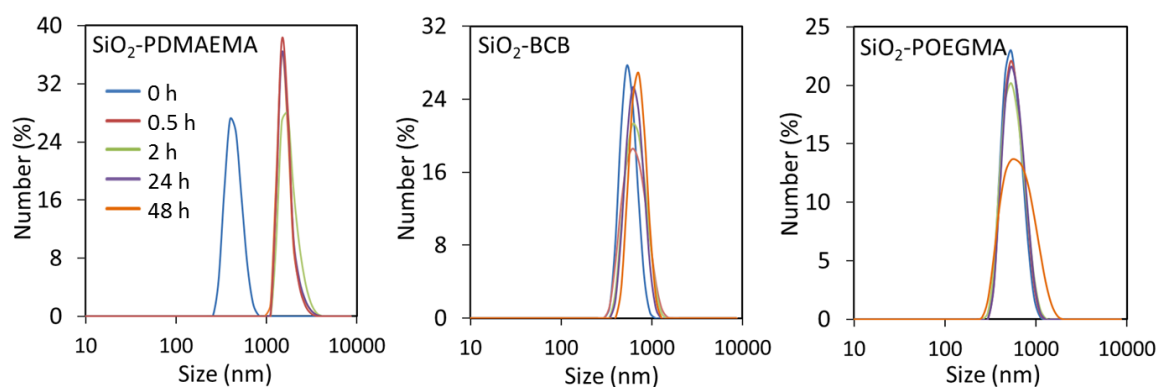
Figure 2.16. Serum stability of SiO_2-PDMAEMA, SiO_2-BCB and SiO_2-POEGMA incubation with 10 % FBS for different time points measured *via* DLS.
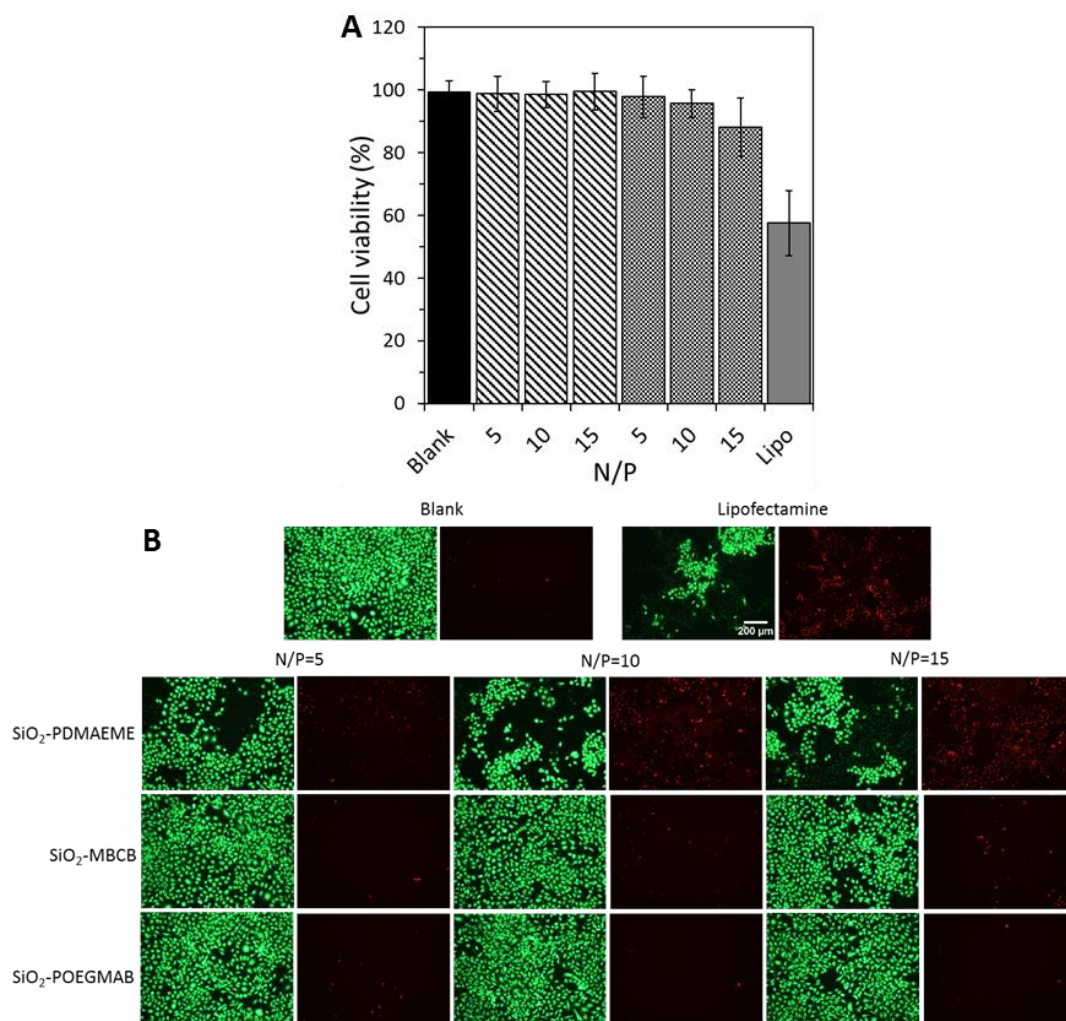
Figure 2.17. HaCaT cell viability with SiO$_2$-POEGMA and SiO$_2$-BCB/siRNA complexes compared with blank and Lipo/siRNA controls (A and B).

2.9 SiO$_2$-BCB mediated knock down in the HaCaT-GFP model and cancer cells

To determine whether SiO$_2$-BCB retained a high siRNA delivery efficiency, the knock down performance of this vector was assessed with our HaCaT-GFP model. Similar transfection levels (near 60 %) were measured with SiO$_2$-BCB (N/P=10), SiO$_2$-PDMAEMA (N/P=10) and lipofectamine (Figure 2.18A and 2.18B). In contrast, no reduction level was observed in any of our controls (Figure 2.18C). Therefore, the addition of a POEGMA

outer block did not prevent siRNA delivery and knock down of the targeted gene, despite the expected reduction in cell membrane interactions, perhaps as a result of the residual positive zeta potential of SiO₂-BCB particles.
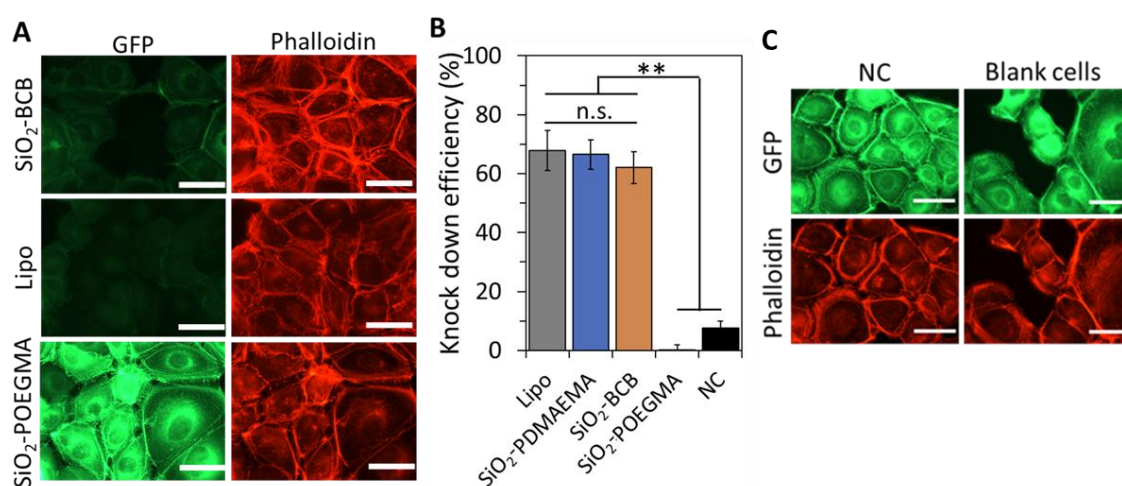
Figure 2.18. Knock down efficiency of SiO₂-BCB/GFP siRNA with HaCaT-GFP cells (A, B and C).

To demonstrate the application of our brush-based vectors, we investigated their use for the knock down of epidermal growth factor receptors (EGFR) in cancer cells, receptors often overexpressed in epithelial malignancies[34, 35]. Gene therapy and knock down of EGFR would allow the reduction of tumor growth, in combination to other therapeutic strategies[36]. An optimised N/P ratio of 10 was used as studied in the case of SiO₂-BCB/EGFR siRNA. Glyceraldehyde 3-phosphate dehydrogenase (GAPDH) was used as internal loading control. No obvious EGFR knock down was observed in groups of blank cells and Lipofectamine/NC siRNA complex. While after transfection, it was demonstrated that SiO₂-BCB nanoparticles allowed efficient knock down of EGFR in

HeLa and A549 non-small lung carcinoma cells through western blotting in Figure 2.19A

and 2.19B. Immunofluorescence staining was further applied to detect the expression

of EGFR visually. Hela and A549 cells were fixed, immunostained with secondary

antibody identified by alexa 488 (green) after transfection. As shown in Figure 2.19C,

EGFR in blank cells or cells transfected with negative control siRNA were bright and with

enhanced signal around cell nucleus. Cells transfected with SiO_2-BCB/EGFR siRNA or

Lipofectamine/EGFR siRNA, the expression of EGFR was weakened significantly, which

suggested successful knock down of EGFR and were in accordance with western blot

results. Hence block copolymer brush-based vectors are versatile agents for efficient

knock down of genes for the treatment of diseases and molecular biology studies.
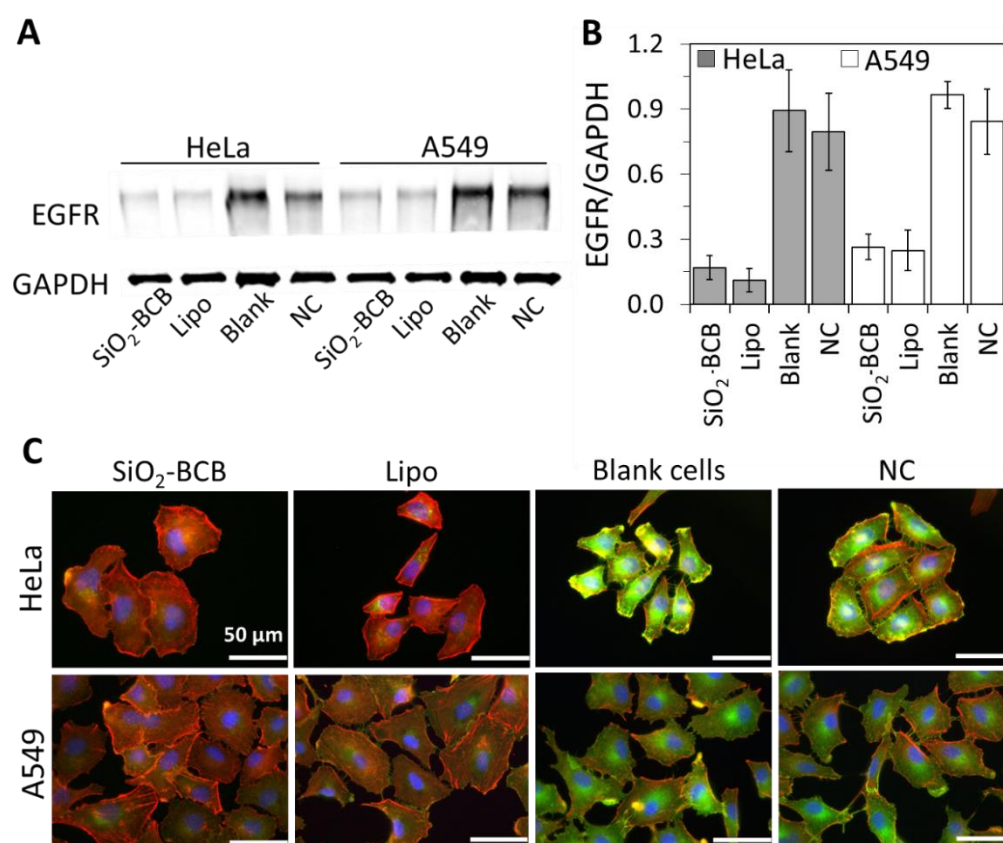
Figure 2.19. Western blot quantification (A and B) and fluorescent immunostaining (C) of EGFR in HeLa and A549 cells after transfectio with SiO_2-BCB/EGFR siRNA.

2.10 Conclusion

In conclusion, we showed that the binding of nucleic acid molecules to cationic polymer brushes depends both on brush density and size of the nucleic acid sequence. We demonstrated that such brushes can be applied to the design of nanoparticles displaying a combination of high knock down efficiency, improved protein resistance and solution stability, as well as low cytotoxicity. In addition to the ease with which polymer brushes can be functionanlised with bioactive moieties (to confer targeting for example) from a wide range of nanomaterials conferring imaging capability, degradability or responsive behavior, such block copolymer brush siRNA delivery vectors are attractive candidates for the design of a new generation of therapeutic platforms. Improving our understanding of parameters (chemical and structural) regulating such RNA-brush interactions, and the stable assembly and dissociation of RNA molecules from brush-based vectors, should enable the improved design of new RNA delivery platforms.

Experimental section

Materials

2-(Dimethylamino)ethyl methacrylate (DMAEMA, Mn = 157.21), oligo(ethylene glycol methyl ether methacrylate) (OEGMA, M_n = 300), copper(I) chloride (Cu(I)Cl), copper(II) bromide (Cu(II)Br$_2$), 2,2'-bipyridyl (bipy), anhydrous toluene, triethylamine (Et$_3$N) and 1-undecanethiol were purchased from Sigma-Aldrich and used as received. All chemicals and solvents were analytical grades unless otherwise stated. Cu(I)Cl was kept under vacuum desiccator until used to avoid oxidisation when exposed to air. Silicon wafers (100 mm diameter, <100> orientation, polished on one side/reverse etched) were purchased from Compart Technology Ltd and cleaned in a Plasma System Zepto from Diener Electronic, for 10 min in air. Gold-coated substrates were obtained through the evaporation of a chromium layer (20 nm followed by the evaporation of a gold layer (200 nm) using an Edwards Auto 500 evaporator. Silica particles (unfunctionalised) were purchased from Bangs Laboratories (supplied as powder, mean diameters of 300 nm). The thiol initiator, ω-mercaptoundecyl bromoisobutyrate was synthesised according to the literature[37], and silane initiator, (3-trimethoxysilyl)propyl 2-bromo-2-methylpropionate was purchased from Gelest. Surface plasmon resonance (SPR) chips (10 x 12 x 0.3 mm) were purchased from Ssens. Triton X-100, gelatin, phallodin–tetramethylrhodamine B isothiocyanate, PFA (paraformaldehyde), DAPI (4,6-diamidino-2-phenylindole), phosphate buffered saline (PBS, 150 mM) were purchased from Sigma Aldrich. Dulbecco's Modified Eagle Medium (DMEM) medium, OPti-MEM™ medium, Fetal Bovine Serum (FBS), trypsin, versene, penicillin-streptomycin, L-glutamine, Alexa Fluor goat anti-rabbit 488 and DNA fragmens were from Thermo-Fisher. Collagen type I

was from BD Bio-science. GFP siRNA (target sequence CGG CAA GCT GAC CCT GAA GTT CAT), EGFR siRNA (target sequence CAG GAA CTG GAT ATT CTG AAA), negative control (NC) siRNA (N/A) were purchased from Qiagen®. The EGFP plasmid was purified by using a plasmid purification kit from PureLink™, thermo fisher. Anti-EGFR monoclonal antibody (rabbit) was purchased from Abcam. Western blot gel, buffers, transfer kit and protein ladder were purchased from Bio-Rad. Secondary IRDye® 800CW Donkey anti-Rabbit IgG (H + L) was from Li-cor.

Polymer brush synthesis on flat surfaces

The brushes were synthesised from the bromo initiator moieties with the 'grafting from' method, using atom transfer radical polymerisation (ATRP).

Deposition of the ATRP silane initiator on silicon wafers. A piece of plasma-oxidised silicon wafer was immersed in a solution of silane initiator (30 μL), Et$_3$N (50 μL), anhydrous toluene (30 mL), and left at room temperature overnight. Then the wafer was rinsed with ethanol and dried under nitrogen stream. Initiator-coated wafers were kept in a dry and dust free nitrogen box until needed. The dry thickness of silane initiator layers was near 2 nm, as measured *via* spectroscopic ellipsometry (JA Woollam, -SE).

Deposition of ATRP thiol initiator on gold substrates and SPR chips. Gold substrate and SPR chips were first plasma-oxidised and immersed in 5 mM thiol initiator ethanoic solutions containing two different ratios of ω-mercaptoundecyl bromoisobutyrate to 1-undecanethiol (100 % and 10 %, depending on the grafting density targeted). The chips were left at room temperature overnight, then washed with ethanol and dried under

nitrogen. The thiol initiator functionalised chips were used to grow polymer brushes freshly. The dry thickness of thiol initiator layers was near 2 nm, as measured *via* ellipsometry.

Synthesis of PDMAEMA brushes. To study PDMAEMA brush growth and the evolution of its thickness as a function of time, a solution of $CuBr_2$ (18 mg, 80 μmol), bipy (320 mg, 2.05 mmol), and DMAEMA (42 mmol, 6.6 g) in water/ethanol (4/1 (v/v), 30 mL) was degassed using argon bubbling for 30 min. CuCl (82 mg, 828 μmol) was added into this solution quickly and the resulting mixture was sonicated to ensure fully dissolve of CuCl and further degassed for 30 min before polymerisation. Initiator-coated silicon/gold substrates (~1 × 1 cm^2 each) were placed in reaction vessels and degassed *via* four cycles of high vacuum/nitrogen gas refilling. Subsequently, 1 mL of DMAEMA solution was transferred to reaction vessels under inert atmosphere *via* a syringe. The polymerisation was stopped at different time points (2.5, 5, 10, 20, 30 min) by immersing the coated substrates in deionised water, followed by washing with copious amounts of ethanol and drying under a nitrogen stream. The dry thickness of PDMAEMA brush was measured *via* ellipsometry afterwards. PDMAEMA brush growth kinetics can be found in Figure. 2.1. For the preparation of sparse PDMAEMA brushes on gold substrates, the thiol initiator was diluted with 1-undecanethiol at a ratio of 1:9.

Synthesis of POEGMA brushes. The procedure of POEGMA brush synthesis was similar as for PDMAEMA brushes except for the difference in monomer solution: the OEGMA solution consisted $CuBr_2$ (18 mg, 80 μmol), bipy (320 mg, 2.05 mmol), and OEGMA (42 mmol, 12.6 g) and CuCl (82 mg, 828 μmol) in water/ethanol (4/1 (v/v), 30 mL). Kinetics for POEGMA brush growth was also studied at time points of 2.5, 5, 10, 20, 30 min.

Synthesis of block copolymer brush (BCB). For preparation of block copolymer brush, 1 mL DMAEMA solution (composition is the same as in PDMAEMA brush synthesis) was add to each reaction vessel containing the initiator-coated silicon wafers, gold substrates or SPR chips under inert atmosphere. After polymerisation for the time corresponding to the targeted thickness (10 nm, 4 min polymerisation, or 30 nm, 20 min polymerisation), according to PDMAEMA brush growth kinetics), 10 mL of OEGMA monomer solution (composition is the same as in POEGMA brush synthesis) was injected and left to polymerise for different time points before the reaction was stopped. Total dry thicknesses were measured afterwards by ellipsometry.

Synthesis of polymer brush coated silica nanoparticles

Initiator deposition. Anhydrous toluene (4 mL) kept under nitrogen was added to 200 mg 300 nm silica nanoparticles. The particles were sonicated for 10 min and were shaken until the suspension turned cloudy and homogenous. The silica particles were then centrifuged at 4000 rpm x 15 min and the toluene was aspirated out. The sonication and centrifugation process were repeated three times and the particles were finally dispersed in 4 mL anhydrous toluene. The initiator grafting process was carried out by adding 200 μL Et$_3$N, 40 μL silane initiator to the 4 mL silica dispersion and stirring overnight. Then the silica particles with silane initiator (SiO$_2$-silane) were washed with 4 mL ethanol three times and stored in final water/ethanol (4/1 (v/v), 10 mL)) in the fridge until needed for polymerisation.

Synthesis of PDMAEMA brushes on silica nanoparticles (SiO₂-PDMAEMA). The polymerisation solution was prepared as described previously by dissolving DMAEMA (6.6 g, 42 mmol), bipy (320 mg, 2.05 mmol), $CuBr_2$ (80 mmol) and CuCl (0.082 g, 828 µmol) in half of the total polymerisation solvent (water/ethanol 4/1 (v/v), 15 mL). 10 mL SiO_2-silane dispersion obtained were degassed for 30 minutes with argon bubbling while stirring. An equal volume of DMAEMA monomer solution was added to the SiO_2-silane suspension. Polymerisation was allowed to proceed under argon at RT for 20 min to get 30 nm of PDMAEMA brush on SiO_2. To terminate the polymerisation, the particle dispersion was diluted using deionised water and bubbled with air until the color changed from dark brown to blue (oxidisation of CuCl). The particles were recovered *via* centrifugation, washed successively with water and ethanol to get rid of the catalysts and residual monomer, during which, sonication was applied to reduce the aggregation and finally the particles were dispersed in 10 mL deionised water and stored in the fridge.

Synthesis of POEGMA brushes on silica nanoparticles (SiO₂-POEGMA). The procedure of POEGMA brush synthesis was similar to that used for PDMAEMA brushes except for the difference in monomer solution. For OEGMA polymerisation on silica nanoparticles, the monomer solution was: OEGMA (12.6 g, 42 mmol), bipy (320 mg, 2.05mmol), $CuBr_2$ (80 mmol) and CuCl (0.082 g, 828 µmol) in 15 mL solvent (water/ethanol 4/1 (v/v), 15 mL).

Synthesis of block copolymer brushes on silica nanoparticles (SiO₂-BCB). For preparation of block copolymer brushes on silica nanoparticles, 2.5 mL DMAEMA monomer solution was added to an equal volume of degassed SiO_2-silane dispersion under inert atmosphere. After achieving 30 nm of PDMAEMA brush (polymerisation for

20 min), 50 mL OEGMA monomer solution was injected and left to polymerise for 120 min according to figure S10 to generate a second block containing POEGMA and PDMAEMA (molar ratio of 10) with a thickness of 30 nm. Polymerisation was stopped, and particles were purified in the same way as for SiO$_2$-PDMAEMA.

Polymer brush coated nanoparticle characterisation

Size and zeta potential measurement. The size and zeta potential of PDMAEMA, POEGMA and block copolymer brush coated silica nanoparticles were measured with a Malvern zetasizer nano ZS. Samples were prepared by dispersing particles in PBS until obtaining a slightly cloudy solution and then sonicated for 10 min with shaking at regular intervals. Each sample was measured in triplicates (three independent samples from at least two batches of particles) at 25°C and the average result was taken as the final hydrodynamic diameter or zeta potential.

Thermogravimetric (TGA) measurement. By using TGA, the dry mass of polymer on silica nanoparticles was determined. Herein, the TGA was performed in air using a TA Instruments Q500. All samples were heated from room temperature to up to 1000 °C at a heating rate of 10 °C/min and dried under vacuum at room temperature prior to TGA runs. It was assumed that the mass change from 100 °C to 900 °C was due to the burning of the organic polymer brush coatings and the remainder was non-combustible silica particles. The polymer brush thickness on silica nanoparticles was calculated according to TGA results in Figure 2.8 and equation 2.3.

Fourier transform infrared - attenuated total reflectance (FTIR-ATR). FTIR was used to characterise the different chemical groups expected within the respective materials through obtaining an infrared spectrum. ATR-FTIR spectroscopy in this study was carried out using a Bruker Tensor 27 with an MCT detector (liquid N2 cooled). Spectra were taken at a resolution of 4 cm^{-1} with a total of 128 scans per run. FTIR spectroscopy was carried out on bare SiO_2, SiO_2-PDMAEMA, SiO_2-POEGMA and SiO_2-BCB, results in Figure 2.14.

Brush density measurement on silica nanoparticles. PDMAEMA brush density on silica nanoparticles can be determined by Equation 2.4, knowing the weight percentage (characterised by TGA) and molecular weight of PDMAEMA on silica nanoparticles. For molecular weight characterisation, PDMAEMA was cleaved from silica nanoparticles and characterised with gel permeation chromatography (GPC). Briefly, 5 mL SiO_2-PDMAEMA particle suspension (20 mg/mL) was added to 25 mL 10 % hydrofluoric acid solution and stirred at room temperature for 4 h. The cloudy particle suspension turned clear after silica cores dissolved completely. The solution was then transferred to a 3.5 KD Spectra/Por® dialysis bag, dialysed with deionised water and freeze dried afterwards. GPC measurements were carried on an Agilent 1260 infinity system operating in dimethylformamide (DMF) with 5 mM ammonium tetrafluoroborate at 50 °C and equipped with refractive index detectors and variable wavelength detectors. The instrument was calibrated with linear narrow polystyrene standards in a range of 550 to 46,890 g/mol. 2 mg of PDMAEMA cleaved from silica nanoparticles was dissolved in 2 mL of DMF completely and filtered before GPC characterisation.

Transmission electron microscopy (TEM). TEM measurements were carried out using a JEOL 2010 transmission electron microscope with a LaB6 filament, operated at 200 kV. Samples were prepared by dropping the diluted brush coated silica nanoparticle suspension on a copper grid with porous carbon film and drying at room temperature.

Characterisation of interactions between polymer brushes and nucleic acids

SPR was used to evaluate the interaction between nucleic acid molecules (10 bp DNA, 100 bp DNA, 22 bp RNA and 4.5 kbp plasmid) and polymer brushes with a Biacore 3000. SPR chips were coated with polymer brushes prior to mounting on a substrate holder. Mounted chips were docked, primed with PBS and equilibrated with PBS at 10 µL/min flow rate until a stable baseline was obtained. 50 µL nucleic acid solutions (plasmid DNA or RNA) were injected at 10 µg/mL. Once the injection was finished, washing with PBS was continued at 10 µL/min flow rate. The nucleic acid adsorption level was measured after washing with PBS for 15 min. Nucleic acid adsorption studies *via* SPR was carried out with chips coated with 30 nm brushes, at densities of 100 % and 10 % for PDMAEMA, POEGMA brushes and 100 % density of block copolymer brush (PDMAEMA, 10 nm, + POEGMA, 10 nm). All measurements were carried out in triplicates (three separate chips freshly prepared).

Characterisation of protein adsorption to polymer brushes

Proteins adsorption to polymer brush coated SPR chips. SPR was used to investigate the binding of proteins on polymer brushes. Similar methods to those used for the characterisation of nucleic acid adsorption were used, but chips were exposed to 50 μL of 10 % FBS during injection of the protein samples. Measurements were carried on 10 nm PDMAEMA, POEGMA brushes and 100 % density of block copolymer brushes (PDMAEMA, 10 nm, + POEGMA, 10 nm). All measurements were carried out in triplicates (three separate chips freshly prepared).

Nanoparticle aggregation in serum solutions. SiO_2-PDMAEMA, SiO_2-POEGMA and SiO_2-BCB were dispersed in 10 % FBS (PBS) solution for 30 min, 2 h, 24 h and 48 h respectively. Subsequently, particles were centrifuged and washed three times and redispersed in PBS before characterisation *via* DLS. Changes in size after incubation in FBS solutions indicated the aggregation of particles following protein adsorption. Each sample was measured in triplicate at 25°C.

Cell viability assay

HaCaT Cell culture and passage. DMEM media supplied with 10 % FBS, 1 % Penicillin-Streptomycin (P/S) and 1 % glutamine was used to culture HaCaT cells in 37°C/5 % CO_2 incubator. To harvest HaCaT cells (T75), cells were washed twice with pre-warmed PBS solution and then cells were detached from the flask by trypsinisation (versene/trypsin, 4/1 v/v, 5 mL, 37°C). 15 mL of DMEM medium was then added to the flask to quench the trypsin. Cells were transferred to a 50 mL centrifuge tube and centrifuged at 1200

rpm for 5 min. After discarding the supernatant solution, the pellet was resuspended in 10 mL FAD medium and the concentration of cells was measured with a haematocytometer.

Cell viability test. Cells were seeded at a density of 50 k cells per well (in 500 µL of DMEA medium) in 24-well plates 24 h prior. SiRNA (with a final concentration of 50 nM/well) complexed with SiO_2-PDMAEMA, SiO_2-POEGMA, SiO_2-BCB at N/P=5, 10, 15 and Lipofectamine/siRNA were added into each well for 4 h in serum free OPTI-MEM medium and then the medium was replaced by full culture DMEM medium for further 24 h incubation. Cell viability was carried out by live/dead assay in which, cells were incubated in 500 µL DMEM medium of 4 mM calcein AM and 2 mM ethidium homodimer for 30 min prior to imaging. Fluorescence imaging was used to capture the live-dead cells, and these were counted *via* ImageJ to obtain the percentage of live cells of total number of cells.

Transfection assay

Establishment of stable HaCaT Cells expressing green fluorescence protein (HaCaT-GFP). Stable HaCaT cell lines expressed EGFP-actin were generated by transfection with linearised plasmids for EGFP-actin (Clontech, Mountain View, CA) as previously described (Sharili 2016)[38]. Cells were transfected using Lipofectamine 2000 according to the manufacturer's instructions and selected with 0.5 mg/mL G418 until a stable GFP positive population was established.

Knock down assay with SiO₂-PDMAEMA and SiO₂-BCB. The protocol for culturing and passaging HaCaT-GFP cells was the same as for HaCaT cells. HaCaT-GFP cells were seeded at a density of 50 k/well on glass cover slips pre-treated with collagen in 24 well plates, 24 h prior to the transfection assay. A final siRNA concentration of 50 nM/well was used for all transfection assays described in this report. 100 µL SiO₂-PDMAEMA/GFP siRNA (or SiO₂-BCB/GFP siRNA) complexes were prepared at N/P=5, 10 and 15, in serum free OPTI-MEM medium. After removing the DMEM medium, cells were washed twice with pre-warmed serum free OPTI-MEM medium and another 400 µL was added. 100 µL siRNA complex was then added dropwise to each well and mixed by shaking gently. Cells were incubated with siRNA complexes for 4 h in the incubator and the medium was then replaced by 500 µL full culture DMEM medium for a further 24 h of incubation. Lipofectamine® 2000 complexed with GFP siRNA/negative control (NC) siRNA (protocol according to the manufacturer's instruction with a final siRNA concentration of 50 nM/well) was used as a positive/negative control. The transfected cells were washed with PBS three times, fixed in paraformaldehyde (PFA, 4 %, 10 min) and permeabilised with Triton X-100 (0.2 %, 5 min). Cells were then stained with TRITC-phalloidin (1:1000) and DAPI (4,6-diamidino-2-phenylindole, 1:1000) in blocking buffer (10% FBS and 0.25% gelatin from cold water fish skin, Sigma-Aldrich) and kept at room temperature for 1 h. Cover slips with fixed cells were mounted on glass slides before imaging with a Leica DMI4000 fluorescence microscope.

SiO₂-BCB/EGFR siRNA on cancer cells (immunostaining and western blot). Cancer cells used in this study were HeLa cells and A549 cells. The culture medium and protocol were similar with HaCaT cells except for shorter trypsinisation times. Both cancer cells were

transfected with SiO$_2$-BCB/EGFR siRNA, lipofectetamine/EGFR siRNA and lipofectetamine/NC siRNA at N/P ratio of 10. After transfection, cells were washed with PBS, fixed and permeabilised. Non-specific protein binding was blocked by incubating the cover-slips for 1 h in blocking buffer (10% FBS and 0.25% gelatin in PBS). Subsequently, the cover-slips were incubated with anti-EGFR monoclonal antibody (anti-EGFR, 1:200, Abcam) in blocking buffer for 1 h at room temperature. After washing with PBS three times, cells were then incubated with Alexa Fluor 488-conjugated secondary antibody (goat anti-rabbit, 1:1000, Thermo-Fisher), phalloidin (1:1000) and DAPI (1:1000) in blocking buffer for 1 h at room temperature. Samples were washed and mounted onto glass slides prior to imaging. The relative protein abundance across samples was determined for western blot. After transfection, cells were harvested, lysised and the protein content was quantified (Pierce™ BCA Protein Assay Kit, Thermo-Fisher). Equal protein loadings was further confirmed by GAPDH. Bands were separated on a 4% to 15% SDS-PAGE gradient gels (Bio-Rad) and semi-dry transferred on to PVDF membranes. Blots were incubated with blocking buffer (5 % milk powder and 5 % FBS in TBS buffer) at room temperature for 1 h before incubating with an anti-EGFR monoclonal antibody 1:1000 (identical to that used for immunostaining) in blocking buffer at 4 °C overnight. After washing three times with TBS + tween buffer, secondary IRDye® 800CW Donkey anti-Rabbit IgG (H + L) (1:15000, Li-cor) in blocking buffer was applied for a further 1 h incubation at room temperature. Bands were visualised using an Odyssey® imaging system (Li-cor).

Statistics

Data are reported as averages ± stdev for groups of at least three replicates, or as individual values with the average indicated. An unpaired, two-tailed Student's t test was used for assessing of statistical significance (*$p<0.05$, **$p<0.01$, ***$p<0.001$).

References

(1) Barbey, R.; Lavanant, L.; Paripovic, D.; Schuwer, N.; Sugnaux, C.; Tugulu, S.; Klok, H. A., *Chem Rev* **2009,** *109* (11), 5437-527.

(2) Edmondson, S.; Osborne, V. L.; Huck, W. T., *Chem Soc Rev* **2004,** *33* (1), 14-22.

(3) Krishnamoorthy, M.; Hakobyan, S.; Ramstedt, M.; Gautrot, J. E., *Chem Rev* **2014,** *114* (21), 10976-11026.

(4) Cheng, G.; Zhang, Z.; Chen, S.; Bryers, J. D.; Jiang, S., *Biomaterials* **2007,** *28* (29), 4192-4199.

(5) Li, G.; Xue, H.; Cheng, G.; Chen, S.; Zhang, F.; Jiang, S., *J Phys Chem B* **2008,** *112* (48), 15269-15274.

(6) Rzhepishevska, O.; Hakobyan, S.; Ruhal, R.; Gautrot, J.; Barbero, D.; Ramstedt, M., *Biomate Sci* **2013,** *1* (6), 589-602.

(7) Gautrot, J. E.; Trappmann, B.; Oceguera-Yanez, F.; Connelly, J.; He, X.; Watt, F. M.; Huck, W. T. S., *Biomaterials* **2010,** *31* (18), 5030-5041.

(8) Ma, H.; Hyun, J.; Stiller, P.; Chilkoti, A., *Adv Mater* **2004,** *16* (4), 338-341.

(9) Gautrot, J. E.; Wang, C.; Liu, X.; Goldie, S. J.; Trappmann, B.; Huck, W. T. S.; Watt, F. M., *Biomaterials* **2012,** *33* (21), 5221-5229.

(10) Di Cio, S.; Bøggild, T. M. L.; Connelly, J.; Sutherland, D. S.; Gautrot, J. E., *Acta Biomater* **2017,** *50*, 280-292.

(11) Schallon, A.; Synatschke, C. V.; Jérôme, V.; Müller, A. H. E.; Freitag, R., *Biomacromolecules* **2012,** *13* (11), 3463-3474.

(12) Krishnamoorthy, M.; Li, D.; Sharili, A. S.; Gulin-Sarfraz, T.; Rosenholm, J. M.; Gautrot, J. E., *Biomacromolecules* **2017,** *18* (12), 4121-4132.

(13) Zhang, P.; Yang, J.; Li, W.; Wang, W.; Liu, C.; Griffith, M.; Liu, W., *J Mater Chem* **2011,** *21* (21), 7755-7764.

(14) Yan, P.; Zhao, N.; Hu, H.; Lin, X.; Liu, F.; Xu, F.-J., *Acta Biomater* **2014,** *10* (8), 3786-3794.

(15) Majewski, A. P.; Stahlschmidt, U.; Jérôme, V.; Freitag, R.; Müller, A. H. E.; Schmalz, H., *Biomacromolecules* **2013,** *14* (9), 3081-3090.

(16) Ohno, K.; Mori, C.; Akashi, T.; Yoshida, S.; Tago, Y.; Tsujii, Y.; Tabata, Y., *Biomacromolecules* **2013,** *14* (10), 3453-3462.

(17) Zeng, H. C., *J Mater Chem* **2011,** *21* (21), 7511-7526.

(18) Christau, S.; Moller, T.; Yenice, Z.; Genzer, J.; von Klitzing, R., *Langmuir* **2014,** *30* (43), 13033-13041.

(19) Sanjuan, S.; Perrin, P.; Pantoustier, N.; Tran, Y., *Langmuir* **2007,** *23* (10), 5769-5778.

(20) Bhat, R. R.; Genzer, J., *Appl Surf Sci* **2006,** *252* (7), 2549-2554.

(21) Gautrot, J. E.; Huck, W. T. S.; Welch, M.; Ramstedt, M., *ACS Appl Mater Interfaces* **2010,** *2* (1), 193-202.

(22) Shen, Z. L.; Xia, Y. Q.; Yang, Q. S.; Tian, W. D.; Chen, K.; Ma, Y. Q., *Topics Curr Chem* **2017,** *375* (2), 2364-2408.

(23) Katas, H.; Alpar, H. O., *J Control Release* **2006,** *115* (2), 216-225.

(24) Gary, D. J.; Puri, N.; Won, Y. Y., *J Control Release* **2007,** *121* (1-2), 64-73.

(25) Cun, D.; Jensen, L. B.; Nielsen, H. M.; Moghimi, M.; Foged, C., *J Biomed Nanotechnol* **2008,** *4* (3), 258-275.

(26) Synatschke, C. V.; Schallon, A.; Jerome, V.; Freitag, R.; Muller, A. H., *Biomacromolecules* **2011,** *12* (12), 4247-4255.

(27) Huang, Y. Y.; Lin, D. S.; Jiang, Q.; Zhang, W. D.; Guo, S. T.; Xiao, P.; Zheng, S. Q.; Wang, X. X.; Chen, H. B.; Zhang, H. Y.; Deng, L. D.; Xing, J. F.; Du, Q.; Dong, A. J.; Liang, Z. C., *Biomaterials* **2012,** *33* (18), 4653-4664.

(28) Hwang, S. J.; Davis, M. E., *Curr Opin Mol Ther* **2001,** *3* (2), 183-191.

(29) Tan, K. Y.; Lin, H.; Ramstedt, M.; Watt, F. M.; Huck, W. T.; Gautrot, J. E., *Integr Biol (Camb)* **2013,** *5* (6), 899-910.

(30) Ladd, J.; Zhang, Z.; Chen, S.; Hower, J. C.; Jiang, S., *Biomacromolecules* **2008,** *9* (5), 1357-1361.

(31) Rodriguez Emmenegger, C.; Brynda, E.; Riedel, T.; Sedlakova, Z.; Houska, M.; Alles, A. B., *Langmuir* **2009,** *25* (11), 6328-6333.

(32) Kizhakkedathu, J. N.; Kumar, K. R.; Goodman, D.; Brooks, D. E., *Polymer* **2004,** *45* (22), 7471-7489.

(33) He, X. H.; Wu, X. M.; Cai, X.; Lin, S. L.; Xie, M. R.; Zhu, X. Y.; Yan, D. Y., *Langmuir* **2012,** *28* (32), 11938-11947.

(34) Sasaki, T.; Hiroki, K.; Yamashita, Y., *Biomed Res Int* **2013**, 546318.

(35) Normanno, N.; De Luca, A.; Bianco, C.; Strizzi, L.; Mancino, M.; Maiello, M. R.; Carotenuto, A.; De Feo, G.; Caponigro, F.; Salomon, D. S., *Gene* **2006,** *366* (1), 2-16.

(36) Zheng, D.; Giljohann, D. A.; Chen, D. L.; Massich, M. D.; Wang, X. Q.; Iordanov, H.; Mirkin, C. A.; Paller, A. S., *P Natl Acad Sci USA* **2012,** *109* (30), 11975-11980.

(37) Jones, D. M.; Brown, A. A.; Huck, W. T. S., *Langmuir* **2002,** *18* (4), 1265-1269.

(38) Sharili, A. S.; Kenny, F. N.; Vartiainen, M. K.; Connelly, J. T., *Sci Rep* **2016***,* 6, 33893

CHAPTER 3

Preparation of Fluorescent Polymer

Brushes on Different Templates with

Macroinitiators

Abstract

Macroinitiators represent an attractive alternative to conventional small-molecule initiators such as silane and thiol, since they can be synthesised on a large scale with relative ease and applied to a variety substrates to achieve dense polymer brush coatings. Herein, a cationic copolymer macroinitiator was synthesised by the statistical copolymerisation of 2-(dimethylamino)ethyl methacrylate (DMAEMA) with 2-hydroxyethyl methacrylate (HEMA) *via* ATRP and used for coating a variety of templates including 70 nm, 300 nm silica nanoparticles, graphene oxide and calcium carbonate. A controlled linear PDMAEMA brush growth was achieved by tuning the adsorbed macroinitiator layers and polymerisation conditions. We further demonstrate the ease of labelling fluorescence on the templates by deposition a negatively charged and stable fluorescent polyelectrolyte during the layer-by-layer process. Additionally, the resulting nanomaterials can be applied to study cell-nanomaterials interactions and promote siRNA delivery. Thus, this novel methodology is of particular interest for fabricating labelled nanomaterials with controlled polymer brush shells for biomedical applications.

3.1 Introduction

The unique properties of polymer brushes generated *via* surface-initiated polymerisation confer its great interests in many biomedical applications as they allow to tailor diverse architectural and functional features: grafting density, thickness of coatings and chemistry.[1] Majority of the 'grafting from' polymerisation process such as atom transfer radical polymerisation (ATRP) requires surface functionalisation of initiators. Generally, ATRP initiators are attached to surfaces *via* either covalent chemical binding (e.g. mono-functional initiator: thiol–gold (or other noble metal) bonding or silane–silanol bonding) or physical adsorption (e.g. polyelectrolyte macroinitiators (MIs)).[2] However, the synthesis of silane initiators typically involves using expensive and toxic reagents (e.g. H_2PtCl_6 and $HSiCl_3$) and cannot be applied in aqueous solution due to hydrolytic cleavage.[3, 4] In addition, thiol-gold bonds are prone to spontaneous redox cleavage over various time scales.[5]

To overcome the limitations of mono-functional initiators, MIs were developed, which typically adsorb to surfaces *via* non-covalent bindings such as hydrophobic, hydrogen bonding and electrostatic interactions.[6, 7] The production process of MIs is much easier and safer than silane and thiol initiators that MIs can be synthesised on a large scale in mild conditions, [3, 4] which is an obvious advantage for high-surface-area substrates such as colloidal particles[8, 9]. Long shelf lives also seem to be less problematic. Moreover, MIs are more flexible for generating polymer brushes independently of surface chemistry, size and shape. It has been shown in previous reports to use MIs to coat a range of substrates[7, 10] and generate polymer brushes *via* ATRP.

Fluorescent materials offer great potential for many applications in both basic and applied research, such as microscopy, cellular studies, delivery systems, diagnostics and sensing as fluorescence microscopy is selective, rich in contrast and quantitative.[11, 12] Approaches have been developed to label particles, substrates and scaffolds with fluorescent molecule *via* conjugation chemistry[13-15] (*e.g.* click chemistry, thiol-ene coupling, esterification *etc.*) that display high labelling efficiencies. However, this process on the other hand often requires additional chemical modifications of the templates or their polymeric coatings. Fluorescent conjugated polyelectrolytes (FCP) have drawn particular attention for their applications in polymer light-emitting diodes (PLEDs)[16-19], solar cells[20, 21] and biosensors[22-24]. As a result of highly electron-delocalised backbones, FCP has larger absorption extinction coefficient and more efficient intramolecular/intermolecular energy transfer than small fluorophores and fluorescent proteins.[25-27] These unique properties are particularly attractive in the field of biomedical imaging[27] to avoid photo bleaching[28] when samples are irradiated during long exposure times. Yet, FCP haven't been explored to label particles from which to generate polymer brushes for biomedical applications.

In this research, we aimed to fabricate polymer brush from MI adsorbed to a variety of templates (70 nm, 300nm silica nanoparticles, graphene oxide sheets and micro-size calcium carbonate) with different core sizes, surface chemistries and shapes. Firstly, the layer-by-layer coating process of positively charged MI and anionic FCP on templates and polymer brush growth kinetics were investigated. The fluorescent polymer brush coated templates were then carefully characterised *via* zetasizer, FTIR, TGA, confocal imaging and TEM. Selected candidates were used to study the interaction of different

brush chemistry coated particles with epidermal cells. Eventually, cationic polymer

brush coated silica nanoparticles were applied for the delivery of siRNA.

3.2 Synthesis of macroinitiator(MI) and fluorescent conjugated polyelectrolyte
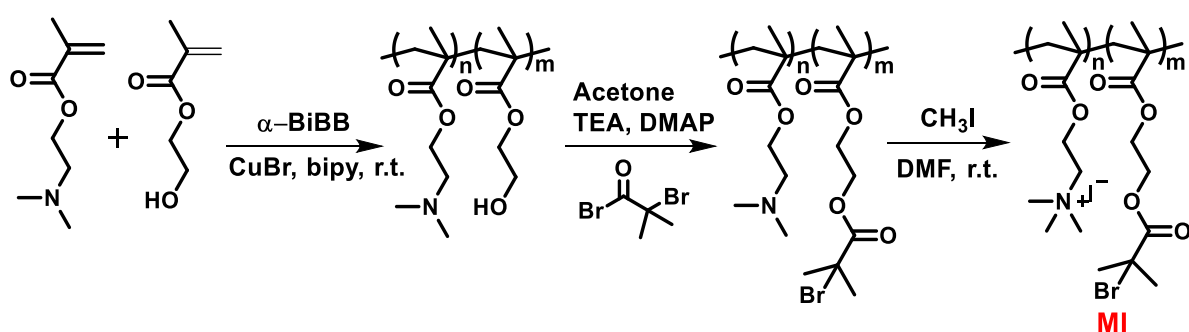

Figure 3.1. Reaction scheme for the three-step synthesis of the cationic macroinitiator used for the surface ATRP.

The MI was synthesised *via* a three-step reaction as described in Figure 3.1, H[1]-NMR was

used to characterise the chemical composition of the purified products after each step.

Firstly, the random co-polymer of DMAEMA and HEMA was synthesised by ATRP using

a molar ratio of 4 (DMAEMA: HEMA=4) and DP target = 20. According to ^{1}H-NMR the

monomer conversion exceeded 95% and the ratio of DMAEMA: HEMA was

approximately 4 : 1. Secondly, the hydroxyl (OH) groups of HEMA were esterified by

bromoisobutyryl bromide (α-BiBB) to introduce an ATRP moiety. The α-BiBB reaction

was efficient with full conversion of the OH-groups according to ^{1}H-NMR as both the 4

and 5 peaks shifted to 9 and 10 in Figure 3.2. Finally, the ternary amine groups in the

DMAEMA-units were quaternised by methyl iodide. Quaternised amines are

distinguishable in ^{1}H-NMR through peaks 14. The result was in agreement with the previous report. The synthesised compound was subsequently used as MI.
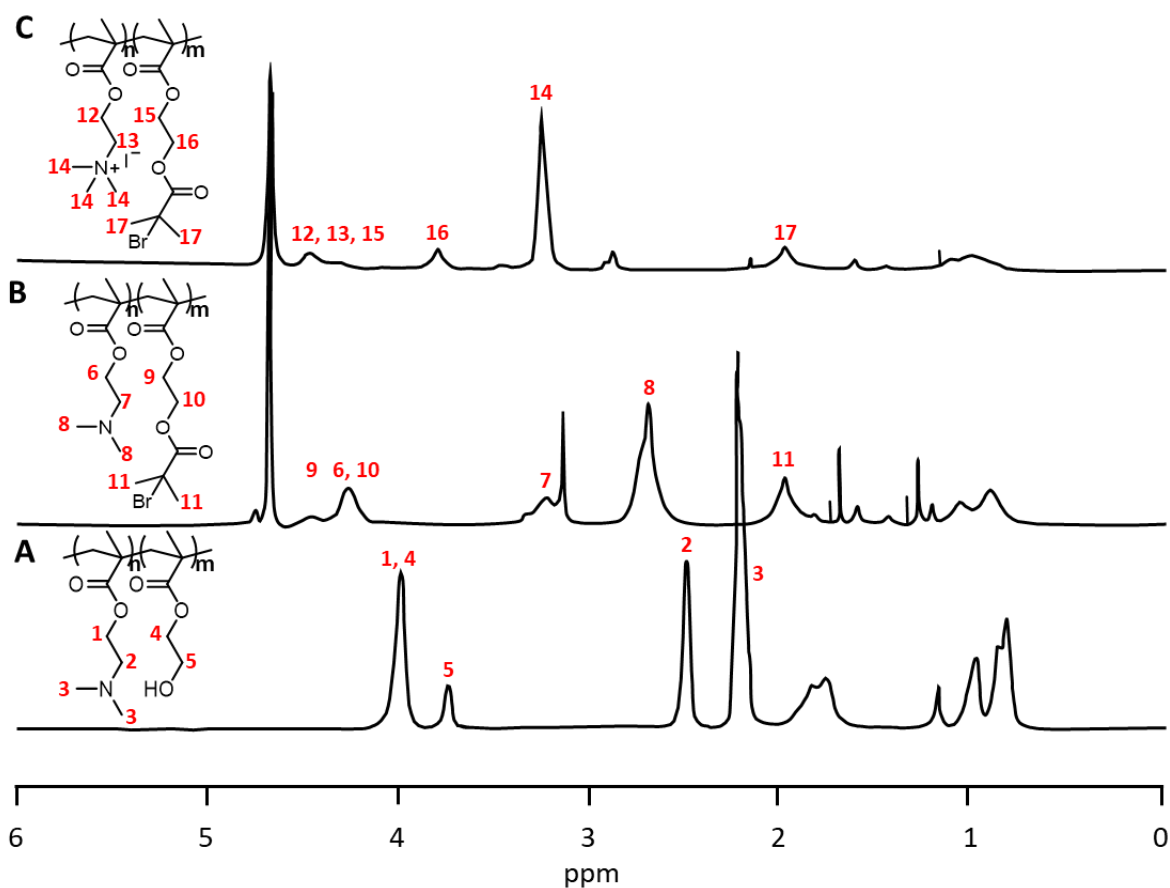

Figure 3.2. ^{1}H NMR spectra for the synthesis of the cationic macroinitiator: DMA-HEMA statistical copolymer (A, deuterated chloroform), copolymer after grafting ATRP initiator (B, deuterium oxide), and the quaternised macroinitiator (C, deuterium oxide).

3.3 Layer-by-layer on silicon wafer and polymer brush growth kinetics

Polymer brush growth kinetics was first studied on silicon wafers. In order to estimate the number of MI layers allowing to achieve a high grafting density of brushes, the kinetics of polymerisation was compared to that of brushes initiated from mono-functional silane initiators. The general idea is illustrated in Figure 3.3, in which polyelectrolytes were deposited on silicon wafer *via* LBL.
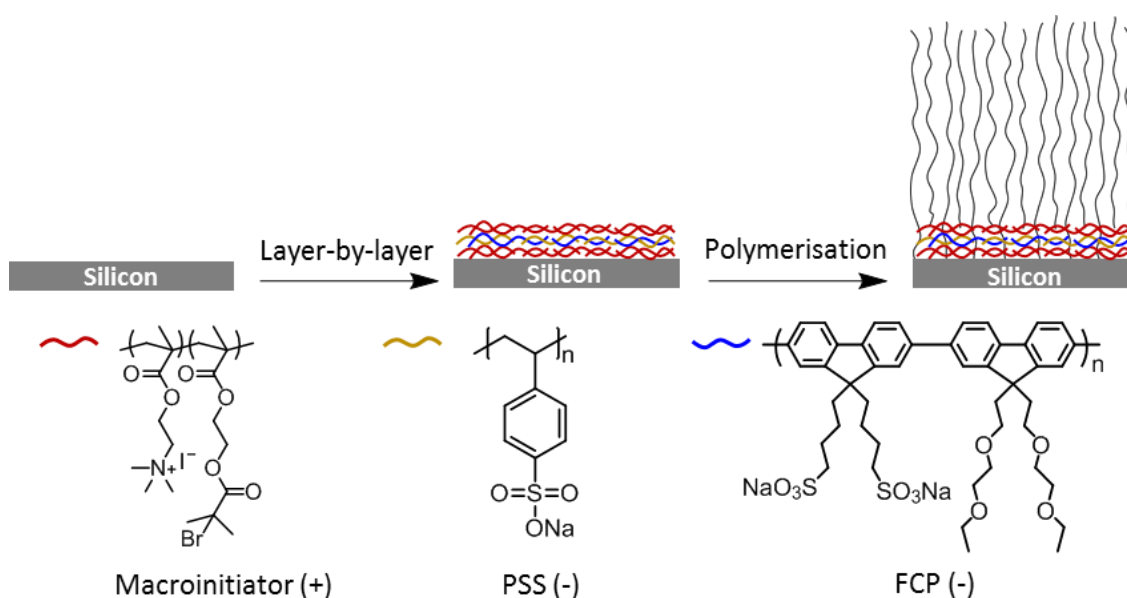
Figure 3.3. Scheme illustration of layer-by-layer (LBL) process of macroinitiator (MI), fluorescent conjugated polyelectrolyte (FCP) / Poly(sodium 4-styrenesulfonate) (PSS) on silicon wafer and brush polymerisation.

Firstly, positively charged MI (2 mg/mL in 0.5 M NaCl) was deposited on plasma treated silicon wafers. To prepare the negatively charged polyelectrolyte solution, FCP was dissolved in DMSO before mixing with the other negatively charged

poly(styrenesulfonate) PSS NaCl solution due to the poor solubility of FCP in aqueous salt solution. The ratio and concentration of FCP to PSS was optimised to ensure full solubility of FCP in mixed solvent and still retain adequate fluorescence. Thus, the coating of the negatively charged layer was a mixture of PSS (2 mg/mL in 0.5 M NaCl) and FCP (0.5 mg/mL in DMSO) at a volume ratio of 10:1 (PSS:FCP). By repeating the above process, multiple layers of MI coated on silicon wafers were obtained. Ellipsometry measurements allowed the quantification of polymer adsorption after deposition of each layer as shown in Figure 3.4A. An increasing of dry thickness was detected with around 3 nm for one layer of MI, 8 nm for two layers of MI and 14 nm for 3 layers of MI. Subsequently, these MI coated chips were used to investigate PDMAEMA brush growth kinetics. Different layers of MI and polymerisation solvent were systematically studied and compared with mono-silane initiator. As shown in Figure 3.4B, with one layer of MI (blue dots) in water/ethanol (volume ratio of 4, dielectric constant of 69), very thin layer of PDMAEMA brush (below 10 nm) was generated after 120 min polymerisation. By increasing the layer of MI to two (green dots), the polymerisation was faster compared with one layer at the initial time points, however, the reaction slowed down after 20 min with no obvious increase of thickness. The maximum thickness was obtained at 120 min with around 20 nm PDMAEMA. With three layers of MI (red dots), a jump of thickness increase was detected within the initial 10 min, where PDMAMEA brush thickness reached 40 nm. Whilst we could not fit the ellipsometry data after that point (showed as red crosses), indicating the formation of a thicker, but more heterogeneous coating. Substrates coated with mono-silane initiators, with polymerisation in the same solvent, monomer concentration and catalytic system, were used as controls (black dots). In order to control the growth of PDMAEMA brush with no

initial thickness jump, polymerisation conditions were optimised as shown in Figure 3.4C. Thus, a less polar solvent mixture (DMF/water with a volume ratio of 4, dielectric constant of 49) was used. PDMAEMA polymerisations from two layers of MI (orange dots) and mono-functional silane (purple dots) were compared. Though the polymerisation was not as fast as in water/ethanol at early time points, the brush growth turned out to be more controlled, with a linear increase in thickness, at longer time points. With two layers of MI in DMF/water, 30 nm PDMAEMA brushes were obtained with 60 min polymerisation, which was comparable to the brush thickness obtained from mono-functional silane initiators at the similar time point.
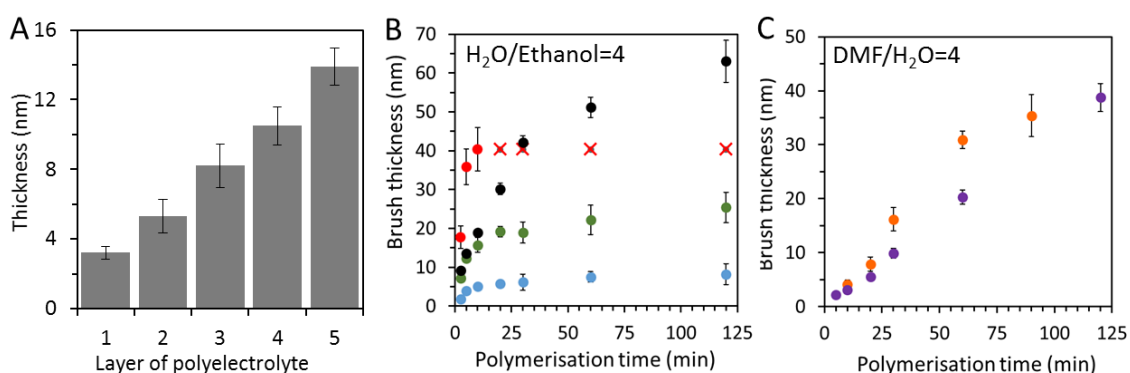
Figure 3.4. Thickness changes of layer-by-layer on silicon wafer tracking by ellipsometry, layer 1: Si-MI, layer 2: Si-MI-FCP, layer 3: Si-MI-FCP-MI, layer 4: Si-MI-FCP-MI-FCP, layer 5: Si-MI-FCP-MI-FCP-MI (A); PDMAEMA brush kinetics study in H_2O/ethanol (V:V=4) with one layer of MI (blue dots), two layers of MI (green dots), three layers of MI (red dots and red cross (out of measurement spectrum)) and mono-silane initiator (black dots) (B); PDMAEMA brush kinetics study in DMF/water (V:V=4) with two layers of MI (orange dots) and mono-silane initiator (purple dots) (C).

3.4 Polymer brush growth from different templates *via* macroinitiator

Growing polymer brushes from MI gives more flexibility as it allows to control and retain brush chemistry and structure independently of the template size, shape as well as surfaces chemistry. Moreover, templates can be easily labelled with stable and bright FCP during LBL without additional chemical modification. To systematically study MI deposition and polymer brush growth on different templates, spherical silica nanoparticles with two different sizes (70 nm and 300 nm respectively), graphene oxide sheets (GO) and micro-size cubic calcium carbonate (CaCO$_3$) were used.
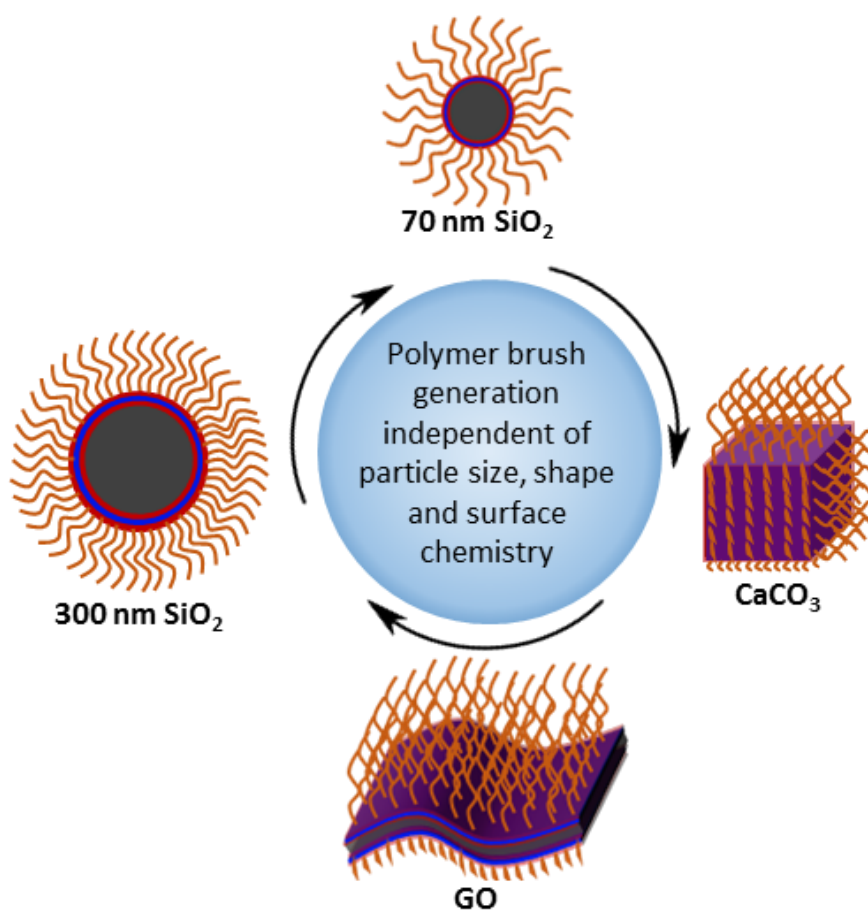

Figure 3.5. Scheme illustration of LBL process of macroinitiator (MI), FCP/PSS on different templates and brush polymerisation.

The general method was similar to that used for the coating of silicon substrates, whilst different incubation times and purification protocols were used (for example to help sedimentation or prevent aggregation). Two layers of MI were deposited for all templates before brush polymerisation, as it showed more controlled brush growth according to the kinetics study on silicon wafers. Zeta potential measurement, although not strictly speaking applicable to non-spherical nanomaterials using the models used for data analysis, is a convenient tool to monitor the deposition of each polyelectrolyte coating, as they indicate the charge reversal that is anticipated after each layer deposition. Figure 3.6A shows the zeta potential change during LBL deposition and after polymerisation of PDMAEMA and POEGMA brushes. A clear trend of charge reversal after each layer confirms the successful deposition process of MI and PSS/FCP.
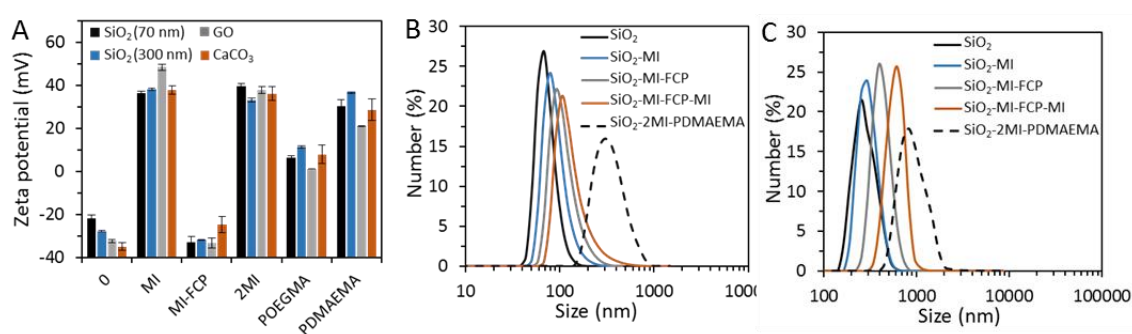
Figure 3.6. Zeta potential change on SiO_2, graphene oxide and calcium carbonate after LBL and polymerisation with PDMAEMA and POEGMA (A); Size changes by DLS measurement of layer-by-layer and polymerisation on 70 nm SiO_2 (B) and 300 nm SiO_2 (C).

After polymerisation of POEGMA, the zeta potential became nearly neutral as the formed POEGMA brush do not carry any charges. The slightly positive zeta potential values may result from the only partial screening of the cationic MI layers by POEGMA

brushes. In contrast, after PDMAEMA polymerisation, the zeta potential of templates remained positive due to the positive charge PDMAEMA itself. Size measurement was also carried out to track the change in size of silica nanoparticles, as shown in Figure 3.6B (70 nm) and 3.6C (300 nm). Sizes of silica nanoparticles increased slightly whilst retaining good dispersity after deposition of each layer of polyelectrolytes. More pronounced size changes were observed after PDMAEMA polymerisation and the associated swelling of the brush in water.
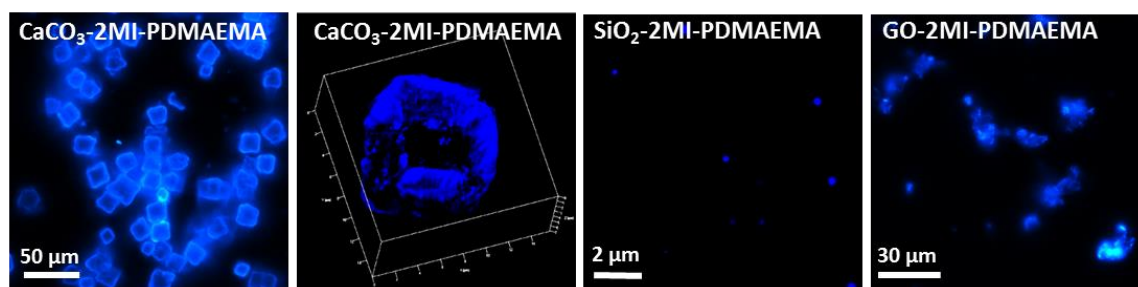
Figure 3.7. Fluorescent images of particles after polymerisation.

During the LBL process, a stable blue fluorescent conjugated polyelectrolyte was introduced in the coating of the second layer, thus allowing the visualisation of the coated templates by fluorescent microscopy. As shown in Figure 3.7, all templates were coated with FCP successfully showing bright and stable blue colour, which was useful in application for the cellular tracking of particles without further chemical modification of the templates. After PDMAEMA brush growth, silica nanoparticles were observed by TEM, which showed the formation of clear organic layers around SiO_2 compared with bare silica nanoparticles for both 70 and 300 nm in Figure 3.8.
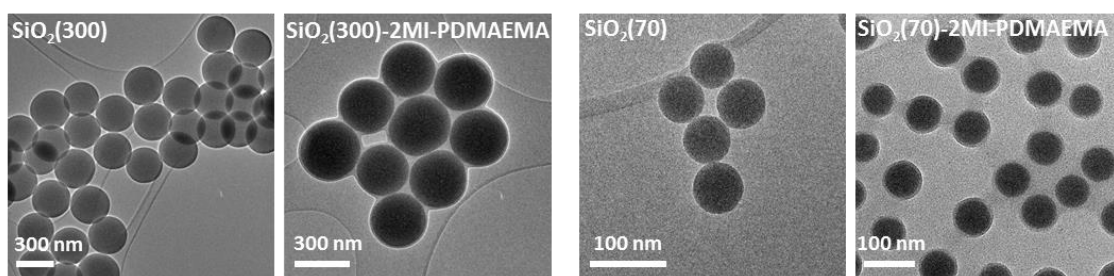
Figure 3.8. TEM images of SiO$_2$-2MI-PDMAEMA for both 70 nm and 300 nm compared to bare silica nanoparticles.

The FTIR data of SiO$_2$(300) and GO after coating with PDMAEMA and POEGMA brush demonstrated successful polymerisation of both brushes from MI as the spectra contain characteristic peaks of PDMAEMA at 1730 cm^{-1} (C=O stretching), 2767 cm^{-1} and 2820 cm^{-1} (CH$_2$ stretching of –N(CH$_3$)$_2$). Vibrations at 1730 cm^{-1} (C=O stretching) and 2870 cm^{-1} (CH$_2$ stretching) were peaks for POEGMA brush in Figure 3.9. For CaCO$_3$, as the volume fraction of polymer brush is negligible compared with that of CaCO$_3$, characteristic peaks were not detectable in FTIR spectra.
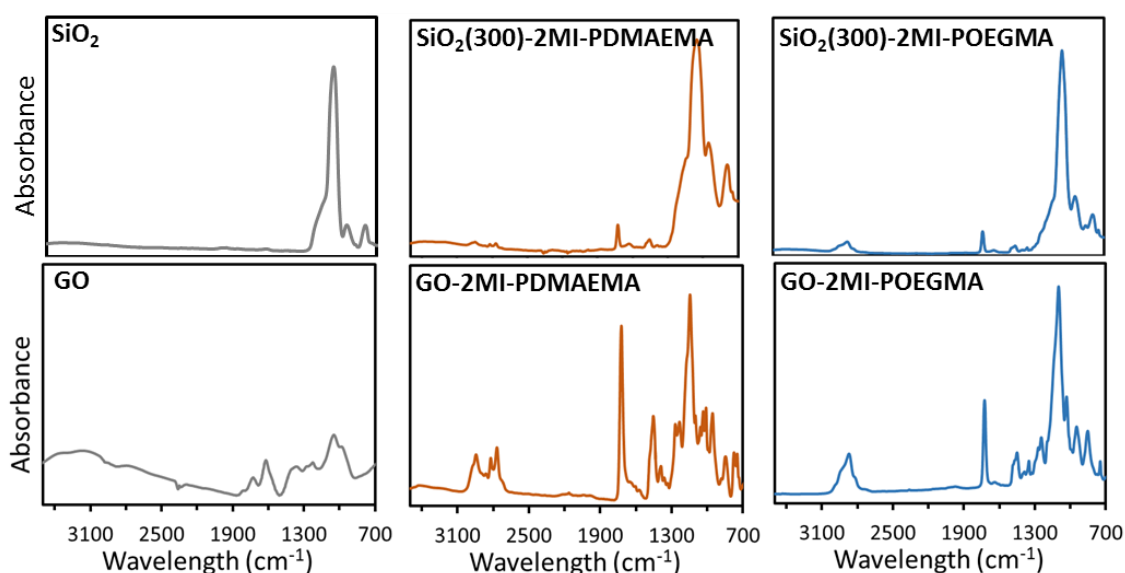
Figure 3.9. FTIR measurement of bare SiO$_2$(300) and GO and after polymerisation of PDMAEMA and POEGMA.

To determine the amount of polymer brush on $SiO_2(300)$ and GO, thermal analysis was carried out. According to Figure 3.10, the amount of MI coated on SiO_2 was 7 wt% compared with bare silica nanoparticles. After polymerisation, the weight percentages of PDMAEMA and POEGMA brush on SiO_2 are 18 % and 43 % respectively, which equal to 20 nm PDMAEMA brush and 60 nm POEGMA brush according to Equation 2.3 in chapter 2. For GO, the main weight loss of GO occurs between 100–250 °C and the loss is mainly due to decomposition of the oxygen-containing functional groups. Based on TGA curves, the weight percentage of MI on GO was 10 %. After polymerisation, the percentage of PDMAEMA and POEGMA brush on GO was 30 % and 35 % respectively.
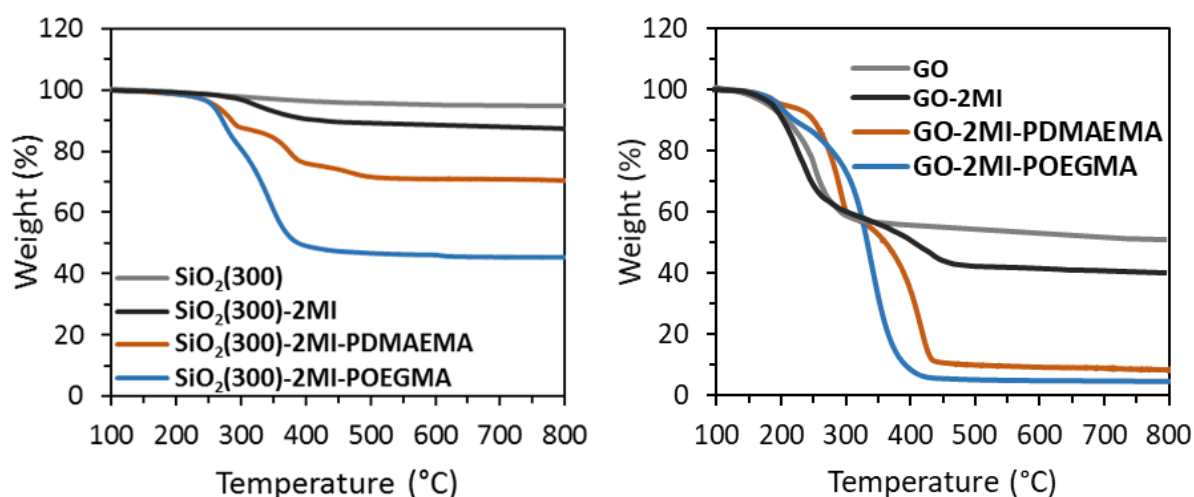
Figure 3.10. TGA measurement of $SiO_2(300)$ and GO before and after polymerisation with PDMAEMA and POEGMA brush.

3.5 Cell viability test

The cytocompatibility of all brush coated nanomaterials was evaluated *via* live/dead assay. HaCaT cells were exposed to PDMAEMA/POEGMA brush coated templates at a concentration of 10 μg/mL for 4 h in serum free OPTIMEM medium and then the

medium was replaced with full culture medium for a further 24 h. Live cells appeared green and dead cells were seen red in colour. The images of live/dead cells and the quantified cell viability were shown in Figure 3.11
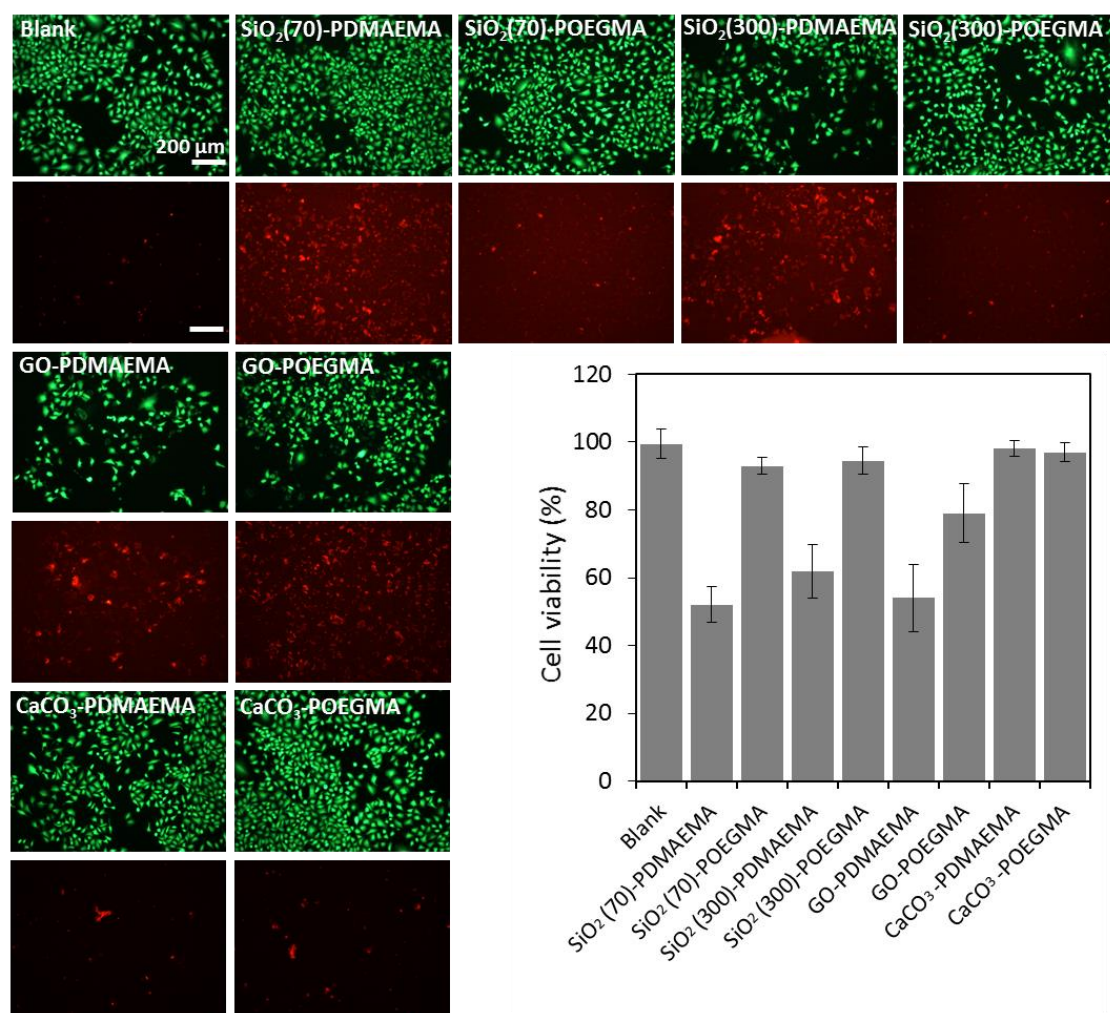
Figure 3.11. Cell viability of PDMAEMA/POEGMA brush coated templates incubated with HaCaT cells by live/dead assay.

Generally, POEGMA brush coated templates showed much better cell viability than PDMAEMA brush coated particles due to the excellent protein resistant properties of POEGMA brush, whilst dense positive charged PDMAEMA brush presented cell toxicity in our previous work. With smaller core size, 70 nm silica nanoparticles with PDMAEMA

showed slightly more toxicity than 300 nm silica nanoparticles. This could be the result from the increase in surface area of the corresponding particles. GO showed higher cell toxicity than other particles on both polymer brush coatings which was possibly due to the high aspect ratio and surface area compared to silica particles. When it was coated with dense cationic polymer brushes, the interaction between cells and materials was promoted and enhanced. For $CaCO_3$, no obvious cytotoxicity was found due to the larger and heavier nature of $CaCO_3$, on which the amount of polymer brushes was negligible that cannot be detected by either FTIR or TGA measurements.

3.6   Cellular interactions

The interaction between nanomaterials and cells is one of the important issues towards understanding the nature of nanomaterials-mediated biological effects. Several routes have been discovered to reveal the mechanism of cellular uptake of nanomaterials, including phagocytosis, macropinocytosis, clathrin-mediated endocytosis, caveolin-mediated endocytosis, and non-clathrin- and noncaveolin-mediated endocytosis.[29] Considering the effect of surface charge of nanomaterials on their cellular uptake, in this study, positively charged PDMAEMA brush and neutral POEGMA brush coated SiO_2 (300 nm) and graphene oxide were involved to study the interaction with HaCaT-GFP cells. Coating of FCP also allows the visualisation of nanomaterials *via* fluorescence microscopy.

SiO_2-PDMAEMA and SiO_2-POEGMA were incubated with HaCaT-GFP cells at 10 µg/mL in serum free OPTIMEM medium for 4 hours before replacing with full culture medium for

further 24 h culture. Cells were then fixed and visualised under confocal microscopy as shown in Figure 3.12A. There was no clear evidence in co-localisation of silica nanoparticles and cells between the different charges (chemistries) of the coatings.
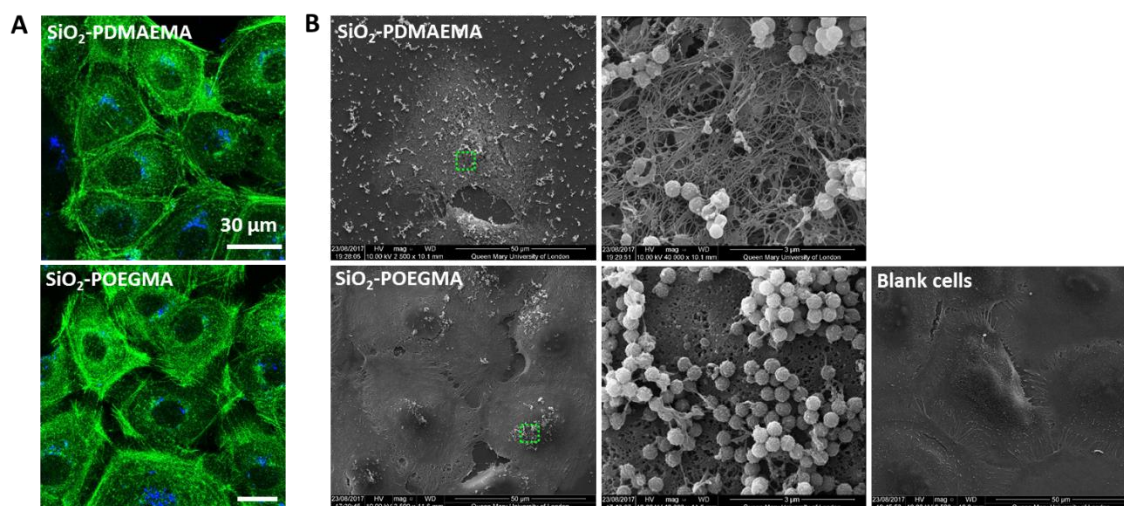
Figure 3.12. Confocal images (A) and SEM images (B) of SiO_2-PDMAEMA and SiO_2-POEGMA particles incubated with HaCaT-GFP cells.

As this result is surprising, considering the known protein resistance of POEGMA brushes and their absence of interactions with most biomacromolecules and cells, SEM was carried out to further explore cell-nanomaterials interactions. After incubating with SiO_2-PDMAEMA and SiO_2-POEGMA the same as described above, HaCaT-GFP cells were fixed, dehydrated, dried and coated with gold before SEM scanning. According to SEM images in Figure 3.12B, more PDMEAMA coated particles were observed at the cell membrane than POEGMA coated particles. Compared with confocal images in which the nanoparticles visualised were those internalised inside cytoplasm, under SEM, only those on the cell membranes can be observed. This may suggest although less POEGMA

coated particles can land and interact with cell membranes due to the protein resistant nature of POEGMA coatings, they were still able to be internalised by the cells. Moreover, it may also result from the neutral surface charge of the POEGMA coated particles, which can cause more particle aggregations that were much easier to observe than single or small accumulations of positively charged SiO_2-PDMAEMA. In additions, under SEM, more cell membrane damage was displayed with SiO_2-PDMAEMA particles, whilst no obvious membrane morphology change was observed with SiO_2-POEGMA compared with blank cells. This also correlates with the cytotoxicity of PDMAEMA brush coated silica nanoparticles showed in Figure 3.11.

3.7 SiRNA delivery with PDMAEMA brush coated silica nanoparticles

Positively charged PDMAEMA brush coated SiO_2 (300) was selected for applications in siRNA delivery. A keratinocyte cell line expressing actin-GFP was selected for simple quantification of siRNA efficiency, using GFP siRNA (allowing imaging of endogenous actin after phalloidin staining). A transfection assay was carried out with nanomaterials and RNA sequences mixed at different N/P ratios of 5, 10 and 15. The commercial transfection agent lipofectamine 2000 was used as a positive control and non-targeting siRNA and blank cells were used as a negative control. The fluorescent intensity ratio of GFP (green)/ phalloidin (red) was measured and compared with the ratio of blank cells which was then determined as the knocking down efficiency. Highest knock down efficiencies (53 $\pm$ 8 %) were measured at N/P=15, slightly less efficient with those measured with lipofectamine (64 $\pm$ 6 %, Figure 15).
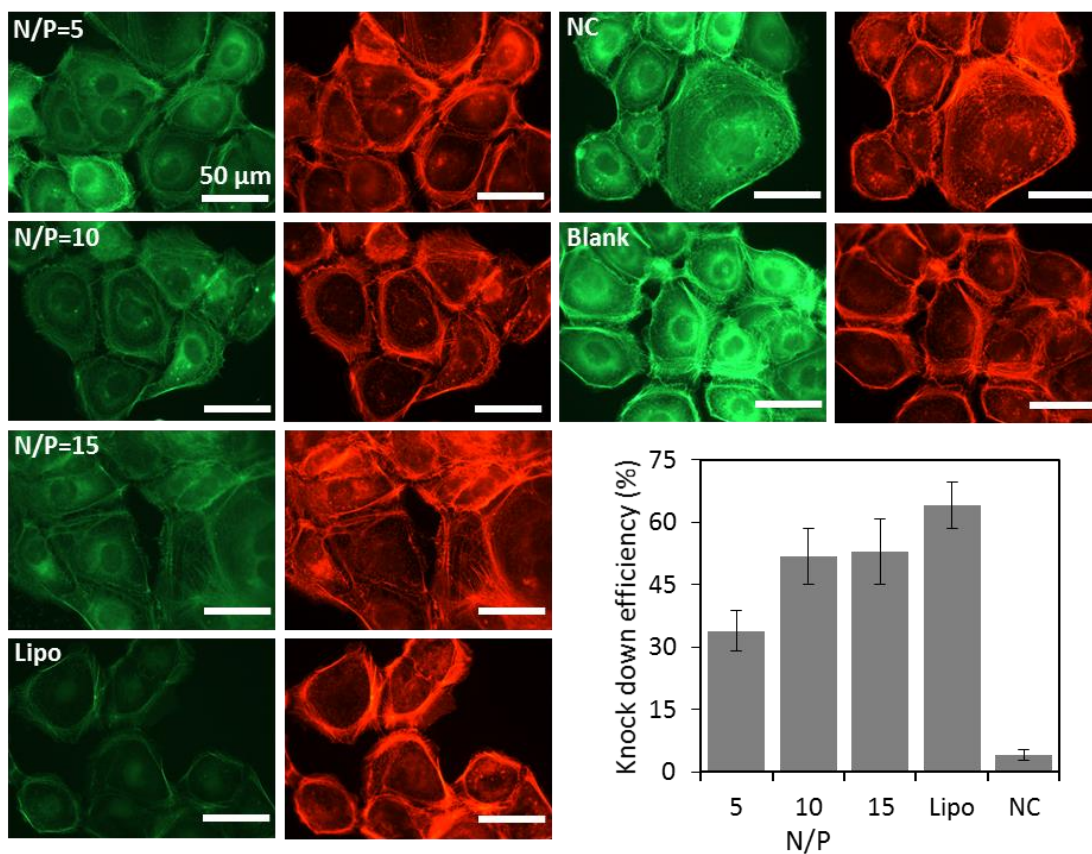
Figure 3.14. Knock down efficiency of SiO$_2$-PDMAEMA/GFP siRNA with HaCaT-GFP cells at different N/P ratio.

In comparison, green fluorescence in the blank and negative control (NC) siRNA groups remained unaltered. In our previous study in chapter 2, a slightly higher transfection efficiency (66 $\pm$ 6 %) of SiO$_2$-PDMAEMA functionalised from mono-silane initiator was observed. It could result from a slightly thinner PDMAEMA brush (20 nm) that achieved in this study compared with previous one (28 nm) in chapter 2.

3.8 Conclusion

In this work, we have developed a novel route to graft polymer brushes and label stable fluorescent dye from templates with different core sizes, shape and surface chemistry using a cationic MI and FCP via LBL and ATRP. Polymer brush growth kinetics was systematically investigated and optimised by coating different layers of MI and conducting polymerisation in solvents of different polarity. Detailed characterisation techniques were applied during the LBL process and after polymerisation to ensure the successful preparation of PDMAEMA or POEGMA coated templates. For particle-cell interactions, POEGMA brush coated nanomaterials displayed improved cytocompatibility compared to PDMAEMA brush coated templates. PDMAEMA brush coated silica nanoparticles were applied to deliver siRNA to HaCaT-GFP cells, successful knock down was observed and compared with commercialised product. In summary, we demonstrated that the LBL of MI and FCP can offer a greater flexibility in the growth and design of polymer brushes and their labelling from templates with a wide range of shapes, sizes and chemistries without additional chemical modification. Moreover, we showed that the resulting nanomaterials can be applied to study cell-nanomaterials interactions and promote siRNA delivery. We believe this novel methodology will provide a simple way of fabricating labelled nanomaterials with controlled polymer brush shells for biomedical applications.

Experimental section

Materials:

2-(Dimethylamino)ethyl methacrylate (DMAEMA, Mn = 157.21), oligo(ethylene glycol methyl ether methacrylate) (OEGMA, M_n = 300), copper (I) chloride (Cu(I)Cl), copper (II) bromide (Cu(II)Br$_2$), 2,2'-bipyridyl (bipy), anhydrous toluene, triethylamine (Et$_3$N) and poly(styrenesulfonate) were purchased from Sigma-Aldrich and used as received. All chemicals and solvents were analytical grades unless otherwise stated. Cu(I)Cl was kept under vacuum until used. Silicon wafers (100 mm diameter, <100> orientation, polished on one side/reverse etched) were purchased from Compart Technology Ltd and cleaned in a Plasma System Zepto from Diener Electronic, for 10 min in air. Silica particles (300 nm, unfunctionalised) were purchased from Bangs Laboratories (supplied as powder). Silica particles (70 nm) were synthesis according to previous report. Calcium carbonate were synthesis according to previous report. Graphene oxide was synthesis by Maria. Triton X-100, gelatin, phallodin–tetramethylrhodamine B isothiocyanate, PFA (paraformaldehyde), DAPI (4,6-diamidino-2-phenylindole), phosphate buffered saline (PBS, 150 mM) were purchased from Sigma Aldrich. Dulbecco's Modified Eagle Medium (DMEM) medium, OPti-MEM™ medium, Fetal Bovine Serum (FBS), trypsin, versene, penicillin-streptomycin, L-glutamine and hoechst 33342 were from Thermo-Fisher. Collagen type I was from BD Bio-science. GFP siRNA (target sequence CGG CAA GCT GAC CCT GAA GTT CAT) and negative control (NC) siRNA (N/A) were purchased from Qiagen®.

Synthesis of macroinitiator (MI):

The synthesis of macroinitiator was reported previously by Chen *et al.*[9] Briefly, it was prepared in a three-step reaction in Figure 1. First, a copolymer of DMAEMA and HEMA was synthesised *via* ATRP, then the hydroxyl groups of HEMA was esterified with 2-bromoisobutyryl bromide and finally DMAEMA was quaternised by methyl iodide. A typical procedure for preparation of the macroinitiator was described below.

Firstly, a solution of DMAEMA (16.9 g, 107.6 mmol), HEMA (3.43 g, 26.4 mmol), 2-propanol (50.39 g), ethyl α-bromoisobutyrate (1.3 g, 6.6 mmol), Cu(II)Br (0.15 g, 0.6 mmol) and 2,2'-bipyridine (bpy, 2.60 g) was degassed with argon for 40 min with continuous stirring at room temperature. The Cu(I)Br catalyst (0.97 g, 6.7 mmol) was added under nitrogen to start the polymerisation. After 15 h, the reaction was terminated by exposure to air. To remove the spent Cu(II) catalyst, the reaction mixture was diluted with DCM and passed through a basic Al_2O_3-colume. The resulting solution was then concentrated and precipitated into diethyl ether. The purified white DMA-HEMA copolymer was filtered, dried under vacuum at room temperature, and characterised by ^{1}H NMR spectroscopy. The final product contained 80 % DMA and 20 % HEMA.

Secondly, esterification of the hydroxy groups of the DMA-HEMA copolymer with excess 2-bromoisobutyryl bromide was carried out. Thus triethylamine (TEA, 26.4 mmol), DMAP (26.4 mmol), and THF (50 mL) were mixed and cooled to 0 °C, followed by the addition of 2-bromoisobutyryl bromide (0.0528 mol). A solution of the DMA-HEMA statistical copolymer (12 g) in THF (50 mL) was added dropwise to this yellow reaction solution over a period of 1 h under dry nitrogen. Subsequently, the reaction

temperature was allowed to rise slowly to room temperature and the esterification was stirred for a further 18 h. The reaction was terminated by addition of EtOH and the white HBr-salt was removed by centrifugation (8000 rpm, 10 min and 15 °C). The product was carefully concentrated using a rotary evaporator below 30 °C and the product was precipitated in diethyl ether (cooled by dry ice). The off-white product was re-dissolved in THF and the purification procedure was repeated once. The product was characterised by ^{1}H-NMR.

Finally, quaternisation was achieved by dissolving this esterified copolymer (6 g) in DMF (50 mL). Then, methyl iodide (2 mL) was added to this stirred solution and quaternisation was allowed to continue for 24 h at 20 °C. This reaction mixture was added to a large excess of THF, and the isolated cationic macroinitiator was redissolved in water and freeze-dried overnight to obtain an off-white solid and then characterised with ^{1}H NMR.

Synthesis of fluorescent conjugated polyelectrolyte (FCP)

Fluorescent conjugated polyelectrolyte was a gift from Prof. Guoli Tu in Wuhan National Laboratory for Optoelectronics, Huazhong University of Science and Thchnology in China, detailed synthesis and characterisation can be found in the reported literature[18].

Layer-by-layer MI on silicon wafers

A piece of plasma-oxidised silicon wafer was immersed in a solution of positively charged MI (2 mg/mL in 0.5 M NaCl) for 1 h at room temperature. Then the wafer was

rinsed with copious of DI water and dried under nitrogen stream. The sample was named as Si-MI. A mixed solution of negatively charged polyelectrolytes was prepared by mixing 10 mL PSS (2 mg/mL in 0.5 M NaCl) with 1 mL FCP (0.5 mg/mL in DMSO) under votex. Then Si-MI was immersed in the above solution for 1 h at room temperature before washing with DI water and drying with nitrogen stream. The sample was names as Si-MI-FCP. By repeating the process of each polyelectrolyte, different layer of MI coated silicon wafers can be obtained. Herein, one layer of MI (Si-MI), two layers of MI (Si-MI-FCP-MI, Si-2MI) and three layers of MI (Si-MI-FCP-MI-FCP-MI, Si-3MI) were prepared to study polymer brush growth kinetics. The dry thickness of each step was measured *via* spectroscopic ellipsometry (JA Woollam, -SE).

Polymer brush growth kinetics on different layers of macroinitiator

To study PDMAEMA brush growth and the evolution of its thickness as a function of time, a solution of $CuBr_2$ (18 mg, 80 µmol), bipy (320 mg, 2.05 mmol), and DMAEMA (42 mmol, 6.6 g) in water/ethanol (4/1 (v/v), 30 mL) or in DMF/water (4/1 (v/v), 30 mL) was degassed using argon bubbling for 30 min. CuCl (82 mg, 828 µmol) was added into this solution quickly and the resulting mixture was sonicated to ensure fully dissolve of CuCl and further degassed for 30 min before polymerisation. MI-coated silicon wafers (~1 × 1 cm^2 each) were placed in reaction vessels and degassed *via* four cycles of high vacuum/nitrogen gas refilling. Subsequently, 1 mL of DMAEMA solution was transferred to reaction vessels under inert atmosphere *via* a syringe. The polymerisation was stopped at different time points (2.5, 5, 10, 20, 30, 60 and 120 min) by immersing the substrates in deionised water, followed by washing with ethanol and drying under a

nitrogen stream. The dry thickness of PDMAEMA brush was measured *via* ellipsometry afterwards.

Layer-by-layer MI on different particle templates

Particles of different size, shape and surface chemistry were investigated to coat MI and generate polymer brushes. Sphere silica nanoparticle (SiO_2, 70 nm and 300 nm), micro-sized cubic calcium carbonate ($CaCO_3$) and graphene oxide sheets (GO) were applied in LBL process. Briefly, 10 mL MI solution (2 mg/mL in 0.5 M NaCl) was prepared and stirred vigorously. 10 mL particle suspension (0.5 mg/mL in DI water) was added to MI solution dropwise and slowly. The resulting suspension was left for stirring at RT for 4 h. The particles were then centrifuged at proper conditions (8000 rpm x 15 min for 70 nm SiO_2 and GO, 4000 rpm x 15 min for 300 nm SiO_2, 2000 rpm x 5 min for $CaCO_3$) before the supernatant was aspirated out. Particles were then washed with 10 mL DI water. The above process repeating for three times. MI coated particles (SiO_2(70)-MI, SiO_2(300)-MI, GO-MI and $CaCO_3$-MI,) were resuspended to 10 mL DI water and added dropwise to 10 mL PSS/FCP mixed solution described before whilst with vigorous stirring for 4 h at RT. The washing and centrifuging process was the same as described above. Eventually, all the particles were coated with two layers of MI, namely SiO_2(70)-MI-FCP-MI (SiO_2(70)-2MI), SiO_2(300)-2MI, GO-2MI and $CaCO_3$-2MI respectively before polymerisation.

Polymer brush growth on different particles

PDMAEMA brush. The polymerisation solution was prepared as described previously by dissolving DMAEMA (6.6 g, 42 mmol), bipy (320 mg, 2.05 mmol), $CuBr_2$ (80 mmol) and CuCl (0.082 g, 828 μmol) in half of the total polymerisation solvent (DMF/water 4/1 (v/v), 15 mL). 10 mL particle-2MI dispersion in DMF/water 4/1 (v/v) obtained in above were degassed for 30 minutes with argon bubbling while stirring. An equal volume of DMAEMA monomer solution was added to the suspension. Polymerisation was allowed to proceed under argon at RT for 60 min. To terminate the polymerisation, the particle dispersion was diluted using deionised water and bubbled with air until the colour changed from dark brown to blue (oxidisation of CuCl). The particles were recovered *via* centrifugation, washed successively with water to get rid of the catalysts and residual monomer and finally the particles were dispersed in 10 mL deionised water and stored in the fridge.

POEGMA brushes. The procedure of POEGMA brush synthesis was similar to that used for PDMAEMA brushes except for the difference in monomer solution and polymerisation time. For OEGMA polymerisation, the monomer solution was: OEGMA (12.6 g, 42 mmol), bipy (320 mg, 2.05mmol), $CuBr_2$ (80 mmol) and CuCl (0.082 g, 828 μmol) in 15 mL solvent (DMF/water 4/1 (v/v), 15 mL). The reaction was kept in room temperature for 120 min before termination.

Polymer brush coated particle characterisation

Size and zeta potential measurement. Zeta potential measurement was applied to track the change of polyelectrolyte layer on all the particles after each LBL process and polymerisation. Size measurement was applied to only silica nanoparticles (both 70 nm and 300 nm) after each LBL step and polymerisation with a Malvern zetasizer nano ZS. Samples were prepared by dispersing particles in DI water until obtaining a slightly cloudy solution and then sonicated for 10 min with shaking at regular intervals. Each samples were measured in triplicates at 25°C and the average result was taken as the final hydrodynamic diameter or zeta potential.

Thermogravimetric (TGA) measurement. By using TGA, the dry mass of polymer particles was determined. Herein, the TGA was performed in air using a TA Instruments Q500. All samples were heated from room temperature to up to 1000 °C at a heating rate of 10 °C/min and dried under vacuum at room temperature prior to TGA runs.

Fourier transform infrared - attenuated total reflectance (FTIR-ATR). FTIR was used to characterise the different chemical groups expected within the respective materials through obtaining an infrared spectrum. ATR-FTIR spectroscopy in this study was carried out using a Bruker Tensor 27 with an MCT detector (liquid N2 cooled). Spectra were taken at a resolution of 4 cm^{-1} with a total of 128 scans per run. FTIR spectroscopy was carried out on polymer brush coated silica nanoparticles and graphene oxide.

Scanning electron microscopy (SEM). SEM measurements were carried out using a JEOL 2010 transmission electron microscope with a LaB6 filament, operated at 200 kV.

Samples were prepared by dropping the diluted brush coated silica nanoparticle suspension on a copper grid with porous carbon film and drying at room temperature.

Transmission electron microscopy (TEM). TEM measurements were carried out using a JEOL 2010 transmission electron microscope with a LaB6 filament, operated at 200 kV. Samples were prepared by dropping the diluted brush coated silica nanoparticle suspension on a copper grid with porous carbon film and drying at room temperature.

Fluorescent imaging. Due to the coating of fluorescent conjugated polyelectrolyte, particles were able to be visualised by fluorescent microscope. Herein, Zeiss LSM710 Confocal and Elyra supperresolution microscope was applied to detect the fluorescent particles after polymerisation. Briefly, samples were prepared by dropping the particles suspension on a glass slide and drying at RT before mounting to another coverslip.

Cell viability

HaCaT Cell culture and passage. DMEM media supplied with 10 % FBS, 1 % Penicillin-Streptomycin (P/S) and 1 % glutamine was used to culture HaCaT cells in 37°C/5 % CO_2 incubator. To harvest HaCaT cells (T75), cells were washed twice with pre-warmed PBS solution and then cells were detached from the flask by trypsinisation (versene/trypsin, 4/1 v/v, 5 mL, 37°C). 15 mL of DMEM medium was then added to the flask to quench the trypsin. Cells were transferred to a 50 mL centrifuge tube and centrifuged at 1200 rpm for 5 min. After discarding the supernatant solution, the pellet was resuspended in 10 mL FAD medium and the concentration of cells was measured with a haematocytometer.

Cell viability test. Cells were seeded at a density of 35 k cells per well (in 500 μL of DMEA medium) in 24-well plates 24 h prior. Templates coated with PDMAEMA and POEGMA brush with final concentration of 10 ug/mL were added into each well for 4 h in 0.5 mL serum free OPTI-MEM medium and then the medium was replaced by full culture DMEM medium for further 24 h incubation. Cell viability was carried out by live/dead assay in which, cells were incubated in 500 μL DMEM medium of 4 mM calcein AM, 2 mM ethidium homodimer and hoechst 33342(for staining cell nucleus) for 30 min at 37 °C prior to imaging. Fluorescence imaging was used to capture the live-dead cells and these were counted *via* ImageJ to obtain the percentage of live cells of total number of cells.

Particle-cell interaction

Fluorescent. The protocol for culturing and passaging HaCaT-GFP cells was the same as for HaCaT cells. $SiO_2(300)$ and GO coated with PDMAEMA and POEGMA brush with final concentration of 10 ug/mL were added into each well for 4 h in 0.5 mL serum free OPTI-MEM medium and then the medium was replaced by full culture DMEM medium for further 24 h incubation before imaging.

SEM. After uptaken silica nanoparticles with different polymer brush coating, cell samples were characterised *via* SEM to check the morphology. Cells seeded on class coverslips were fixed after 24 h particle uptake with 2.5% glutaraldehyde in PBS for 2 h at room temperature. Then washed 3 times with 0.1 M PBS and dehydrated with a series of ethanol washings by increasing the ethanol content from 20% to 100%, each wash

repeated twice for 5 min. Critical Point Drying was then performed (EMS 850 Critical Point Dryer) to dry the cell samples and then they were coated with Gold (SC7620 Mini Sputter Coater, Quorum Technologies) for 60 s coating at 20 mA process current before SEM imaging.

Transfection assay

HaCaT-GFP cells were seeded at a density of 35 k/well on glass cover slips pre-treated with collagen in 24-well plates, 24 h prior to the transfection assay. A final siRNA concentration of 50 nM/well was used. 100 μL SiO_2-PDMAEMA/GFP siRNA complexes were prepared at N/P=5, 10 and 15, in serum free OPTI-MEM medium. After removing the DMEM medium, cells were washed twice with pre-warmed serum free OPTI-MEM medium and another 400 μL was added. 100 μL siRNA complex was then added dropwise to each well and mixed by shaking gently. Cells were incubated with siRNA complexes for 4 h in the incubator and the medium was then replaced by 500 μL full culture DMEM medium for a further 24 h of incubation. Lipofectamine® 2000 complexed with GFP siRNA/negative control (NC) siRNA (protocol according to the manufacturer's instruction with a final siRNA concentration of 50 nM/well) was used as a positive/negative control. The transfected cells were washed with PBS three times, fixed in paraformaldehyde (PFA, 4 %, 10 min) and permeabilised with Triton X-100 (0.2 %, 5 min). Cells were then stained with TRITC-phalloidin (1:1000) and DAPI (4,6-diamidino-2-phenylindole, 1:1000) in blocking buffer (10% FBS and 0.25% gelatin from cold water fish skin, Sigma-Aldrich) and kept at room temperature for 1 h. Cover slips with fixed

cells were mounted on glass slides before imaging with a Leica DMI4000 fluorescence

microscope.

References

(1) Krishnamoorthy, M.; Hakobyan, S.; Ramstedt, M.; Gautrot, J. E., *Chemical Reviews* **2014,** *114* (21), 10976-11026.

(2) Barbey, R.; Lavanant, L.; Paripovic, D.; Schuwer, N.; Sugnaux, C.; Tugulu, S.; Klok, H. A., *Chemical Reviews* **2009,** *109* (11), 5437-5527.

(3) Edmondson, S.; Armes, S. P., *Polymer International* **2009,** *58* (3), 307-316.

(4) Edmondson, S.; Vo, C. D.; Armes, S. P.; Unali, G. F.; Weir, M. P., *Langmuir* **2008,** *24* (14), 7208-7215.

(5) Lee, M. T.; Hsueh, C. C.; Freund, M. S.; Ferguson, G. S., *Langmuir* **1998,** *14* (22), 6419-6423.

(6) Estillore, N. C.; Park, J. Y.; Advincula, R. C., *Macromolecules* **2010,** *43* (16), 6588-6598.

(7) Liu, Y.; Klep, V.; Zdyrko, B.; Luzinov, I., *Langmuir* **2004,** *20* (16), 6710-6718.

(8) Chen, X. Y.; Armes, S. P., *Advanced Materials* **2003,** *15* (18), 1558.

(9) Chen, X. Y.; Armes, S. P.; Greaves, S. J.; Watts, J. F., *Langmuir* **2004,** *20* (3), 587-595.

(10) Wei, Q. B.; Wang, X. L.; Zhou, F., *Polymer Chemistry* **2012,** *3* (8), 2129-2137.

(11) Kolanowski, J. L.; Liu, F.; New, E. J., *Chem Soc Rev* **2018,** *47* (1), 195-208.

(12) Liang, J.; Tang, B. Z.; Liu, B., *Chem Soc Rev* **2015,** *44* (10), 2798-811.

(13) Yee, D. W.; Schulz, M. D.; Grubbs, R. H.; Greer, J. R., *Advanced Materials* **2017,** *29* (16).

(14) Jiang, R. M.; Liu, H.; Liu, M. Y.; Tian, J. W.; Huang, Q.; Huang, H. Y.; Wen, Y. Q.; Cao, Q. Y.; Zhang, X. Y.; Wei, Y., *Materials Science & Engineering C-Materials for Biological Applications* **2017,** *81*, 416-421.

(15) Oz, Y.; Arslan, M.; Gevrek, T. N.; Sanyal, R.; Sanyal, A., *Acs Applied Materials & Interfaces* **2016,** *8* (30), 19813-19826.

(16) Gao, X.; Hu, B.; Tu, G., *Organic Electronics* **2014,** *15* (7), 1440-1447.

(17) Liu, Z.; Fang, C.; Cai, X.; Gao, X.; Li, P.; Zhang, Q.; Tu, G., *Dyes and Pigments* **2018,** *156*, 39-44.

(18) Zhu, X.; Xie, Y.; Li, X.; Qiao, X.; Wang, L.; Tu, G., *Journal of Materials Chemistry* **2012,** *22* (31), 15490-15494.

(19) Qin, W.; Yu, W.; Zi, W.; Liu, X.; Yuan, T.; Yang, D.; Wang, S.; Tu, G.; Zhang, J.; Liu, F. S.; Li, C., *Journal of Materials Chemistry A* **2014,** *2* (37), 15303-15307.

(20) Zhang, Y.; Shi, J.; He, X.; Tu, G., *Journal of Materials Chemistry A* **2016,** *4* (35), 13519-13524.

(21) Liu, J.; Li, J.; Liu, X.; Li, F.; Tu, G., *ACS Applied Materials and Interfaces* **2018,** *10* (3), 2649-2657.

(22) Chen, L.; McBranch, D. W.; Wang, H.-L.; Helgeson, R.; Wudl, F.; Whitten, D. G., *Proceedings of the National Academy of Sciences* **1999,** *96* (22), 12287-12292.

(23) Wang, D.; Gong, X.; Heeger, P. S.; Rininsland, F.; Bazan, G. C.; Heeger, A. J., *Proceedings of the National Academy of Sciences* **2002,** *99* (1), 49-53.

(24) Liu, B.; Bazan, G. C., *Chemistry of Materials* **2004,** *16* (23), 4467-4476.

(25) McQuade, D. T.; Pullen, A. E.; Swager, T. M., *Chemical Reviews* **2000,** *100* (7), 2537-2574.

(26) Pu, K.-Y.; Liu, B., *Biosensors and Bioelectronics* **2009,** *24* (5), 1067-1073.

(27) Kan-Yi, P.; Bin, L., *Advanced Functional Materials* **2011,** *21* (18), 3408-3423.

(28) Waters, J. C.; Wittmann, T., Chapter 1 - Concepts in quantitative fluorescence microscopy. In *Methods in Cell Biology*, Waters, J. C.; Wittman, T., Eds. Academic Press: 2014; Vol. 123, pp 1-18.

(29) Deng, J.; Gao, C. Y., *Nanotechnology* **2016,** *27* (41).

CHAPTER 4

Quaternised Cationic Polymer Brush

Coated Silica Nanoparticles for SiRNA

Long-term and Efficient Delivery

Abstract：

Long-term and efficiency siRNA delivery is of particular interest during gene therapy to avoid repeated administration of siRNA therapeutics and other biological research which requires long-term RNA transfection. To achieve more sustained RNA delivery, three different types of polymer brushes: PDMAEMA brush coated silica nanoparticles SiO_2-PDMAEMA, SiO_2-PDMAI (quaternised with methyl iodide) and SiO_2-PDMABr (quaternised with acid cleavable acetal molecule) were prepared and investigated for their binding affinity to oligonucleotides and long-term siRNA transfection ability. SiO_2-PDMAI exhibited the longest and highest siRNA transfection among the three vectors with improved cell viability. The results from co-localisation study revealed that SiO_2-PDMAI has the best siRNA retention ability.

4.1 Introduction

Gene delivery relies on the encapsulation of DNA/RNA coding for a gene of interest, which is ideally delivered to targeted cells, providing the treatment of both inherited and acquired diseases.[1] Short interfering RNA (siRNA)[2, 3] is proposed to be at the centre of the next-generation therapeutics because of its merits of having unrestricted application to target any protein, simple manufacturing process, and low cost.[4] However, effective therapies using siRNA for a sufficient period of time has been restricted due to the lack of an efficient delivery systems (but some siRNA based therapies are currently in late phases of clinical trials).[5, 6] SiRNA typically achieves only transient silencing, which is limited to relatively short time frames.[7] Hence, repeated administration of siRNA therapeutics[8] is required during the process of gene therapy (especially for some chronic diseases[9]), which is relatively constraining for patients, and can lead to poor therapeutic efficiency.

The interest in designing non-viral vectors for gene delivery has never waned as they are less hazardous in terms of antigen-specific immune responses compared to viral vectors, although in general transfection efficiency of non-viral vectors are lower.[10, 11] Encapsulation of naked RNA by cationic polymers[12], polypeptides[13], or lipids[14] such as Lipofectamine 2000 have been a major player in commercial products although their present high cytotoxicity[15] and short-term transfection[16] is restrictive. Previously, we have reported using dense poly(2-(dimethylamino)ethyl methacrylate) (PDMAEMA) brush coated silica nanoparticles prepared *via* 'grafting from' method for the encapsulation and delivery of siRNA.[17] SiO_2-PDMAEMA showed excellent siRNA uptake and transfection in a short period of time (24 h after transfection) and reached

comparable levels as Lipofectamine 2000. However, longer-term transfections are required, although the mechanisms enabling such longer-term delivery are not clear.

To achieve more sustained RNA delivery, we proposed to alter the chemistry of polymer brushes and therefore their binding affinity to oligonucleotides. Three different types of polymer brushes, differing by the chemistry of their side-chains were investigated: polymer brush (PDMAEMA) coated silica nanoparticles SiO_2-PDMAEMA, SiO_2-PDMAI (PDMAEMA quaternised with methyl iodide) and SiO_2-PDMABr (quaternised with 1-acetoxyethyl-2-bromoacetate (acetal bromide)) were prepared in this work. As a tertiary amine methacrylate, SiO_2-PDMAEMA has attracted much attention due to its pH-responsive characteristics[18]. After quaternisation with methyl iodide, SiO_2-PDMAI becomes permanently charged, regardless of pH (strong polyelectrolyte). This strong polyelectrolyte PDMAI brush was expected to provide more stable siRNA encapsulation, which should affect the long-term release of siRNA and resulting transfection efficiency. On the other hand, changes in pH in different cellular compartments, such as lysosomes (pH 4.5–5), endosomes (pH 5.5–6), and the cytosol (pH 7.4), can be exploited to speed up the release of oligonucleotides.[19-22] Indeed, acid-sensitive acetal functions makes then optimal agents for the targeting of endosomes/lysosomes as site of pH-induced cleavage. PDMABr brush will be cleaved under acidic environment (e.g. in the endosome/lysosome) and become zwitterionic, which would be expected to promote the release of siRNA molecules.

Hence, the development of the proposed three vectors, with different chemistry and pH responsiveness, will help understand the kinetics of RNA dissociation and the mechanism *via* which cationic polymer brush coated particles promote effective siRNA

molecule delivery. We observed a strong siRNA binding on PDMAEMA and PDMAI brushes that wasn't affected by changes in pH, whilst siRNA molecules bound slightly less with PDMABr and displayed a strong pH-induced release. SiRNA silencing kinetics of the three delivery vectors in HaCaT-GFP cells were evaluated over different transfection periods. Finally, fluorescent labelled vectors and siRNA were used to track the cellular uptake and release of siRNA *in vitro*.

4.2 Preparation of methyl iodide and acetal functionalised PDMAEMA on silicon substrates.

Acetals and ketals have attracted significant attention as pH responsive materials since a few decades ago, because they yield charge-neutral and potentially non-toxic by products upon cleavage.[23] They have been widely used as building blocks for polymers[24, 25], nanoparticles[26], and antibody-drug conjugates[27], as well as in protein purification[28] and solid phase synthesis[29]. More recently, they have been pursued in a variety of areas including controlled release applications and nucleic acid delivery.[30]
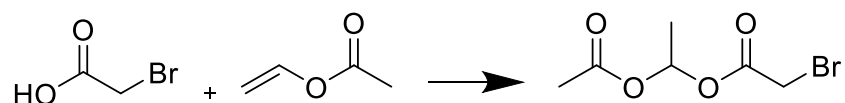

Figure 4.1. Synthesis route of 1-acetoxyethyl-2-bromoacetate (acetal bromide).

In this project, to prepare acid-cleavable brush coated silica particles, acetal bromide was synthesised *via* the reaction route described in Figure 4.1. After reaction, the

product was purified through a chromatography and characterised by H^1-NMR, with identified peaks shown in Figure 4.2.

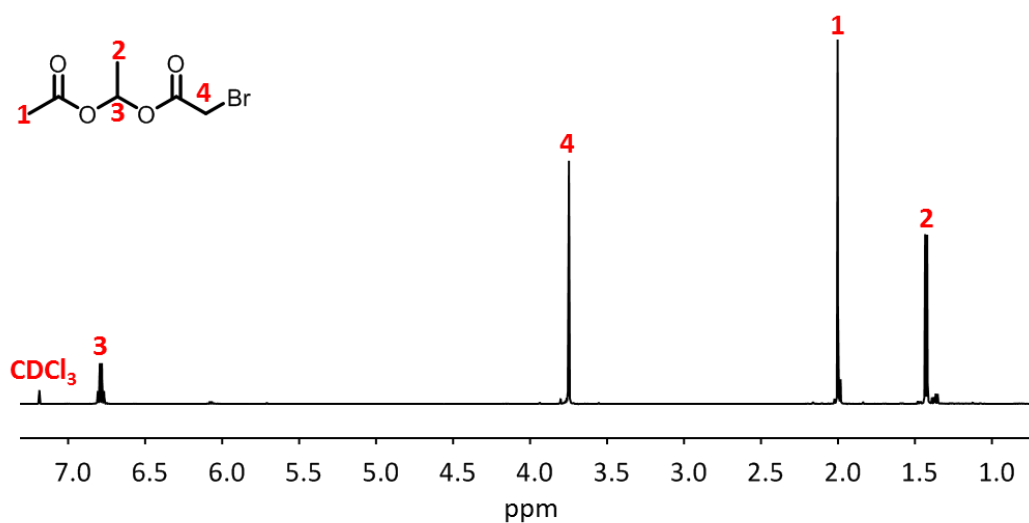**Figure 4.2.** H^1-NMR spectrum of acetal bromide in CDCl$_3$.

To determine the successful reaction of acetal bromide with PDMAEMA, free PDMAEMA polymer was firstly synthesised and then reacted with acetal bromide. acetal bromide functionalised PDMAEMA was then characterised with H^1-NMR.
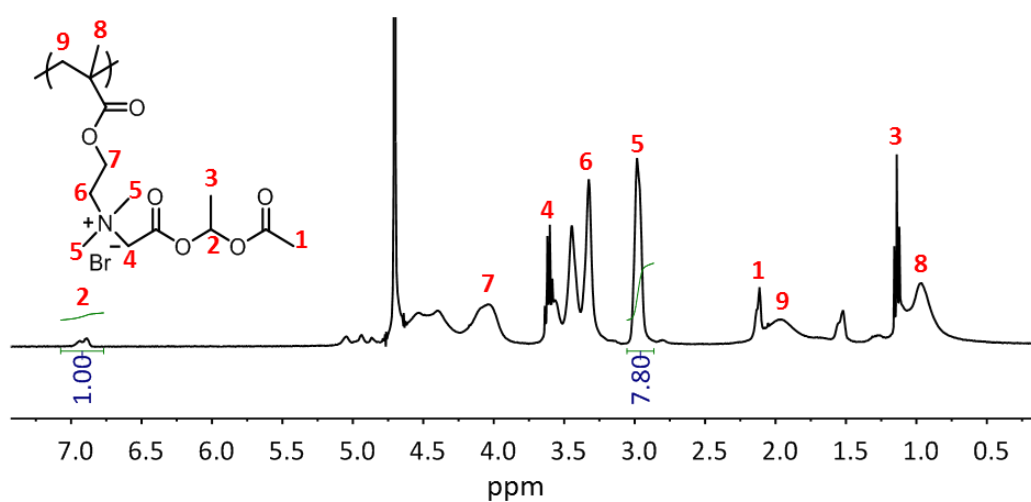

Figure 4.3. H^1-NMR spectrum of acetal bromide functionalised free PDMAEMA (PDMABr) in D$_2$O.

The characteristic peaks of 1, 2, 3 and 4 from acetal bromide shown in the spectrum in Figure 4.3 suggested the successful functionalisation. 77 % of tertiary amine on PDMAEMA were functionalised with acetal bromide, calculated from the integration ratio of peak 2 and 5 in Figure 4.3.
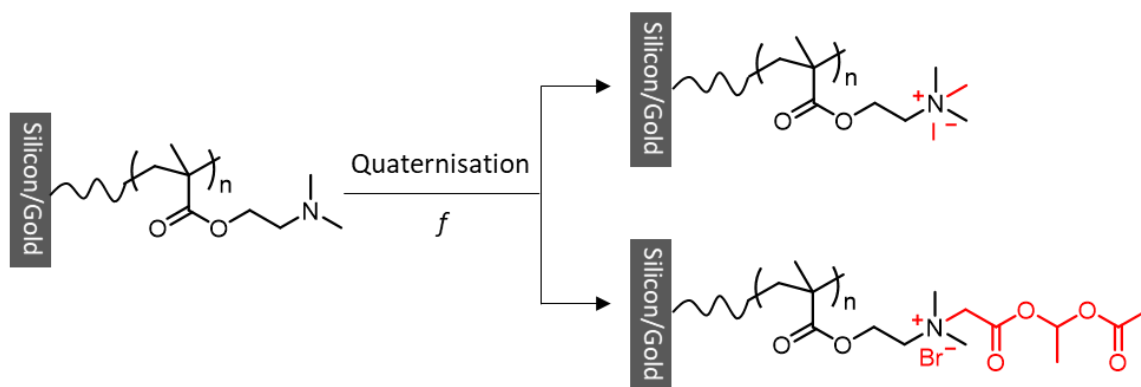
Figure 4.4. Synthesis route and chemical structure of methyl iodide functionalised PDMAEMA (PDMAI) and acetal bromide functionalised (PDMABr).

Methyl iodide and the obtained acetal bromide were then used to quaternise tertiary amine of PDMAEMA brush coated silicon wafers, as illustrated in Figure 4.4. 30 nm PDMAEMA brush coated silicon substrates were prepared according to previous report. After quaternisation, 12 nm and 10 nm dry thickness increase were detected from methyl iodide and acetal bromide functionalised PDMAEMA brush respectively *via* ellipsometry, indicating the successful quaternisation.

4.3 Characterisation of methyl iodide and acetal functionalised PDMAEMA on silicon substrates.

The chemical composition of PDMAEMA, PDMAI and PDMABr brushes coated silicon substrates was further characterised by X-ray photoelectron spectroscopy (XPS, see Figure 4.5).
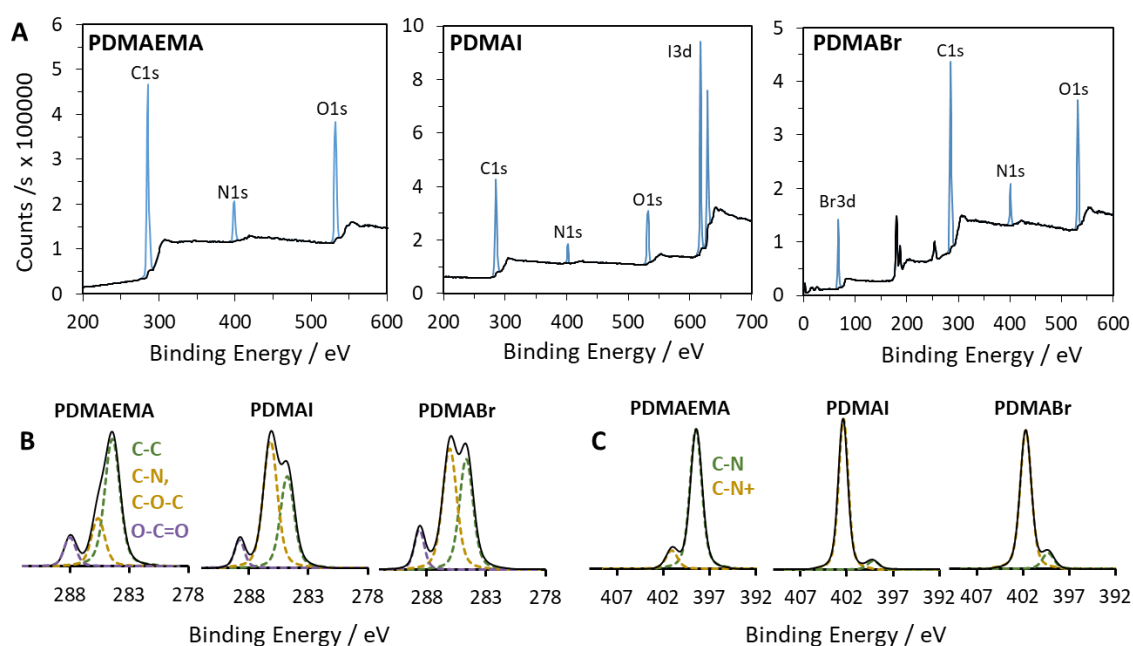
Figure 4.5. XPS wide scan spectrum (A) and high-resolution spectrum (B and C) for composite measurement of silicon-PDMAEMA, Silicon-PDMAI and Silicon-PDMABr.

The brush thicknesses used (above 30 nm) are greater than the sampling depth of XPS, which is typically up to ~10 nm for Al Kα radiation, depending upon the specific core level photoelectrons.[31] Thus the majority of detected photoelectrons are originated from the brush layer rather than the initiator layer. The appearance of N 1s, C 1s and O 1s signals in the wide scan spectrum (Figure 4.5A) was attributable to atoms in

PDMAEMA brushes. The iodide/bromide peaks in the survey spectra were associated with the counterions of quaternary ammonium salts generated after quaternisation.

High-resolution XPS of the C 1s photoemission envelope for PDMAEMA brush shown in Figure 4.5B were fit to the three unique carbon moieties of PDMAEMA: C-C (284.5 eV), C-N (285.9 eV) and O-C=O (288.5 eV). After quaternisation, the percentage of C-N was increased. The most notable changes in the XPS results were observed in the high resolution N 1s spectra in Figure 4.5C. Around 10 % of the N 1s peak corresponded to C-N+ on the unquaternised surfaces, likely due to some degree of amine protonation, this increased to around 90% following quaternisation with methyl iodide/acetal bromide. Unquaternised nitrogen was observed for both PDMAI and PDMABr brush indicated that the reaction did not reach 100% completion. This can likely be attributed to the reduced accessibility of some amines within the brush and is in agreement with the H^1-NMR results obtained on free PDMAEMA polymers (see Figure 4.3).
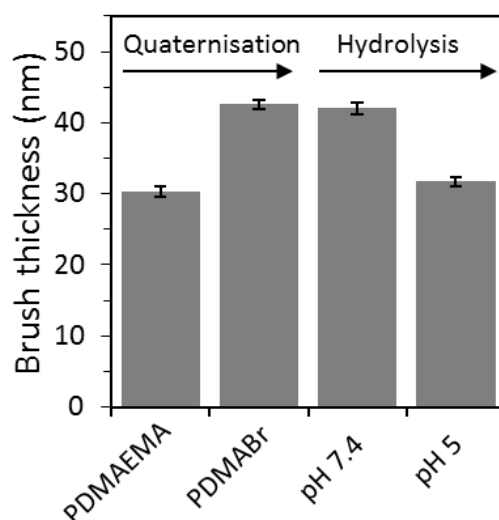

Figure 4.6. PH responsiveness: dry thickness changes of PDMABr brush on silicon wafer at pH 5 and 7.4 PBS after 4 h incubation.

Addition of acidic aqueous solutions to acetals will transform them back into ketones (or aldehydes). Hence, the dry brush thickness of PDMABr before and after hydrolysis in pH 5 PBS was measured. PDMABr brush incubated in neutral pH was used as control. A decrease of brush thickness around 12 nm back to unfunctionalised PDMAEMA brush (30 nm) was detected after hydrolysis in acidic solutions (Figure 4.6), which suggested the full cleavage of acetal on PDMABr brush after 4 h incubation. While, the thickness of PDMABr brush incubated in pH 7.4 PBS remains unchanged.

The behaviour of polyelectrolyte brushes is governed by several factors, including excluded volume, electrostatic interactions (mainly repulsion between charged monomer units) and osmotic pressure imparted by the absorption of solvent and counterions.[32-36] For weak polybases, such as PDMAEMA brush, at pH values below pKa, PDMAEMA brushes become charged due to protonation of tertiary amine.[37] The charging process causes the brush to swell due to the increase coulombic repulsion between chains and the associated osmotic pressure rise that occurs as a result of ingress of solvent and counterions into the brush. Whilst at high pH, above the repeat unit pKa, the brush is deprotonated and becomes neutral.[37] The reverse neutralisation of the charged groups causes the brush to collapse as expulsion of both the water and counterions from inter- and intra-chains.[35]

To characterise the brush responsiveness under different salt and pH conditions, *in situ* ellipsometry was used. All brushes were equilibrated in solution to allow the polymer brush chains to fully disentangle. In this study, the brushes were exposed to DI water, 150 Mm NaCl, pH 7.4 PBS, pH 5 PBS and pH 9 PBS until an equilibrium brush thickness

was observed. In DI water, PDMAEMA brushes were partially protonated and undergo a slight swelling with a ratio of 1.5, as shown in Figure 4.7.
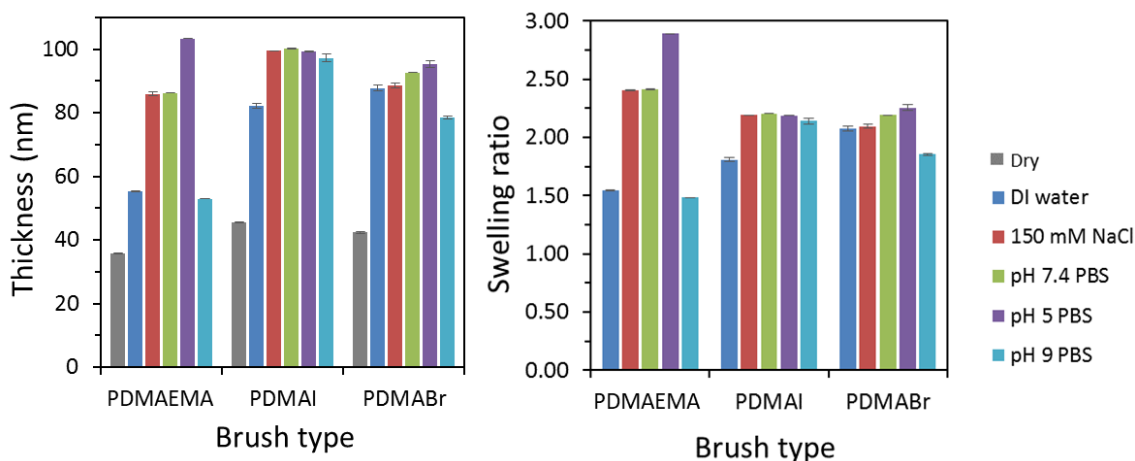
Figure 4.7. Wet ellipsometry measurements of PDMAI and PDMABr brushes in different buffers and at different pH.

The brushes incubated in 150 mM NaCl and pH 7.4 PBS presented a higher degree of swelling than in DI water. At low ionic strength, the brush behaves more like an "osmotic brush" due to the weak dissociation of the charged group on PDMAEMA brush. Here hydroxide ions are associated with the brush to preserve electroneutrality and increase the pH of the environment within the brush, resulting in the low level of charge of the brush. When increasing the ionic strength, the tertiary amine moieties on the PDMAEMA brush becomes more protonated and the electrostatic repulsion between the brush chains increases.

At pH 5, well below the pKa of the free polymer, the brush chains are highly protonated and undergo significant swelling with a ratio near 3. In contrast, when the pH was

adjusted above the pKa, the brush became hydrophobic, with decreased brush swelling, though still observed to display a degree of water association within the structure. After quaternisation, PDMAI and PDMABr become permanently charged, regardless of the pH and ionic strength. No significant thickness change was observed with PDMAI brush when incubated in different salt solutions and at different pH, which indicated that most of the tertiary amine of PDMAEMA brush were quaternised by methyl iodide. Moreover, the permanent charge groups can increase the brush chain repulsion to help the swelling of PDMAI brush. For PDMABr brushes, a slight increase of swelling and collapse observed in pH 5 and 9, which could result from unfunctionalised tertiary amine groups, implying incomplete quaternisation with acetal bromide.

4.4   SiRNA binding on quaternised PDMAEMA brushes

Previously, we have reported the effect of the PDMAEMA brush density on the binding and infiltration of oligonucleotides, and observed highly stable siRNA binding on dense PDMAEMA brushes, compared to sparse brushes.[17] Herein, the binding and release of siRNA by dense PDMAEMA (30 nm), PDMAI and PDMABr brushes was investigated and monitored *via* surface plasmon resonance (SPR). Fast adsorption of siRNA was observed on all brushes as shown in Figure 4.8, though 1/3 reduced adsorption of siRNA was achieved on PDMABr brushes compared to PDMAEMA and PDMAI brushes (which reached similar levels of adsorption). This could be due to the increased steric hindrance between polymer chains associated wtih PDMABr after quaternisation, resulting in the reduced infiltration of oligonucleotides. After injection, all surfaces were equilibrated in PBS for 300 s and the absorption of siRNA was measured. Subsequently, an acidic

solution of pH 5 PBS was introduced to monitor the siRNA release on different pH responsive brushes. Upon continuous washing with pH 5 PBS, stable retention was observed on PDMAEMA and PDMAI brushes with negligible loss of siRNA. An expected siRNA release and binding fluctuation correlated with the cleavage of acetal on PDMABr brushes. The siRNA binding level dropped to less than half compared with initial binding levels. Consequently, high binding and stable retention of siRNA may be beneficial for long-term siRNA delivery, whilst the unique properties of PDMABr brushes could promote siRNA release through hydrolytic cleavage.
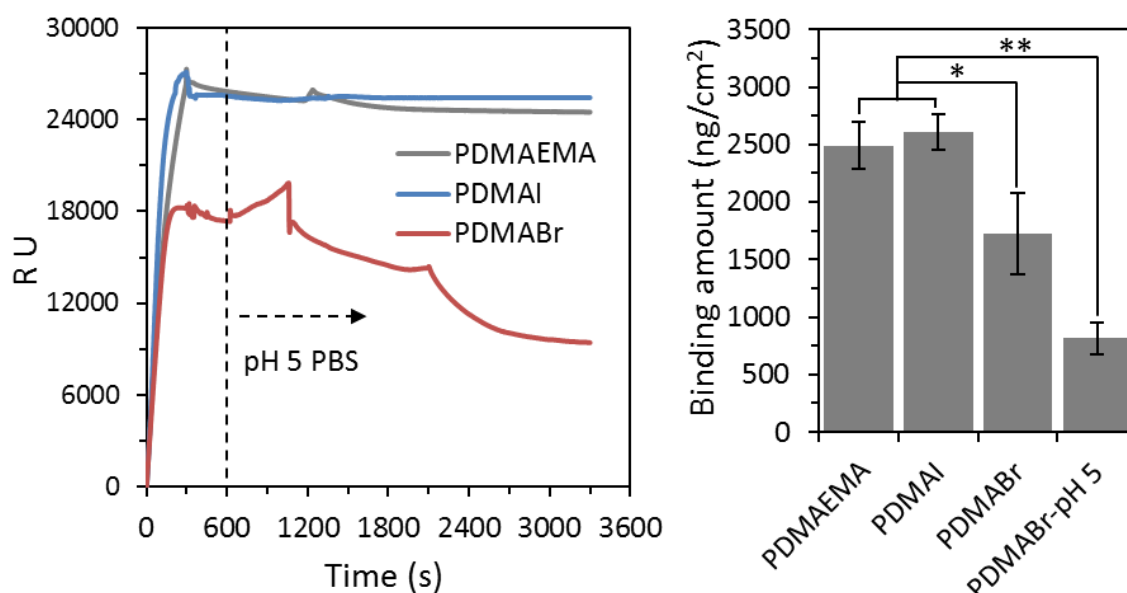

Figure 4.8. SiRNA binding on PDMAEMA, PDMAI and PDMABr brushes and responsiveness to acidic environment (pH 5 PBS was applied after finishing siRNA injection and equilibration showing dash lines in the figure).

4.5   Preparation and characterisation quaternised PDMAEMA brush on silica nanoparticles

The synthesis of PDMAEMA brush-coated 300 nm silica nanoparticles and the control of the brush growth at targeted thicknesses were reported previously.[18] Subsequently, SiO_2-PDMAEMA particles were quaternised with methyl iodide and acetal bromide for preparing SiO_2-PDMAI and SiO_2-PDMABr. The size distribution of these brush coated particles was characterised in pH 7.4 PBS with dynamic light scattering (DLS). The obtained SiO_2-PDMAEMA particles were well-dispersed in PBS with a size of 460 ± 11 nm (Figure 4.9) and zeta potential of 14.2 ± 3.1 mV. After quaternisation, the steric hindrance between polymer chains was enhanced due to the increased molecular weight and this effect was more pronounced with SiO_2-PDMABr, possibly due to the increased size of the acetal groups. The size increase of SiO_2-PDMAI (530 ± 23 nm) and SiO_2-PDMABr (651 ± 17 nm) are reported in Figure 4.9.
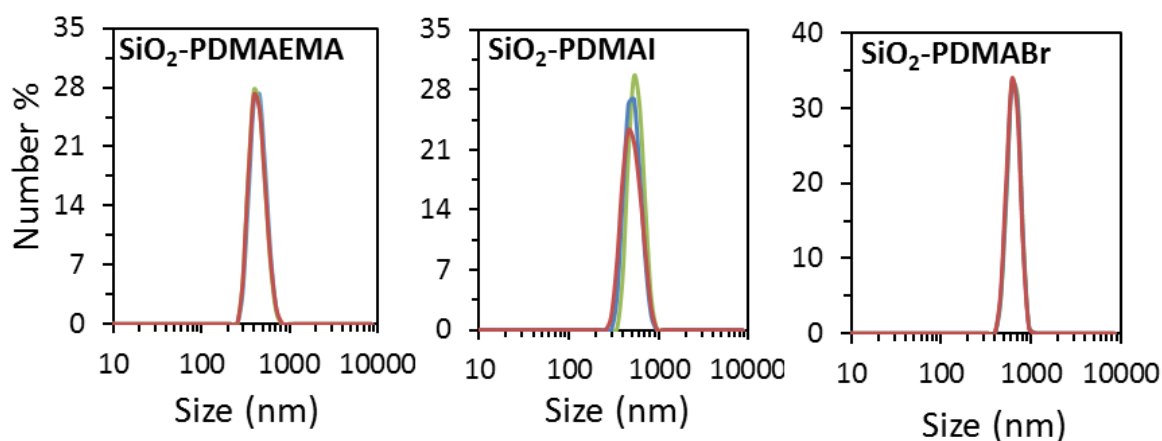
Figure 4.9. DLS measurement of SiO_2-PDMAEMA, SiO_2-PDMAI and SiO_2- PDMABr in PBS at 0.1 mg/mL, 25 °C, measurements were carried out in triplicate.

The associated changes in surface chemistry were confirmed by fourier transform infrared spectroscopy (FTIR, Figure 4.10), with the appearance of a band at 1730 cm^{-1}, characteristic of C=O vibrations in all spectrum. Extra peaks of SiO$_2$-PDMAI and SiO$_2$-PDMABr (at about 1650 cm^{-1}) were attributed to –N$^+$(CH$_3$)$_3$ groups, which provides some evidence of the quaternisation reaction.
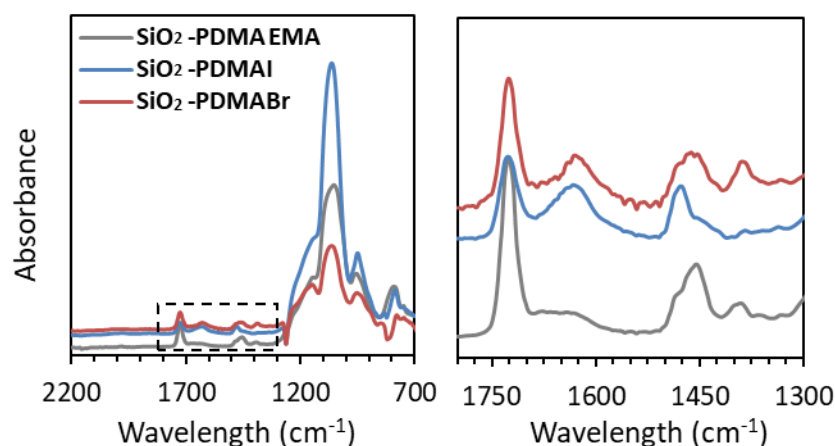
Figure 4.10. FTIR characterisation of SiO$_2$-PDMAEMA, SiO$_2$-PDMAI and SiO$_2$- PDMABr.

The amount of polymer brush on the surface of SiO$_2$ was determined by thermogravimetric analysis (TGA) in Figure 4.11, with 38 %, 48 % and 57 % weight loss associated with the polymer coating for SiO$_2$-PDMAEMA, SiO$_2$-PDMAI and SiO$_2$-PDMABr.
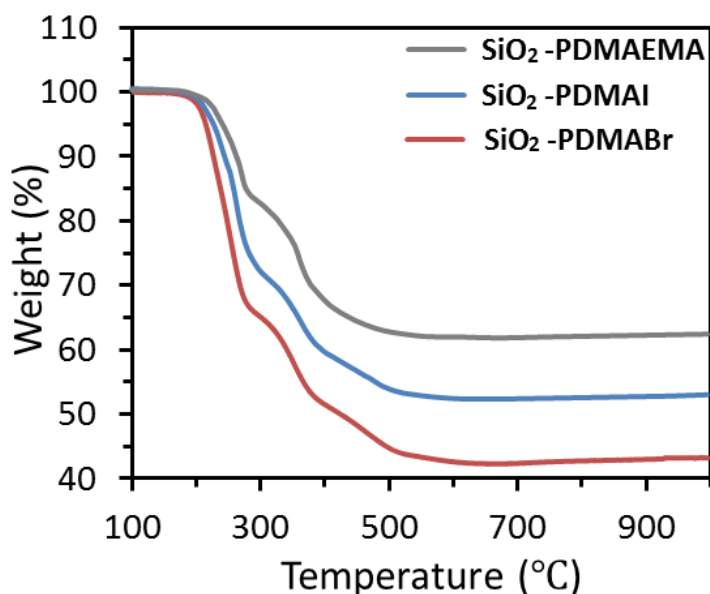
Figure 4.11. TGA characterisation of SiO_2-PDMAEMA, SiO_2-PDMAI and SiO_2- PDMABr at a heating degree of 10 °C/min from room temperature to 1000 °C, weight loss was determined at 900 °C.

According to our previous results[17], the weight loss from bare silica particles and initiator layer on silica particles was around 10 %, hence the weight loss specifically attributed to PDMAEMA brushes can be calculated (28 %), which equal to 33 nm PDMAEMA brush according to Equation 2.3 in chapter 2. The increased weight loss of SiO_2-PDMAI and SiO_2-PDMABr was due to the quaternisation reaction.

To demonstrate the lability of acetal groups of SiO_2-PDMABr in acidic conditions, particle sizes and zeta potentials were measured after incubation in PBS solutions with pH 5 and 7.4 at different time points (see Figure 4.12). No significant size and zeta potential change was observed for particles incubated in pH 7.4 PBS. Whilst for those in pH 5 PBS, the zeta potential decreased for longer incubation and reversed to slightly negative after 6 h, which indicated the cleavage of acetal groups on SiO_2-PDMABr. In addition, the increase in the size of particles was attributed to the formation of aggregates, as electrostatic repulsion between particles was reduced after acetal cleavage.
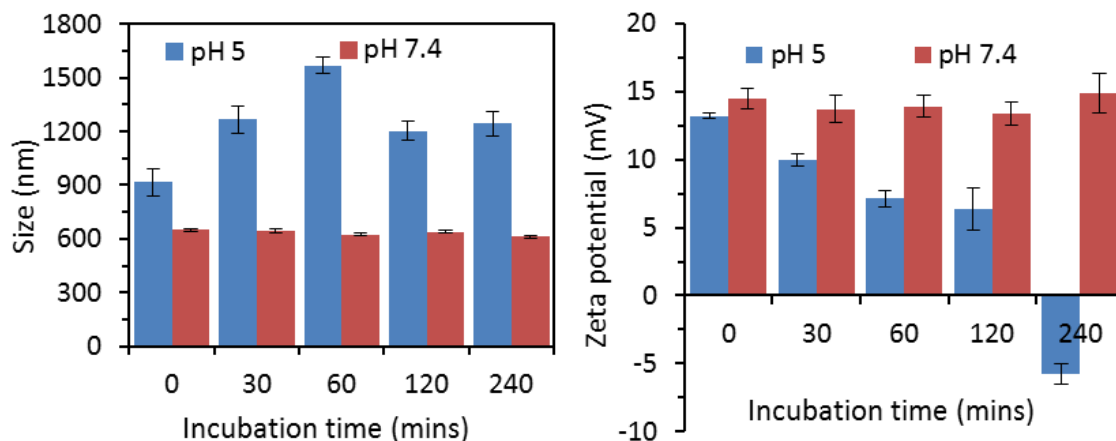
Figure 4.12. Size and zeta potential change of SiO$_2$-PDMABr incubated in pH 5 and pH 7.4 PBS for different time points.

4.6 Transfection kinetics study

A keratinocytes cell line expressing actin-GFP was selected for the simple quantification of siRNA efficiency[17], using GFP siRNA (allowing simultaneous imaging of endogenous and GFP-tagged actin after phalloidin staining for quantification) as described in our previous report[17]. Knock down levels of SiO$_2$-PDMAEMA, SiO$_2$-PDMAI and SiO$_2$-PDMABr complexes were determined for different N/P ratios (10 and 20) and compared with the commercialized transfection agent lipofectamine 2000. The fluorescence intensity ratio of GFP (green)/ phalloidin (red) was measured and compared with the ratio of non-transfected cells to determine the knock down efficiency.
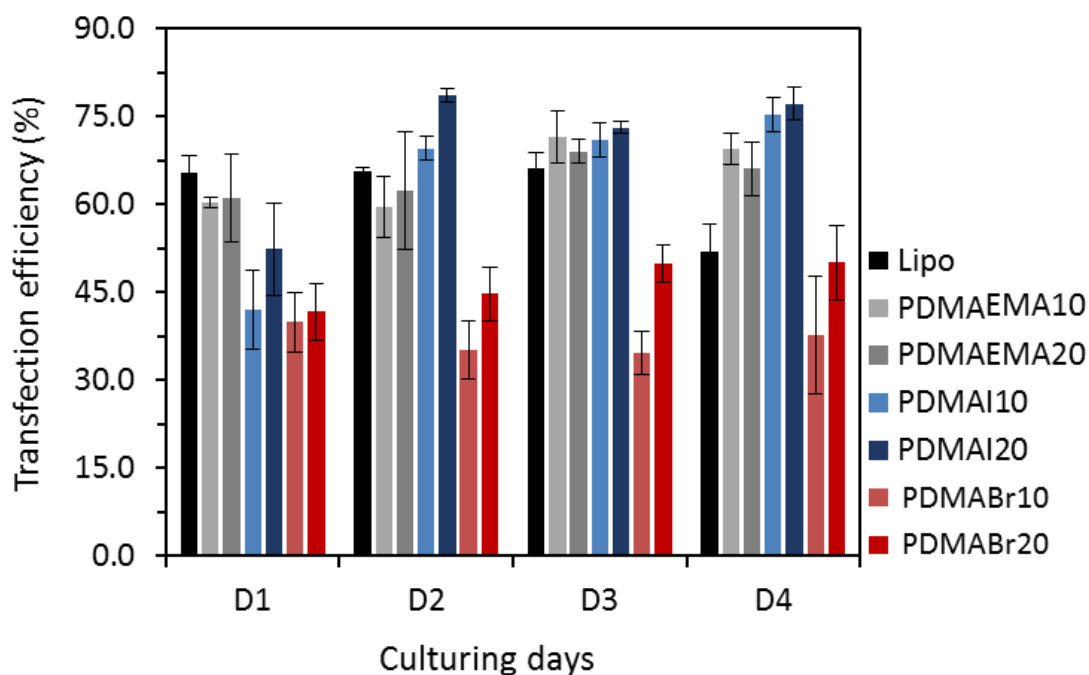
Figure 4.13. HaCaT-GFP cell transfection efficiency kinetics study with SiO_2-PDMAEMA, SiO_2-PDMAI and SiO_2-PDMABr compared with lipofectamine 2000 (Lipo) at NP ratio of 10 and 20, following by transfection from one day to four days; Data analysis was based on three independent experiments, knock down efficiency was determined by the decreased ratio of green to red fluorescence intensity compared with blank cell group. Cells were further cultured for one, two, three and four days to determine the transfection kinetics. After culturing cells for one day, highest knock down efficiencies (above 60 %) were measured with SiO_2-PDMAEMA vectors, comparable with those measured with lipofectamine (Figure 4.13), whilst there was no significant difference in transfection levels at different N/P. This result is in good agreement with our previous report[17].

Table 4.1. Significant difference analysis for transfection kinetics with SiO_2-PDMAEMA, SiO_2-PDMAI and SiO_2-PDMABr compared with lipofectamine, highlighted values represents where there's a significant difference (p<0.5).

TTEST (p value)	D1	D2	D3	D4
lipo vs PDMAEMA10	0.055	0.214	0.317	0.035
lipo vs PDMA20	0.461	0.659	0.046	0.035
lipo vs PDMAI10	0.011	0.055	0.260	0.029
lipo vs PDMAI20	0.052	0.001	0.022	0.027
lipo vs PDMABr10	0.004	0.012	0.014	0.206
lipo vs PDMABr20	0.032	0.017	0.035	0.763

Quaternised vectors were shown a relatively low transfection levels (below 50 %) at both N/P after 1 day of incubation. It is possibly due to the low siRNA encapsulation ability of SiO_2-PDMABr presented according to SPR result and the slower release of siRNA from SiO_2-PDMAI vector as its permanent charge allows to further condense and stabilise siRNA. However, a significant increase of transfection level occurred with SiO_2-PDMAI vector for the following days, in particular at day 2, 78 % knock down efficiency was achieved with SiO_2-PDMAI at N/P=20. Conversely, no significant changes in knock down were observed with SiO_2-PDMABr for the remaining of the experiment, except for a slightly increase for those at N/P=20 although the overall efficiency was still below 50 %. Interestingly, in the case of SiO_2-PDMAI, higher N/P resulted in higher transfection levels whilst the situation conversed for SiO_2-PDMAEMA. The possible cytotoxicity of SiO_2-PDMAEMA at high N/P (will be discussed later) may explain the lower transfection level achieved. Furthermore, for lipofectamine, similar and comparable knock down level was observed for the first three days, however, at day 4, the transfection efficiency reduced significantly lower (around 52 %) than SiO_2-PDMAEMA and SiO_2-PDMAI, although it is still higher than SiO_2-PDMABr.
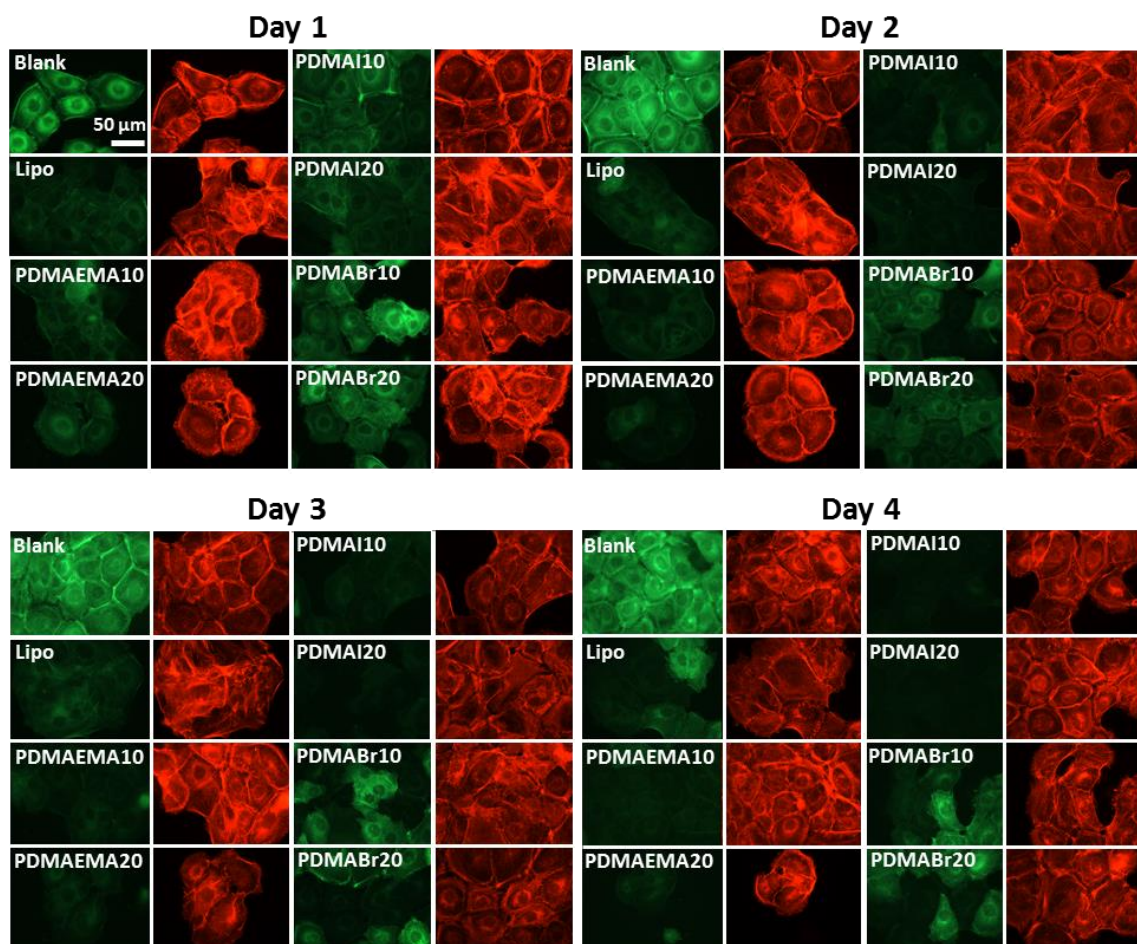
Figure 4.14. Representative images for HaCaT-GFP cell transfection kinetics study with SiO$_2$-PDMAI and SiO$_2$-PDMABr compared with lipofectamine and SiO$_2$-PDMAEMA at NP ratio of 10 and 20 stated at the end of the vector name for different transfection days from one day to four days; Red: phalloidin staining of cytoskeleton, green: GFP-tagged actin.

It implies the polylipid based siRNA delivery materials may not be suitable for its long-term and sustainable transfection, while SiO$_2$-PDMAEMA and SiO$_2$-PDMAI can efficiently condense, encapsulation and release siRNA in a continuous manner and are ideal for the sustained delivery of siRNA molecules. Representative images for each condition and detailed significance comparison and representative images are shown in Figure 4.14 and Table 5.1 respectively.

4.6 Cell viability test

The inherent toxicity of non-viral cationic vectors remains an important issue to address in the field of gene delivery. In our previous report[17], a block copolymer brush consisting of an out block of POEGMA brush was introduced to reduce the binding of serum and increase cell viability. Herein, HaCaT cell viability was tested by incubation the cells with SiO_2-PDMAEMA, SiO_2-PDMAI and SiO_2-PDMABr siRNA complex for N/P ratio 10, 20 and time points (from 1 day to 4 days) compared with lipofectamine. Live/dead assay was used to quantify the percentage of live cells (shown in green) out of total cells. High cell toxicity was observed with Lipofectamine on day 1 that almost 40 % cells died, however, the cell viability increased to above 80 % for the following days as shown in Figure 4.15. It could imply that cell membrane damage occurred on the first day when most of the Lipo/siRNA complexes interact and were internalised within the cells, and that cells subsequently recovered and proliferated at later time points.

Figure 4.15. HaCaT cell viability test *via* live/dead assay with SiO_2-PDMAEMA, SiO_2-PDMAI and SiO_2-PDMABr siRNA complexes compared with lipofectamine/siRNA at NP ratio of 10 and 20 for different transfection days from one day to four days; Data analysis was based on three independent experiments, all cell viabilities were compared with the blank cell group that used in the experiments; Cell viability was determined by calculating the live cells out of total cell number.

For SiO_2-PDMAEMA/siRNA complex, most of cell viability during four days culturing was below 80 % except for SiO_2-PDMAEMA on day 4 at N/P=10 and higher cytotoxicity was observed at N/P=20 compared with N/P=10. Surprisingly, quaternised particle/siRNA complex displayed no obvious cytotoxicity for both N/P ratio and for all days after transfection. Representative images were shown in Figure 4.16. Thus, we propose that the high positive charge alone is not responsible for cell toxicity in this case. Even though a few reports[38, 39] gave evidence that introducing quaternary ammonium groups could increase cytotoxicity, our results are in agreement with other reports[40, 41] that indicated increased cell viability upon quaternisation. For liposome-based systems, a positive

correlation of transfection efficiencies and the degree of toxicity in glioma cell lines was observed by Bell *et al*[42]. leading to the proposal that some degree of cell membrane damage is required for optimal transfection, bearing a fine margin between optimised transfection and cytotoxicity.[43]
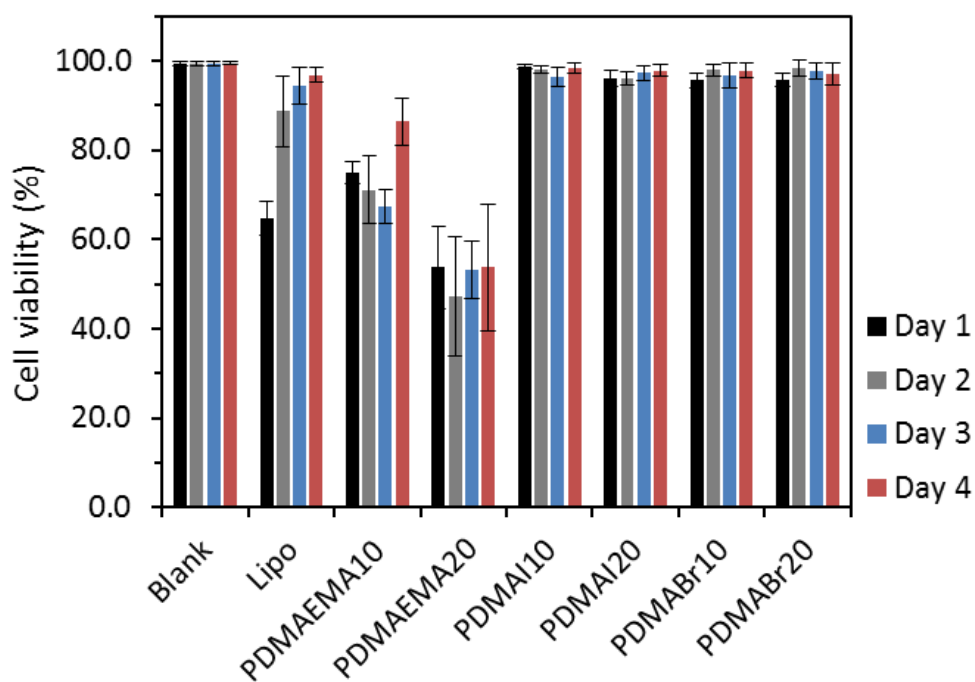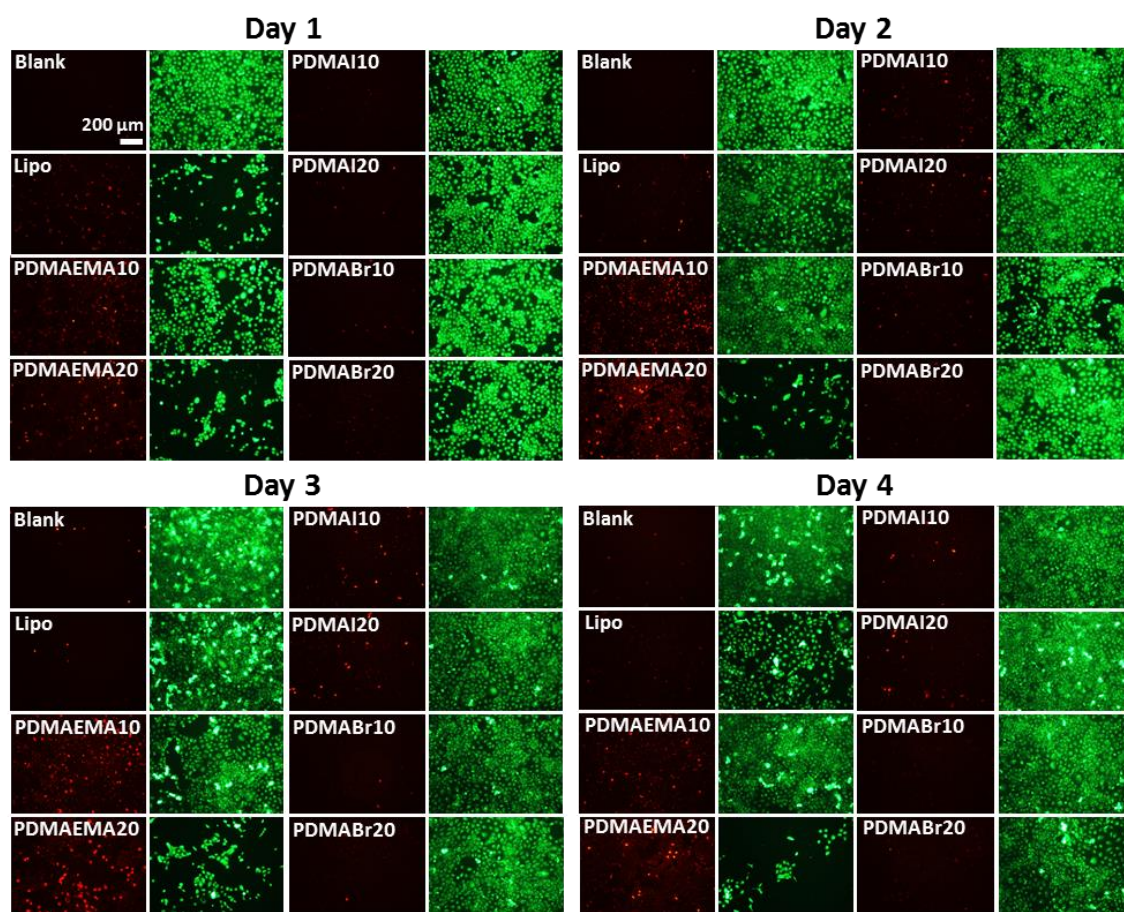

Figure 4.16. Representative images for HaCaT cell viability test *via* live/dead assay with SiO$_2$-PDMAEMA, SiO$_2$-PDMAI and SiO$_2$-PDMABr siRNA complexes compared with lipofectamine/siRNA at NP ratio of 10 and 20 stated at the end of the vector name for different days from one day to four days; Red: dead cells, green: live cells.

However, SiO$_2$-PDMAI complexes successfully transfected cells to a higher degree without causing obvious cell toxicity. It might be due to a different biophysical mechanism regarding the entry of the complexes into the cytosol, or the higher

hydrophobicity associated with unquaternised SiO$_2$-PDMA vectors in physiological environments that will cause much stronger cell membrane disruption compared with quaternised vectors.

4.7 Cellular uptake and tracking of RNA release with labelled particles and siRNA molecules

To understand and visualise particle cellular uptake and siRNA retention and release process *in vitro*, labelled vectors (with fluorescent conjugated polymers, as described in chapter 3) and siRNA were used.

Figure 4.16. SiRNA and particle uptake (average area)/cell analysed with image J for labelled particles and siRNA (A); SiRNA release (free siRNA in cytoplasm) and retention (siRNA still within particles) efficiency analysis for three vectors based on calculation in table 4.2.

Firstly, stable blue fluorescent particles were prepared according to previous reports shown in chapter 4, in which macroinitiators and 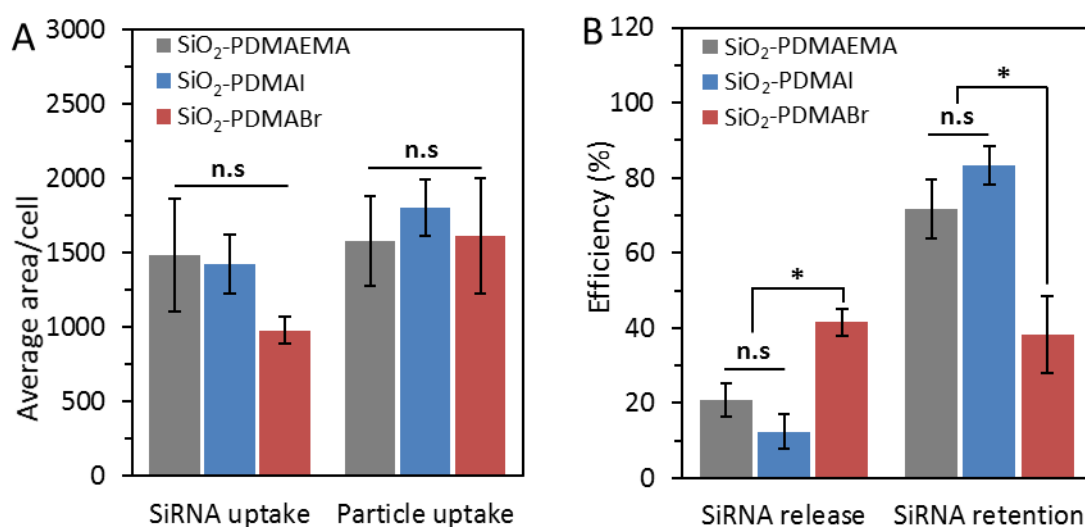fluorescent polyelectrolytes were coated with silica nanoparticle *via* a layer-by-layer approach before polymerisation *via* ATRP. The obtained SiO_2-PDMAEMA particles were then quaternised to afford the corresponding SiO_2-PDMAI and SiO_2-PDMABr particles. Vector/siRNA complexes were formed as before, according to the protocol used in transfection studies. These complexes were then incubated on HaCaT cells with serum free medium for 4 h and followed by a further culturing of 48 h. Cells were subsequently fixed and stained with lysotracker Deep Red dye. Images were analysed and quantified with image J. As shown in Figure 4.16A (detailed calculation on representative examples were shown in Table 4.2), siRNA and particle uptake was determined by measuring the related fluorescent area per cell, both quaternised particles shows a slightly increase of uptake compared with SiO_2-PDMAEMA, which could probably due to the permanent positive charge on quaternised particles that facilitates particle cellular internalisation. In terms of siRNA uptake, similar levels was observed with SiO_2-PDMAEM and SiO_2-PDMAI, whereas the uptake level drops about 30 % on SiO_2-PDMABr, which correlates with SPR and transfection data, although not as pronounced. The ability encapsulation and retention of siRNA allows to release siRNA to cytoplasm in a sustained manner, and establish a long-term transfection effect. Endosomal escape is a major barrier for efficient siRNA delivery *via* non-viral delivery systems as endosomal/lysosomal content are acidified (pH ~5) and contain various nucleases that promote the degradation of the siRNA. Thus, the siRNA release and retention efficiencies were quantified (detailed calculation on representative examples were shown in Table 4.2).

Table 4.2 Calculation of particle/siRNA uptake and siRNA retention/release efficiency (where shows *) based on representative examples; a to g was the measured area with image J co-localisation protocol, i to o was calculated based on values of a to g, detailed calculation was illustrated in the first column.

	Calculation	SiO$_2$-PDMAEMA	SiO$_2$-PDMAI	SiO$_2$-PDMABr
a	Total particles	21310	23821	18104
b	Total siRNA	25670	19153	12204
c	Total Lysosome	65165	54022	63576
d	Particels in lysosome	8802	8723	8179
e	SiRNA on particles (siRNA complex)	16969	15807	4613
f	SiRNA in lysosome	9927	6527	4971
g	SiRNA complex in lysosome	7312	5720	2341
h	Total cell number	16	16	18
i=b-e	Released siRNA from particles	8701	3346	7591
j=f-g	Free siRNA in lysosome	2615	807	2630
k=i-j	Free siRNA in cytoplasma	6086	2539	4961
l=a/h	# Particle uptake / cell	1332	1588	1293
m=b/h	# SiRNA uptake (siRNA/cell)	1604	1277	872
n=e/b*100	# SiRNA retention efficiency (%)	66	83	38
o=k/b*100	# SiRNA release efficiency (%)	24	13	41

As shown in Figure 4.16 B, more than 70 % siRNA was still within SiO$_2$-PDMAEMA and SiO$_2$-PDMAI, whilst less than 40 % of siRNA was in SiO$_2$-PDMABr, which was reflected on the hand by the siRNA release efficiencies that faster release was observed on SiO$_2$-PDMABr due to its acidic cleavable property within endosome/lysosome to promote the disassociation of siRNA from polymer brushes. However, the less siRNA retention and faster release could also bring issues in siRNA transfection that the released siRNA may not be efficiently used and will undergo degradation over time. In contrast, the better retention ability and gradual release of siRNA work synergistically to provide SiO$_2$-PDMAI with a prolonged siRNA knock down ability, which was particularly favoured in clinical trials and biological research where long-term and efficient siRNA delivery is

required. Representative images of labelled particle, siRNA and lysosome/endosome co-localisation was shown in Figure 4.17.
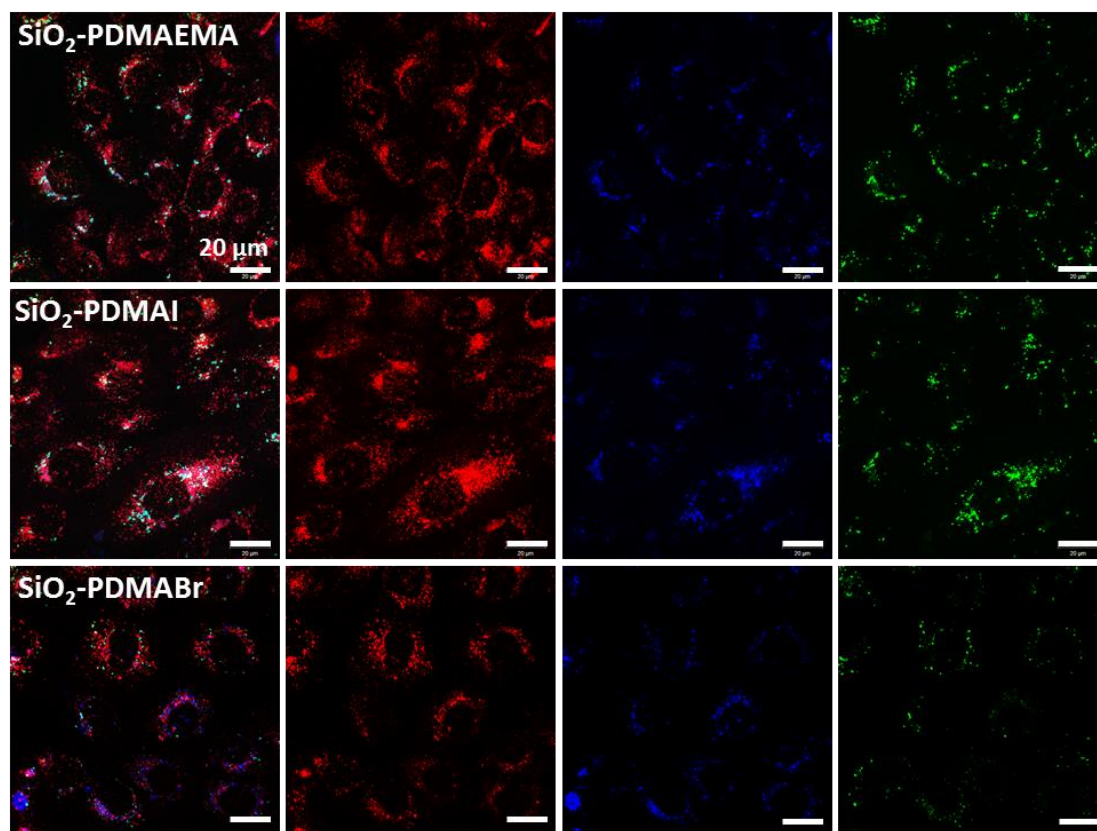
Figure 4.17. Representative images of labelled particle, siRNA and lysosome/endosome co-localisation HaCaT cells; Blue (third column): fluorescent labelled SiO$_2$-PDMAEMA/SiO2-PDMAI/SiO2-PDMABr *via* LBL of macroinitator and fluorescent conjugated polyelectrolytes to generate polymer brush *via* ATRP, green (fourth column): labelled non-targeting siRNA, red (second column): lysosome and endosome stained with lysotracker, merged images were shown in the first column.

Conclusion

Herein, we have reported three different polymer brushes coated silica nanoparticles (SiO$_2$-PDMAEMA, SiO$_2$-PDMAI and SiO$_2$-PDMABr) synthesised *via* ATRP as siRNA delivery vectors. The latter two were derived from SiO$_2$-PDMAEMA by quaternisation tertiary

amine of methyl iodide and acetal bromide respectively. We studied the preparation and characterisation of these particles with different coating chemistries, confirmed their chemical composition, pH responsiveness and charge shifting ability *via* different techniques. PDMAEMA and PDMAI brushes showed higher siRNA encapsulation and stabilisation ability than PDMABr brush, in which overall siRNA binding is decreased and that is displaying extensive siRNA release upon cleavage of acetal groups in acidic solutions. Additionally, in cell transfection kinetics studies, SiO_2-PDMAI exhibited a long-term and efficient siRNA delivery compared to SiO_2-PDMBr. We hypothesise that this is due to the more hindered structure of PDMABr brush after quaternisation with relatively larger side chains that reduce its ability to stabilise oligonucleotides, compared to permanently charged SiO_2-PDMAI vectors. Furthermore, SiO_2-PDMAI and SiO_2-PDMABr displayed improved cell viability than unquaternised SiO_2-PDMAEMA, although the mechanism behind this effect remains unclear. Finally, fluorescently labelled vectors and siRNA were used to visualise siRNA complex uptake and siRNA release in HaCaT cells. Co-localisation study reveals that SiO_2-PDMAI exhibited the best siRNA retention ability and the lowest siRNA release efficiency compared with the rest two vectors which facilitates the long-term and efficient siRNA delivery. Therefore, the novel cationic polymer brush coated nano-vectors could be a useful platform to develop new generations of siRNA delivery agent for sustained RNA delivery.

Experimental section

Mateirals:

2-(Dimethylamino)ethyl methacrylate (DMA, Mn = 157.21), copper chloride (Cu(I)Cl), copper bromide (Cu(II)Br2), 2,2'-bipyridyl (bipy), anhydrous toluene, triethylamine (Et$_3$N), methyl iodide, Ethyl α-bromoisobutyrate initiator, bromoacetic acid and vinyl acetate were purchased from Sigma-Aldrich and used as received. All chemicals and solvents were analytical grades unless otherwise stated. Cu(I)Cl was kept under vacuum until used. Silicon wafers (100 mm diameter, <100> orientation, polished on one side/reverse etched) were purchased from Compart Technology Ltd and cleaned in a Plasma System Zepto from Diener Electronic, for 10 min in air. Silica particles (unfunctionalised) were purchased from Bangs Laboratories (supplied as powder, mean diameters of 300 nm). The silane initiator, (3-trimethoxysilyl)propyl 2-bromo-2-methylpropionate was purchased from Gelest. Surface plasmon resonance (SPR) chips (10 x 12 x 0.3 mm) were purchased from Ssens. Triton X-100, gelatin, phallodin–tetramethylrhodamine B isothiocyanate, PFA (paraformaldehyde), DAPI (4,6-diamidino-2-phenylindole), phosphate buffered saline (PBS, 150 mM) and 6-FAM fluorescent labelled siRNA (MISSION® siRNA Fluorescent Universal Negative Control, 6-FAM) were purchased from Sigma Aldrich. Dulbecco's Modified Eagle Medium (DMEM) medium, OPTI-MEM™ medium, Fetal Bovine Serum (FBS), trypsin, versene, penicillin-streptomycin, L-glutamine, hoechst 33342, live/dead assay kit and LysoTracker® Red DND-99 were from Thermo-Fisher. Collagen type I was from BD Bio-science. GFP siRNA (target sequence CGG CAA GCT GAC CCT GAA GTT CAT) was purchased from Qiagen®.

Synthesis of 1-acetoxyethyl-2-bromoacetate (acetal bromide)

1-acetoxyethyl-2-bromoacetate (Mw: 224) was synthesised by an addition reaction according to previous report. Briefly, 4.168 g (30 mmol, 1.5 eq) bromoacetic acid was mixed with 1.721 g (20 mmol, 1 eq) vinyl acetate in a 100 mL round-bottomed flask. The reaction was heated to 95 °C and left for 19 h until all vinyl acetate was consumed. After 19 h, the mixture was allowed to cool down and purified with column chromatography (petroleum ether/ethyl acetate=6). The desired product was yield at 40% as a yellowish liquid.

Synthesis of free PDMAEMA polymer

Free PDMAEMA polymer was synthesis by ATRP controlled radical polymerisation according to previous report. Briefly, in a 100mL round bottom flask, the monomer (15 g DMAEMA, 95.5 mmol, 500 eq), the Ethyl α-bromoisobutyrate initiator (EBiB, 0.073 g, 0.374 mmol, 2 eq) and 2,2'-bipyridyl ligand (bipy, 0.0297 g, 0.190 mmol, 1.01 eq) were mixed in ethanol and water mixture (10 mL, v:v=1:4). Nitrogen gas was bubbled through the mixture at room temperature for 30 min to remove oxygen, then copper(I) chloride (0.0186 g, 0.188 mmol, 1 eq) was added to the mixture. The reaction was heated to 50 °C. A small flow of nitrogen gas was maintained during the polymerisation. After 5 h the polymerisation was cooled and exposed to the atmosphere. The solution was dialyzed against water (2L) using a Spectra/Por regenerated cellulose membrane with a molecular weight cut off of 1000 Da . The resulting aqueous solution was then lyophilised to yield the final polymer as off white solid.

Quaternisation of free PDMAEMA with acetal bromide

A mixture of PDMAEMA polymer (500 g, 3.2 mmol, 1 eq) and 1-acetoxyethyl-2-bromoacetate (1.075 g, 4.8 mmol, 1.5 eq) was dissolved in 5 mL DMF and added to 25 mL round bottom flask. The reaction heated to 70 °C and left stirring at room temperature overnight. Subsequently, the polymer was purified by precipitating in precooled ethanol twice and the obtained powder under vacuum.

Quaternisation of PDMAEMA brush with acetal bromide and methyl iodide

30 nm PDMAEMA brushes on silicon wafer was preparation according to previous report. Subsequently, the wafers coated with PDMAEMA brushes were immersed in 100 mM ABr or methyl iodide DMF solution for 12 h. The quaternised PDMAEMA brushes, namely PDMAI for methyl iodide quaternisation, PDMABr for acetal bromide one were washed with copious of ethanol and dried with nitrogen stream before ellipsometry characterisation.

Characterisation of quaternised PDMAEMA brush

PH responsiveness of PDMABr. PDMABr brush coated silicon wafers were incubated in PBS buffers with pH 7.4 and pH 5 respectively for 4 h at room temperature. Dry brush thickness was measured with ellipsometry before and after incubation with buffers.

Wet ellipsometry measurement for brush swelling in different pH. Silicon wafers with silane initiators were cut into 1 cm x 3 cm before polymerisation. 3 pieces of PDMAEMA brushes were prepared with close brush thickness, of which one was quaternised with acetal bromide (PDMABr) and one with methyl iodide (PDMAI). All brushes coated silicon wafers were assembled with liquid chamber before characterisation. Continues argon flow was applied to dry the brushes through the chamber for 10 mins and dry brush thicknesses in the chamber were measured right after drying. Then, 4 mL deionised water was injected in the chamber and equilibrate for 5 mins before measuring brush swelling thickness. Similarly, brush swelling thickness was measured in 150 Mm NaCl, pH 7.4 PBS, pH 5 150 Mm NaCl and pH 9 150 Mm NaCl subsequently.

SiRNA binding on quaternised PDMAEMA brush

PDMAEMA brush coated SPR chips were prepared according to previous report. PDMAI and PDMABr coated SPR chips were prepared with same method describe above. Surface plasmon resonance (SPR) was used to evaluate the interaction between siRNA (22 bp) and polymer brushes with a Biacore 3000. SPR chips were coated with polymer brushes prior to mounting on a substrate holder. Mounted chips were docked, primed with PBS and equilibrated with PBS at 10 µL/min flow rate until a stable baseline was obtained. 50 µL siRNA solutions were injected at 10 µg/mL. Once the injection was finished, washing with PBS was continued at 10 µL/min flow rate. The adsorption level was measured after stabilised. All measurements were carried out in triplicates (three separate chips freshly prepared).

Preparation of quaternised PDMAEMA coated silica nanoparticles

PDMAEMA brush coated silica nanoparticles (SiO$_2$-PDMAEMA) were prepared according to previous report. Then, PDMAEMA brush was quaternised by incubating SiO$_2$-PDMA (200 mg) in 10 mL DMF with 100 mM acetal bromide and methyl iodide. The obtained particles were named as SiO$_2$-PDMAI and SiO$_2$-PDMABr.

Characterisation of quaternised PDMAEMA coated silica nanoparticles

DLS, FTIR and TGA were applied to characterise the size, chemical structure and polymer brush composite. Detailed methods were reported previously.

PH responsiveness of SiO$_2$-PDMABr. SiO$_2$-PDMABr was incubated in PBS buffers with pH 7.4 and pH 5 respectively for 30, 60, 120 and 240 min at room temperature. Then particles were washed, redispersed again in pH 7.4 PBS and characterised with DLS for size and zeta potential.

Transfection kinetics study

HaCaT-GFP cells were seeded at different densities (25 k/well, 12.5 k/well, 6.25 k/well and 3.125 k/well) on glass cover slips pre-treated with collagen in 24-well plates, 24 h prior to the transfection assay. A final siRNA concentration of 50 nM/well was used. 100 µL SiO$_2$-PDMAEMA/GFP siRNA, SiO$_2$-PDMAI/GFP siRNA and SiO$_2$-PDMABr/GFP siRNA were prepared at N/P=10 and 20, in serum free OPTI-MEM medium. After removing the DMEM medium, cells were washed twice with pre-warmed serum free OPTI-MEM

medium and another 400 µL was added. 100 µL siRNA complex was then added dropwise to each well and mixed by shaking gently. Cells were incubated with siRNA complexes for 4 h in the incubator and the medium was then replaced by 500 µL full culture DMEM medium for a further culturing of 1 day (25 k), 2 days (12.5 k), 3 days (6.25 k) and 4 days (3.125 k). Lipofectamine® 2000 complexed with GFP siRNA/negative control (NC) siRNA (protocol according to the manufacturer's instruction with a final siRNA concentration of 50 nM/well) was used as a positive/negative control. The transfected cells were washed with PBS three times, fixed in paraformaldehyde (PFA, 4 %, 10 min) and permeabilised with Triton X-100 (0.2 %, 5 min). Cells were then stained with TRITC-phalloidin (1:1000) and DAPI (4,6-diamidino-2-phenylindole, 1:1000) in blocking buffer (10% FBS and 0.25% gelatin from cold water fish skin, Sigma-Aldrich) and kept at room temperature for 1 h. Cover slips with fixed cells were mounted on glass slides before imaging with a Leica DMI4000 fluorescence microscope. Transfection efficiency was quantified by Image J.

Cell viability study

HaCaT cells were seeded at different densities (25 k/well, 12.5 k/well, 6.25 k/well and 3.125 k/well) (in 500 µL of DMEA medium) in 24-well plates 24 h prior. A final siRNA concentration of 50 nM/well was used. 100 µL SiO_2-PDMAEMA/GFP siRNA, SiO_2-PDMAI/GFP siRNA and SiO_2-PDMABr/GFP siRNA were prepared at N/P=10 and 20 were added into each well for 4 h in 0.5 mL serum free OPTI-MEM medium and then the medium was replaced by full culture DMEM medium for further culturing of 1 day (25 k), 2 days (12.5 k), 3 days (6.25 k) and 4 days (3.125 k). Cell viability was carried out by

live/dead assay in which, cells were incubated in 500 μL DMEM medium of 4 mM calcein AM, 2 mM ethidium homodimer and hoechst 33342 (for staining cell nucleus) for 30 min at 37 °C prior to imaging. Fluorescence imaging was used to capture the live-dead cells and these were counted *via* ImageJ to obtain the percentage of live cells of total number of cells.

Labelled particle and siRNA co-localisation study in HaCaT cells

HaCaT cells were seeded at a density of 12.5 k/well on glass cover slips pre-treated with collagen in 24-well plates, 24 h prior. SiO_2-PDMAEMA generated from macroinitiator and with fluorescent labelling was prepared according to previous report. SiO_2-PDMAEMA was then quaternised with the same protocol described. 6-FAM fluorescent labelled siRNA (sigma Aldrich, MISSION® siRNA Fluorescent Universal Negative Control, 6-FAM) was used to track siRNA binding and release mechanism. Briefly, a final siRNA concentration of 50 nM/well was used. 100 μL SiO_2-PDMAEMA/6-FAM siRNA, SiO_2-PDMAI/6-FAM siRNA and SiO_2-PDMABr/6-FAM siRNA was prepared at N/P=20, in serum free OPTI-MEM medium. After removing the DMEM medium, cells were washed twice with pre-warmed serum free OPTI-MEM medium and another 400 μL was added. 100 μL siRNA complex was then added dropwise to each well and mixed by shaking gently. Cells were incubated with siRNA complexes for 4 h in the incubator and the medium was then replaced by 500 μL full culture DMEM medium for a further culturing of 2 days. Subsequently, cells were stained with LysoTracker® Red DND-99 at 50 nM for 1 h at 37 °C and fixed in paraformaldehyde (PFA, 4 %, 10 min) before imaging with a Zeiss LSM710

Confocal and Elyra PS.1 Superresolution microscope. Images were analysed and quantified with Image J.

References:

(1) Conwell, C. C.; Huang, L., *Non-Viral Vectors for Gene Therapy, 2nd Edition: Part 1* **2005,** *53*, 3-18.

(2) N, P. P.; J, M. A., *Clinical and Experimental Pharmacology and Physiology* **2006,** *33* (5-6), 504-510.

(3) Hannon, G. J., *Nature* **2002,** *418*, 244.

(4) McManus, M. T.; Sharp, P. A., *Nature Reviews Genetics* **2002,** *3*, 737.

(5) Chakraborty, C.; Sharma, A. R.; Sharma, G.; Doss, C. G. P.; Lee, S. S., *Molecular Therapy-Nucleic Acids* **2017,** *8*, 132-143.

(6) Burnett, J. C.; Rossi, J. J.; Tiemann, K., *Biotechnology Journal* **2011,** *6* (9), 1130-1146.

(7) Castanotto, D.; Rossi, J. J., *Nature* **2009,** *457*, 426.

(8) Akinc, A.; Goldberg, M.; Qin, J.; Dorkin, J. R.; Gamba-Vitalo, C.; Maier, M.; Jayaprakash, K. N.; Jayaraman, M.; Rajeev, K. G.; Manoharan, M.; Koteliansky, V.; Rohl, I.; Leshchiner, E. S.; Langer, R.; Anderson, D. G., *Mol Ther* **2009,** *17* (5), 872-9.

(9) Kim, S. S.; Garg, H.; Joshi, A.; Manjunath, N., *Trends in Molecular Medicine* **2009,** *15* (11), 491-500.

(10) Nayerossadat, N.; Maedeh, T.; Ali, P. A., *Adv Biomed Res* **2012,** *1*, 27.

(11) Li, S.; Huang, L., *Gene Therapy* **2000,** *7* (1), 31-34.

(12) Pack, D. W.; Hoffman, A. S.; Pun, S.; Stayton, P. S., *Nature Reviews Drug Discovery* **2005,** *4* (7), 581-593.

(13) He, C. L.; Zhuang, X. L.; Tang, Z. H.; Tian, H. Y.; Chen, X. S., *Advanced Healthcare Materials* **2012,** *1* (1), 48-78.

(14) de Lima, M. C. P.; Simoes, S.; Pires, P.; Faneca, H.; Duzgunes, N., *Advanced Drug Delivery Reviews* **2001,** *47* (2-3), 277-294.

(15) Fischer, D.; Bieber, T.; Li, Y.; Elsässer, H.-P.; Kissel, T., *Pharmaceutical Research* **1999,** *16* (8), 1273-1279.

(16) Bartlett, D. W.; Davis, M. E., *Nucleic Acids Research* **2006,** *34* (1), 322-333.

(17) Li, D.; Sharili, A. S.; Connelly, J.; Gautrot, J. E., *Biomacromolecules* **2018,** *19* (2), 606-615.

(18) Krishnamoorthy, M.; Li, D.; Sharili, A. S.; Gulin-Sarfraz, T.; Rosenholm, J. M.; Gautrot, J. E., *Biomacromolecules* **2017,** *18* (12), 4121-4132.

(19) Convertine, A. J.; Diab, C.; Prieve, M.; Paschal, A.; Hoffman, A. S.; Johnson, P. H.; Stayton, P. S., *Biomacromolecules* **2010,** *11* (11), 2904-2911.

(20) Malcolm, D. W.; Varghese, J. Y.; Sorrells, J. E.; Ovitt, C. E.; Benoit, D. S. W., *Acs Nano* **2018,** *12* (1), 187-197.

(21) Dehousse, V.; Garbacki, N.; Colige, A.; Evrard, B., *Biomaterials* **2010,** *31* (7), 1839-1849.

(22) Yu, H. J.; Zou, Y. L.; Wang, Y. G.; Huang, X. N.; Huang, G.; Sumer, B. D.; Boothman, D. A.; Gao, J. M., *Acs Nano* **2011,** *5* (11), 9246-9255.

(23) Cordes, E. H.; Bull, H. G., *Chemical Reviews* **1974,** *74* (5), 581-603.

(24) Zhang, Y.; He, J.; Cao, D.; Zhang, M.; Ni, P., *Polymer Chemistry* **2014,** *5* (17), 5124-5138.

(25) Zhang, X. J.; Zhuo, R. X., *Macromolecular Chemistry and Physics* **2016,** *217* (17), 1926-1933.

(26) Liu, J.; Huang, Y.; Kumar, A.; Tan, A.; Jin, S.; Mozhi, A.; Liang, X.-J., *Biotechnology Advances* **2014,** *32* (4), 693-710.

(27) Gillies, E. R.; Goodwin, A. P.; Fréchet, J. M. J., *Bioconjugate Chemistry* **2004,** *15* (6), 1254-1263.

(28) J, T. D.; M, T. G.; D, X.; W, K. L.; F, S. M., *Hepatology* **1996,** *23* (4), 872-880.

(29) Yao, W.; Xu, H. Y., *Tetrahedron Letters* **2001,** *42* (13), 2549-2552.

(30) A., C. J.; T., B. T.; L., C. J.; E., B. K.; M., B. E.; J., F. J. M., *Advanced Materials* **2010,** *22* (32), 3593-3597.

(31) Kohli, R., Chapter 3 - Methods for Monitoring and Measuring Cleanliness of Surfaces. In *Developments in Surface Contamination and Cleaning*, William Andrew Publishing: Oxford, 2012; pp 107-178.

(32) Tan, K. Y.; Gautrot, J. E.; Huck, W. T. S., *Langmuir* **2011,** *27* (4), 1251-1259.

(33) Chen, W.-L.; Menzel, M.; Watanabe, T.; Prucker, O.; Rühe, J.; Ober, C. K., *Langmuir* **2017,** *33* (13), 3296-3303.

(34) Azzaroni, O.; Zheng, Z. J.; Yang, Z. Q.; Huck, W. T. S., *Langmuir* **2006,** *22* (16), 6730-6733.

(35) Willott, J. D.; Murdoch, T. J.; Humphreys, B. A.; Edmondson, S.; Webber, G. B.; Wanless, E. J., *Langmuir* **2014,** *30* (7), 1827-1836.

(36) Galvin, C. J.; Genzer, J., *Macromolecules* **2016,** *49* (11), 4316-4329.

(37) Zhang, Q.; Xia, F.; Sun, T.; Song, W.; Zhao, T.; Liu, M.; Jiang, L., *Chemical Communications* **2008,** (10), 1199-1201.

(38) Bottega, R.; Epand, R. M., *Biochemistry* **1992,** *31* (37), 9025-9030.

(39) Lv, H.; Zhang, S.; Wang, B.; Cui, S.; Yan, J., *Journal of Controlled Release* **2006,** *114* (1), 100-109.

(40) Lee, J. H.; Lim, Y. B.; Choi, J. S.; Choi, M. U.; Yang, C. H.; Park, J. S., *Bulletin of the Korean Chemical Society* **2003,** *24* (11), 1637-1640.

(41) Patil, M. L.; Zhang, M.; Taratula, O.; Garbuzenko, O. B.; He, H. X.; Minko, T., *Biomacromolecules* **2009,** *10* (2), 258-266.

(42) Bell, H.; Kimber, W. L.; Li, M. W.; Whittle, I. R., *Neuroreport* **1998,** *9* (5), 793-798.

(43) Bauer, M.; Kristensen, B. W.; Meyer, M.; Gasser, T.; Widmer, H. R.; Zimmer, J.; Ueffing, M., *Basic & Clinical Pharmacology & Toxicology* **2006,** *98* (4), 395-400.

CHAPTER 5

Conclusions and Future Work

5.1 Conclusions

In this thesis, we focus on the design and preparation of PDMAEMA polymer brush coated silica nanoparticles for the delivery of siRNA. The idea was inspired from the interactions of nucleic acid with PDMAEMA brush, in which the binding of nucleic acid molecules to PDMAEMA brushes depends both on brush density and size of the nucleic acid sequence. The designed PDMAEMA brush coated silica nanoparticles siRNA delivery vectors displayed high knock down efficiency. The introducing of a protein resistant brush layer POEGMA to the vector improved protein resistance and solution stability as well as cell viability. Such block copolymer brush siRNA delivery vectors are attractive candidates for the design of a new generation of therapeutic platforms.

Besides using mono-initiator to generate polymer brush, we also demonstrated that using LBL of MI and FCP can offer a greater flexibility in the growth and design of polymer brushes and their labelling from templates with a wide range of shapes, sizes and chemistries without additional chemical modification. Polymer brush growth kinetics was systematically investigated and optimised by coating different layers of MI and conducting polymerisation in solvents of different polarity. Detailed characterisation techniques were applied during the LBL process and after polymerisation to ensure the successful preparation of PDMAEMA or POEGMA coated templates. Selected candidates were used to study the particle-cell interactions and deliver siRNA to HaCaT-GFP cells. We believe this novel methodology will provide a simple way of fabricating labelled nanomaterials with controlled polymer brush shells for biomedical applications.

In addition, we have reported three different polymer brushes coated silica nanoparticles (SiO_2-PDMAEMA, SiO_2-PDMAI and SiO_2-PDMABr) with different pH

responsiveness as siRNA delivery vectors. We studied the preparation and characterisation of these particles with different coating chemistries, confirmed their chemical composition, pH responsiveness and charge shifting ability *via* different techniques. In cell transfection kinetics studies, SiO_2-PDMAI exhibited a long-term and efficient siRNA delivery compared to SiO_2-PDMBr. Furthermore, SiO_2-PDMAI and SiO_2-PDMABr displayed improved cell viability than unquaternised SiO_2-PDMAEMA, although the mechanism behind this effect remains unclear. Finally, fluorescently labelled vectors and siRNA were used to visualise siRNA complex uptake and siRNA release in HaCaT cells. Therefore, the novel cationic polymer brush coated nano-vectors could be a useful platform to develop new generations of siRNA delivery agent for long-term and efficient RNA delivery.

Briefly, this thesis contributes to existing knowledge of polymer brush-based siRNA delivery systems by providing the findings:

1. Dense cationic polymer (PDMAEMA) brush allows stable and efficient encapsulation of siRNA.

2. Dense PDMAEMA brush coated silica nanoparticles are able to efficiently deliver GFP siRNA to human epidermal cells.

3. Introducing a protein resistant POEGMA brush layer can improve vector serum stability and cell viability.

4. Using LBL technique to coat MI and FCP offers a greater flexibility to grow polymer brushes and label with fluorescence from templates with a wide range of shapes, sizes and chemistries without additional chemical modification.

5. Quanternisation PDMAEMA brush with methyl iodide provides the vectors with long-term and efficient siRNA delivery ability.

5.2 Future work

This thesis has initiated cationic polymer brush coated systems for siRNA delivery. However, there are still some challenges left to be overcome for improvement of these systems.

1. The interaction of nucleic acids interaction with cationic polymer brush will be investigated systematically by using different base paired DNA and RNA molecules to interact with cationic polymer brushes with different thickness and density to better understand the process and mechanism.

2. Nanomaterials with different core or shape may include to study their impact on siRNA delivery efficiency.

3. Other types of nucleic acids such as microRNA can also be applied in this system for particular biomedical applications.

4. The interaction of different chemistry coated particle on cell morphology and internalisation may be further characterised by other techniques such as cryo-SEM and scanning ion-conductance microscopy (SICM).

5. The mechanism of siRNA uptake and release needs further investigation by carefully design the experiment and analysis tool.